UN... OF MICHIGAN
DEC ... 1958
ENGINEERING LIBRARY

JOURNAL OF FLUID MECHANICS

VOLUME 4 PART 6

NOVEMBER 1958

Published by

CAMBRIDGE UNIVERSITY PRESS

BENTLEY HOUSE, 200 EUSTON ROAD, LONDON, N.W.1
AMERICAN BRANCH: 32 EAST 57th STREET, NEW YORK 22, N.Y.

Price 20*s*. (*U.S.A.* $3.25)

The JOURNAL OF FLUID MECHANICS exists for the publication of theoretical and experimental investigations of all aspects of the mechanics of fluids, and is issued in six parts per volume.

Editor

Dr. G. K. BATCHELOR, Cavendish Laboratory, University of Cambridge, Cambridge, England.

Assistant Editors

Dr. T. B. BENJAMIN, Dr. I. PROUDMAN, Dr. P. G. SAFFMAN.

Associate Editors

Prof. G. F. CARRIER, Pierce Hall, Harvard University, Cambridge 38, Massachusetts, U.S.A.

Dr. W. C. GRIFFITH, Research and Development Laboratory, Missile Systems Division, Lockheed Aircraft Corporation, Palo Alto, California, U.S.A.

Prof. M. J. LIGHTHILL, Department of Mathematics, The University, Manchester, England.

Prof. R. R. LONG, School of Engineering, The Johns Hopkins University, Baltimore 18, Maryland, U.S.A.

Authors wishing to have papers published in the JOURNAL should communicate them to any one of the persons named above, choosing one in their own country where possible.

Authors are urged to ensure that their papers are written clearly and attractively, in order that their work will be readily accessible to readers.

Manuscripts should be typed in double spacing on one side of the paper only, with references listed at the end in alphabetical order of authors. Drawings should be done on a large scale in Indian ink on tracing cloth or drawing paper, with the list of captions typed at the end of the manuscript. Proofs of papers from overseas will usually be despatched to authors by airmail. There is no charge for publication. Authors are entitled to receive 50 offprints of a paper in the JOURNAL free of charge, and additional offprints can be purchased if ordered in advance.

SUBSCRIPTIONS

The subscription price for a volume of six parts is £5 10*s.* net, post free, payable in advance; separate parts 20*s.* net, plus postage. Subscriptions may be sent to any bookseller, or to the Cambridge University Press, Bentley House, 200 Euston Road, London, N.W.1.

Subscribers in the United States should send their orders to the Cambridge University Press, American Branch, 32 East 57th Street, New York 22. Subscription price per volume $18.50 post free, payable in advance; separate parts $3.25, plus postage.

Two-dimensional incompressible magneto-hydrodynamic flow across an elliptical solenoid

By NELSON H. KEMP and HARRY E. PETSCHEK
AVCO Research Laboratory, Everett, Massachusetts

(*Received* 30 *April* 1958)

SUMMARY

An analysis has been made of the two-dimensional flow of an incompressible constant-conductivity fluid through an elliptically shaped solenoid containing a constant magnetic field directed normal to the flow plane. The effect of both Hall current and ion slip has been included in the generalized Ohm's law used for the fluid. The analysis is based on a perturbation procedure in two parameters, one being the magnetic Reynolds number R_m and the other the ratio S of magnetic force per unit area to dynamic pressure. Calculations have been carried to the first order in each parameter, and closed-form analytic expressions have been obtained for the force and moment on the solenoid, the current density, stream function, magnetic field and other pertinent physical quantities.

It was found that, to the zeroth order, there is a force but no moment on the solenoid. To the first order in S, where the flow field is modified but the magnetic field is not, there is a moment and a force, the latter being anti-parallel to the zeroth order force. To the first order in R_m, where the magnetic field is modified but the flow field is not, there is a moment but no force. Thus, to the first order the lift to drag ratio is the same as in the zeroth order. Graphs which illustrate some of the effects of angle of attack, fineness ratio of the ellipse, Hall current and ion slip, on the forces and moments are presented.

SYMBOLS

A_m	constant in Fourier expansion of $(\partial\psi_i/\partial\eta)_e$, see (4.7),	C_e	contour of elliptical solenoid,
		c	value of ξ on elliptical solenoid,
a, b	semi-major and semi-minor axes of ellipse,	D	drag,
B	magnetic field vector,	d	see (3.2),
B^0	uniform magnetic field inside ellipse (dimensional),	**E**	electric field vector,
		E	complete elliptic integral of the second kind,
C_m	constant in Fourier expansion of $(\partial\psi_i/\partial\eta)_e$, see (4.7),	e	electronic charge,

$\mathbf{F}$ force,
h fineness ratio b/a of ellipse
I discontinuous factor which is unity inside ellipse, zero outside ellipse,
$\mathbf{j}$ current density vector,
K_i constant in stream function ψ', see (4.28),
K, K_ξ, K_c, K_s constants defined below (4.32 b) and (5.9),
$\mathbf{k}$ unit vector normal to flow plane, forming third vector of a right-handed system,
k Boltzmann's constant,
L lift,
$\mathscr{L}$ reference length,
l coordinate along free-stream direction,
$\mathbf{M}$ moment about centre of ellipse,
m particle mass,
n coordinate perpendicular to free stream direction,
N wake half-width, see (4.19),
N_j number density of j species,
P perimeter of ellipse,
p fluid pressure,
$\mathbf{q}$ velocity vector,
q^0 free-stream speed (dimensional),
Q_{jk} elastic collision cross-section for collision between species j and k,
R_m magnetic Reynolds number $\mu\mathscr{L}\sigma q^0$,
R moment arm,
$\mathbf{r}$ position vector from centre of ellipse,
S dimensionless parameter $\sigma\mathscr{L}(B^0)^2/\rho q^0$,
s arc length along a contour,
T temperature,
$\mathbf{U}$ constant vector, defined below (5.9),
$\mathbf{V}^0$ vector, see (4.32),
$\bar{\mathbf{V}}^0$ constant vector, defined below (5.9),
W_c, W_s constants in vorticity jump, see (4.20 c),
x, y coordinate along and normal to the major axis of the ellipse,
z complex position vector, $z = x + iy$,
α angle of attack, measured between major axes of ellipse and free stream, see figure 1,
α, β, γ, δ constants in the solution of Laplace's equation (with various sub- and superscripts),
Δ_m see (4.7 a),
ϵ eccentricity of ellipse, $\sqrt{(1-h^2)}$,
ϵ_{jk} friction coefficient between species j and k, see (A 3),
ζ $\xi + i\eta$,
η angular elliptic coordinate,
θ polar angle in (x, y)-plane,
κ Hall coefficient, see (A 2 b),
λ ion slip coefficient, see (A 2 c),
μ permeability,
ξ radial elliptic coordinate,
ρ fluid density (dimensional),
σ electrical conductivity of fluid (dimensional),
ϕ electrostatic potential, $E = -\nabla\phi$,
ψ stream function, $\mathbf{q} = -\mathbf{k} \times \nabla\psi$,
$\boldsymbol{\Omega}$ vorticity vector, $\boldsymbol{\Omega} = \nabla \times \mathbf{q}$.

Subscripts

A applied,
e on the elliptical contour,
E electrons,
i inside ellipse,

Subscripts—continued.

I	ions,	w	in wake,
N	neutral atoms or molecules,	x, y	components of vector in x-, y-directions,
l, n	components of vector in l-, n-directions,	1	unit vector,
o	outside ellipse,	ν	outer normal to contour.

Superscripts

0	zero order,	a	first order in R_m,
′	first order in S,	*	dimensional quantity.

1. Introduction

The possibility that magnetohydrodynamic forces may be used advantageously in high speed flight has recently been suggested (Kantrowitz 1953; Patrick 1956; Rosa 1956). At the gas temperatures encountered at speeds corresponding to a re-entering satellite, air becomes a reasonably good conductor of electricity (Lamb & Lin 1957). If this air is allowed to flow through a magnetic field, drag, lift, or control forces may be obtained. It can be shown, on the basis of very rough order-of-magnitude arguments, that it may be possible to obtain larger forces with less heat transfer by using magnetohydrodynamic forces than would be obtained by the conventional method of using gas pressure acting on solid surfaces.

In order to make a more precise evaluation of the possibilities of magnetohydrodynamics in flight, it is necessary to develop methods for treating magnetohydrodynamic flow problems. The work reported here is intended as a step in this direction. Its aim was to analyse a physically realistic magnetohydrodynamic flow problem which maintains some of the features of hypersonic flight. However, some of the simplifications that have been introduced to obtain analytical solutions are such that the direct application of the results to flight is not possible. In particular, we will assume incompressible flow and uniform electrical conductivity in the entire flow field. While this is a case which is physically realizable in either subsonic flows of hot gas or liquid metal flows, it is not a good approximation to hypersonic flight. Nevertheless, it is hoped that the understanding gained will lead towards the solution of realistic flight problems.

For magnetohydrodynamic calculations associated with astrophysical conditions or with the conditions obtained in highly pinched discharges, the magnetic Reynolds number (see (2.9 b)) is usually assumed to be very large. This is frequently stated more crudely as the assumption of infinite conductivity. This is justified in astrophysics because of the large lengths involved and in the pinched discharges because of the high electrical conductivity which is achieved at very high temperatures ($\sim 10^6$ °K).

For large magnetic Reynolds numbers the flow and the magnetic field are very closely coupled and the field lines may be considered almost rigidly attached to the fluid particles. The value of the magnetic Reynolds number that can be expected in flight is, however, of the order of unity or less. The magnetic field is then only slightly distorted by the flow. The general analysis in this paper is oriented towards small magnetic Reynolds numbers and the final calculation is a perturbation calculation based, in part, on an expansion in powers of the magnetic Reynolds number.

In the presence of a magnetic field, the relation between the current and applied electric field—Ohm's law—in a gas is considerably more complex than it is in a solid or liquid conductor. At low densities and high magnetic field strengths the electrons perform many revolutions in their helical orbits in the magnetic field between collisions. Under these conditions the current may be reduced and is not parallel to the electric field, as seen in coordinates moving with the gas. At still lower densities, and in a partially ionized gas, an appreciable difference between the mean velocity of the ions and the gas velocity arises. This results in a reduction of the effective conductivity of the gas. Both of these effects will probably be important under the conditions of interest for flight applications. The generalized form of Ohm's law utilized in this paper is valid for general values of the parameters describing these two effects and is restricted only by the assumption that the degree of ionization is small.

A type of configuration which might be of interest in hypersonic flight is an extended magnetic field such as that produced by a large ring current surrounding a relatively small body. Such a configuration would produce a drag of the order of magnitude of the dynamic pressure acting on an area comparable with the area enclosed by the ring. The area of solid surface exposed to high heat transfer rates is, however, comparatively small. In such a case the flow interacts principally with the magnetic field, and the disturbance due to the presence of the body and the field coils may be neglected to a first approximation.

In the present paper this type of configuration is idealized by considering a two-dimensional flow perpendicular to the axis of an infinitely long solenoid (figure 1). The solenoid is of elliptical cross-section with its major axis at an angle α to the flow direction. It has a uniform magnetic field normal to the flow plane inside the ellipse, and no field outside. We assume that the solenoid itself is completely transparent to the flow; that is, the current-carrying wires are thin enough not to affect the flow. The only interaction with the fluid is that caused by the magnetic field inside the solenoid. To further simplify the problem, we take the fluid to be incompressible, with constant conductivity.

The method of solution of the problem is based on a perturbation in two parameters. One, as mentioned above, is the magnetic Reynolds number which describes the perturbation of the magnetic field about the undisturbed field of the solenoid. The other is a parameter which describes the perturbation of the flow about the uniform flow which would exist

in the absence of a magnetic field. This second perturbation procedure is similar to thin-aerofoil theory, in that it is a small disturbance of a uniform flow. The magnetohydrodynamic case is, however, not restricted to slender cross-sections of the solenoid since for weak magnetic fields the effect on the flow field will be small regardless of the shape. In connection with the remark about aerofoil theory it might be noted that, from an aeronautical point of view, the solenoid behaves as a 'magnetic aerofoil', disturbing the flow and producing a force and moment on itself, as does a solid wing.

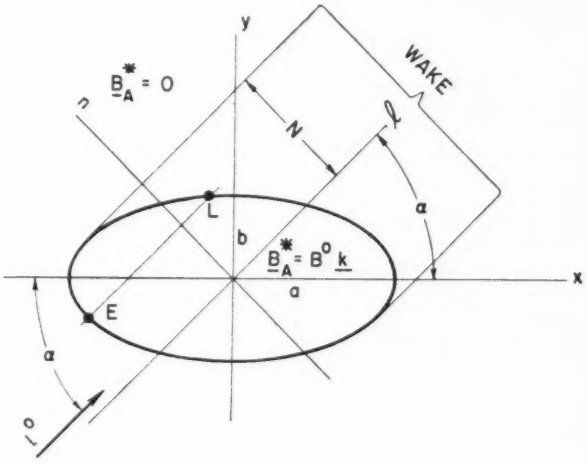

Figure 1. Notation and coordinate systems.

The first-order changes in both the flow and the magnetic field have been computed. The resulting forces and moments on the solenoid are also determined by considering the corresponding forces and moments due to the magnetic body forces on the fluid.

2. Basic equations

The basic equations for the steady motion (with velocity $\mathbf{q}^*$) of an incompressible fluid of density ρ and constant conductivity σ in the presence of a magnetic field $\mathbf{B}^*$ and electric field $\mathbf{E}^*$ are a combination of the Euler, continuity, and Maxwell equations. In rationalized mks. units they are

$$\rho(\mathbf{q}^* \cdot \nabla)\mathbf{q}^* + \nabla^* p^* - \mathbf{j}^* \times \mathbf{B}^* = 0, \qquad \nabla^* \cdot \mathbf{q}^* = 0, \qquad (2.1\,\text{a, b})$$

$$\nabla^* \times \mathbf{E}^* = 0, \qquad \nabla^* \cdot \mathbf{B}^* = 0, \qquad \nabla^* \times \mathbf{B}^* = \mu \mathbf{j}^*, \qquad (2.2\,\text{a, b, c})$$

where μ is the magnetic permeability and $\mathbf{j}^*$ the current density. Equations (2.1 a, b) are the usual incompressible flow equations except

for the presence of the term $\mathbf{j}^* \times \mathbf{B}^*$ which represents the body force exerted by the electromagnetic field on the fluid. (The remaining Maxwell equation which relates the divergence of the electric field to the net charge density may in all cases of magnetohydrodynamic interest be replaced by the quasi-neutrality condition which states that the electron and ion densities are equal at all points in the fluid*. This condition enters into the derivation of the generalized Ohm's law for the gas and is not required directly in the macroscopic equation.) For a partially ionized gas with a low degree of ionization, the current density is related to the electromagnetic and velocity fields by a generalized Ohm's law of the form (see Appendix A)

$$\mathbf{j}^* = \sigma[\mathbf{E}^* + \mathbf{q}^* \times \mathbf{B}^* - \kappa^* \mathbf{j}^* \times \mathbf{B}^* + \lambda^* (\mathbf{j}^* \times \mathbf{B}^*) \times \mathbf{B}^*]. \tag{2.3}$$

We will work with a dimensionless form of the basic equations obtained by introducing the following dimensionless variables:

$$\mathbf{q} = \frac{\mathbf{q}^*}{q^0}, \quad p = \frac{p^*}{\rho (q^0)^2}, \quad \mathbf{B} = \frac{\mathbf{B}^*}{B^0}, \quad \mathbf{E} = \frac{\mathbf{E}^*}{q^0 B^0}, \quad \mathbf{j} = \frac{\mathbf{j}^*}{\sigma q^0 B^0}. \tag{2.4 a, b, c, d, e}$$

Here q^0 and B^0 are the free stream velocity and the constant field inside the solenoid, respectively. The coordinates are also made dimensionless with a characteristic length $\mathscr{L}$. Then (2.1), (2.2) and (2.3) become

$$(\mathbf{q} \cdot \nabla)\mathbf{q} \equiv \tfrac{1}{2} \nabla q^2 - \mathbf{q} \times \boldsymbol{\Omega} = -\nabla p + S \mathbf{j} \times \mathbf{B}, \quad \nabla \cdot q = 0, \tag{2.5 a, b}$$

$$\nabla \times \mathbf{E} = 0, \quad \nabla \cdot \mathbf{B} = 0, \quad \nabla \times \mathbf{B} = R_m \mathbf{j}, \tag{2.6 a, b, c}$$

$$\mathbf{j} = \mathbf{E} + \mathbf{q} \times \mathbf{B} - \kappa \mathbf{j} \times \mathbf{B} + \lambda (\mathbf{j} \times \mathbf{B}) \times \mathbf{B} \tag{2.7}$$

where $\boldsymbol{\Omega} \equiv \nabla \times \mathbf{q}$ and the dimensionless parameters κ and λ are defined by

$$\kappa = \kappa^* \sigma B^0, \qquad \lambda = \lambda^* \sigma (B^0)^2. \tag{2.8 a, b}$$

The two dimensionless numbers S and R_m which appear are defined by

$$S \equiv \frac{\sigma \mathscr{L} (B^0)^2}{\rho q^0}, \qquad R_m \equiv \mu \sigma q^0 \mathscr{L}. \tag{2.9 a, b}$$

R_m is the magnetic Reynolds number and S is a parameter which represents the ratio of electromagnetic body force per unit area to fluid dynamic pressure. Equation (2.6 c) shows that the magnitude of R_m determines the magnitude of the changes in the magnetic field due to the currents in the fluid.

The parameters that appear in the non-dimensional form of the equation depend, of course, on the method of non-dimensionalization. The non-dimensionalization of most of the parameters is fairly straightforward. There is, however, some freedom as far as the current is concerned. For small R_m the non-dimensional current defined by (2.4 e) will be of the order of unity. However, for large R_m the flow and magnetic field adjust themselves so that the current is much less than $\sigma q^0 B^0$. In this case the magnetic field can change by its own order of magnitude in the characteristic length. The current should, therefore, be non-dimensionalized with respect

* For a discussion of this point see, for example, Cowling (1953).

to the magnetic field gradient $B^0/\mu\mathscr{L}$. If this is done the parameters entering into the non-dimensional equations are R_m and S/R_m. It would seem, therefore, that the appropriate parameter for measuring the electromagnetic forces is S/R_m for large R_m, and S for small R_m. The parameter S/R_m is frequently found in the literature because of the preponderance of interest in the large-R_m case. In the present case of small R_m, we will use S.

Equation (2.7) can be solved for $\mathbf{j}$ by expanding the triple vector product, forming $\mathbf{j}\times\mathbf{B}$, and then substituting the resulting expression back into (2.7). This leads to

$$\mathbf{j} = \frac{(1+\lambda B^2)(\mathbf{E}+\mathbf{q}\times\mathbf{B})-\kappa(\mathbf{E}+\mathbf{q}\times\mathbf{B})\times\mathbf{B}+[\kappa^2+\lambda(1+\lambda B^2)][(\mathbf{E}+\mathbf{q}\times\mathbf{B})\,.\,\mathbf{B}]\mathbf{B}}{(1+\lambda B^2)^2+\kappa^2B^2} \tag{2.10}$$

as the generalized Ohm's law with Hall current and ion slip.

In the present two-dimensional case, where the applied magnetic field is normal to the plane of the flow we may also take the induced field to be normal, so that (2.6 b) is automatically satisfied. Then since $\mathbf{q}$ is in the plane, the last term in $\mathbf{j}$ vanishes. Furthermore, in view of (2.5 b) and (2.6 a) we may introduce a stream function and an electrostatic potential by the relations

$$\mathbf{q} \equiv \nabla\times\mathbf{k}\psi \equiv \nabla\psi\times\mathbf{k}, \qquad \mathbf{E} \equiv -\nabla\phi, \tag{2.11 a, b}$$

where $\mathbf{k}$ is the unit vector normal to the flow plane. If we also introduce B, the magnitude of the magnetic field, by

$$\mathbf{B} = \mathbf{k}B, \tag{2.12}$$

then the equation for $\mathbf{j}$ becomes

$$\mathbf{j} = -\frac{(1+\lambda B^2)(\nabla\phi+B\nabla\psi)-\kappa B(\nabla\phi+B\nabla\psi)\times\mathbf{k}}{(1+\lambda B^2)^2+\kappa^2B^2}. \tag{2.13}$$

In view of (2.12) we also find from (2.6 c) that

$$\nabla\times B\mathbf{k} = \nabla B\times\mathbf{k} = R_m\mathbf{j}, \tag{2.14}$$

and of course, in general, from (2.6 c)*

$$\nabla\,.\,\mathbf{j} = 0. \tag{2.15}$$

The nature of the body force in the present two-dimensional case is of interest. Let us break up the magnetic field into two parts. Let $\mathbf{B}_A$ be the applied field produced by applied currents, as for example the constant field inside the ellipse in the present problem. Let $\mathbf{B}_I$ be the induced field, which may be looked on as produced by the induced currents according to (2.14). The body force on the fluid involves only the induced currents, since they are the ones flowing in the gas. Therefore, the body

* This equation could, of course, also be derived directly from charge conservation. Sources and sinks for gas current could exist in the flow if electrodes were introduced. If the current in both the gas and the electrodes is considered it must be divergence free. However, the gas current itself would appear to have sources or sinks at the electrode surfaces. In this paper we will not consider electrodes, although the work here could easily be extended to cover this case.

force may be written with the help of (2.12) and (2.14) as

$$(\nabla \times \mathbf{B}_I) \times (\mathbf{B}_I + \mathbf{B}_A)/R_m = -\nabla B_I^2/2R_m - B_A \nabla B_I/R_m.$$

This shows that in the two-dimensional case the body force due to the induced field is the gradient of a scalar, and wherever the applied field is constant, the whole body force is such a gradient.

The Euler equation (2.5 a) becomes

$$(\mathbf{q} \cdot \nabla)\mathbf{q} = \tfrac{1}{2}\nabla q^2 - \mathbf{q} \times \boldsymbol{\Omega} = -\nabla(p + SB_I^2/2R_m) - SB_A \nabla B_I/R_m. \quad (2.16\,\text{a})$$

Thus, in the regions where B_A is a constant, we have the usual hydrodynamic case of body forces derivable from a potential $SB_I(B_A + \frac{1}{2}B_I)/R_m$, with a Bernoulli constant along each streamline. Further by taking the curl of (2.16 a), with due regard for the two-dimensional nature of the flow, we find that

$$(\mathbf{q} \cdot \nabla)\boldsymbol{\Omega} = 0, \qquad \text{where } B_A = \text{constant}. \quad (2.16\,\text{b})$$

Here we have recognized that $\boldsymbol{\Omega}$ has only one component and put

$$\boldsymbol{\Omega} \equiv \nabla \times \mathbf{q} \equiv \Omega \mathbf{k}, \qquad \Omega = -\nabla^2 \psi. \quad (2.17\,\text{a, b})$$

The last relation, coming from (2.11 a), is the usual one between the vorticity and stream function in plane incompressible flow. Equation (2.16 b) expresses the familiar fact that the vorticity is constant along streamlines. In the present case, it holds everywhere except at the ellipse C_e, across which B_A is discontinuous, so the last term on the right of (2.16 a) cannot be expressed as a gradient. Therefore, vorticity is generated only on C_e, where B_A jumps, and nowhere else in the flow.

To determine how much vorticity is generated on C_e, consider for the moment an applied field B_A which varies rapidly but continuously near C_e. Rewrite the last term on the right of (2.16 a) in its original form $S\mathbf{j} \times \mathbf{B}_A$; where $\mathbf{j}$ is understood to be the induced current. Then take the curl and so obtain

$$\nabla \times [(\mathbf{q} \times \boldsymbol{\Omega}) + S(\mathbf{j} \times \mathbf{B}_A)] = 0.$$

Since the tangential component of a curl-free vector must be continuous across a surface, the jump in vorticity across the surface is defined by requiring that the tangential component of

$$\mathbf{q} \times \boldsymbol{\Omega} + S(\mathbf{j} \times \mathbf{B}_A) \quad (2.18)$$

be continuous.

The other boundary conditions on C_e may be obtained by similar considerations. Since the electric field is also curl-free its tangential component must also be continuous. The induced current density in the gas does not become infinite anywhere. The induced magnetic field is therefore continuous everywhere. In other words the jump in total magnetic field at C_e is just equal to the jump in the applied field. The finite current also implies the absence of infinite forces. The velocity and pressure are, therefore, also continuous. In the absence of electrodes the gas current is everywhere divergence-free and, therefore, the normal component of current is continuous on C_e.

In summary, then, the problem of determining the hydrodynamic and electromagnetic fields consists of solving

$$\nabla \cdot \mathbf{j} = 0, \qquad \nabla B \times \mathbf{k} = R_m \mathbf{j}, \qquad (\mathbf{q} \cdot \nabla)\Omega = 0,$$

both inside and outside C_e. On C_e, where the applied field has a discontinuity, but there is no body, we require:

$$\mathbf{q},\ j_\nu,\ \partial\phi/\partial s,\ B_I \text{ are continuous on } C_e, \tag{2.19a}$$

where $\partial/\partial s$ denotes differentiation along the contour and ν the outer normal to C_e. Far from C_e, the induced fields must vanish, except possibly the velocity in the 'wake' of the contour. Let $\mathbf{l}_1$ be a unit vector in the direction of the free stream flow. Then

$$(\mathbf{q} - \mathbf{l}_1,\ \mathbf{j},\ \mathbf{E},\ B_I) \to 0 \text{ at infinity, except in the wake.} \tag{2.19b}$$

The remaining condition defines the vorticity jump on C_e by continuity of the tangential component of (2.18),

$$\Omega_o - \Omega_i = S(j_\nu/q_\nu)B_{Ai} \text{ on } C_e, \tag{2.20}$$

where the subscript i means inside C_e. To complete the formulation, one must use the relations (2.11), (2.13), and (2.17) between Ω, ψ, ϕ and $\mathbf{j}$.

The set of equations (2.14)–(2.16) are non-linear in ψ and B. In order to obtain approximate analytical solutions a perturbation technique will be used, valid for small values of the dimensionless parameters S and R_m.

The quantities of main interest are the electromagnetic force and moment on the solenoid, which are equal and opposite to those on the fluid. Let $\mathbf{F}^*$ and $\mathbf{M}^*$ be the force and moment on the solenoid, which arise solely from the body force $\mathbf{j} \times \mathbf{B}$ on the fluid. Then

$$\mathbf{F} \equiv \frac{\mathbf{F}^*}{\sigma q^0 \mathscr{L}^2 (B^0)^2} = \frac{\mathbf{F}^*}{\rho (q^0)^2 \mathscr{L} S} = -\iint (\mathbf{j} \times \mathbf{B})\, dA, \tag{2.21}$$

$$\mathbf{M} \equiv \frac{\mathbf{M}^*}{\sigma q^0 \mathscr{L}^3 (B^0)^2} = -\iint \mathbf{r} \times (\mathbf{j} \times \mathbf{B})\, dA = \iint (\mathbf{r} \cdot \mathbf{j})\, dA, \tag{2.22}$$

where the area integrals are taken over the whole plane and $\mathbf{r}$ is the dimensionless position vector of a point so that $\mathbf{M}$ is taken about the origin of coordinates. By analogy with wing-section theory, one might be interested in the drag amd lift of the solenoid, that is, the forces parallel and perpendicular to the stream direction, respectively. These may be defined as

$$D = \frac{D^*}{\sigma q^0 \mathscr{L}^2 (B^0)^2} = \mathbf{F} \cdot \mathbf{l}_1, \tag{2.23}$$

$$L = \frac{L^*}{\sigma q^0 \mathscr{L}^2 (B^0)^2} = \mathbf{F} \cdot (\mathbf{k} \times \mathbf{l}_1) = \mathbf{F} \cdot \mathbf{n}_1, \tag{2.24}$$

where $\mathbf{l}_1$ and $\mathbf{n}_1$ are unit vectors along and normal to the stream direction, as shown in figure 1.

3. Perturbation expansion

All dependent variables are expanded in a double power series in S and R_m. Zero-order terms represent the impressed fluid motion and magnetic field. In the present system of units, the zero-order velocity is a unit vector $\mathbf{l}_1$ in the direction of the free stream. The impressed field is normal to the flow plane and has magnitude unity inside the elliptical contour C_e and zero outside it. The symbol I will be used for this discontinuous quantity. Then we may write

$$\begin{aligned}
\mathbf{q} &= \mathbf{l}_1 + \mathbf{q}'S + \mathbf{q}^a R_m + \ldots, \\
\psi = \mathbf{k}\times\mathbf{q} &= \psi^0 + \psi' S + \psi^a R_m + \ldots, \\
\boldsymbol{\Omega} = \nabla\times\mathbf{q} &= \Omega' S + \Omega^a R_m + \ldots, \\
B &= I + B' S + B^a R_m + \ldots, \\
\mathbf{j} &= \mathbf{j}^0 + \mathbf{j}' S + \mathbf{j}^a R_m + \ldots, \\
\phi &= \phi^0 + \phi' S + \phi^a R_m + \ldots, \\
\mathbf{F} &= \mathbf{F}^0 + \mathbf{F}' S + \mathbf{F}^a R_m + \ldots, \\
\mathbf{M} &= \mathbf{M}^0 + \mathbf{M}' S + \mathbf{M}^a R_m + \ldots .
\end{aligned}$$

If these expansions are inserted into (2.13)–(2.16) and (2.18)–(2.22) and terms containing equal powers of S and R_m equated separately, we obtain the following results.

Zero order

$$\mathbf{j}^0 = -\frac{(1+\lambda I^2)(\nabla\phi^0 + I\nabla\psi^0) - \kappa I(\nabla\phi^0 + I\nabla\psi^0)\times\mathbf{k}}{d}, \tag{3.1 a}$$

$$\nabla\cdot\mathbf{j}^0 = -(1+\lambda I^2)(\nabla^2\phi^0 + I\nabla^2\psi^0)/d = 0. \tag{3.1 b}$$

Here d is a constant which has different values inside and outside C_e. It is defined by

$$d \equiv (1+\lambda I^2)^2 + \kappa^2 I^2. \tag{3.2}$$

$$j_v^0,\ \partial\phi^0/\partial s \text{ are continuous on } C_e, \tag{3.1 c}$$

$$\mathbf{F}^0 = -\iint (\mathbf{j}^0\times\mathbf{k}I)\, dA = \mathbf{k}\times\iint_i \mathbf{j}_i^0\, dA, \tag{3.1 d}$$

$$\mathbf{M}^0 = \iint I\mathbf{k}(\mathbf{r}\cdot\mathbf{j}^0)\, dA = \mathbf{k}\iint_i (\mathbf{r}\cdot\mathbf{j}_i^0)\, dA. \tag{3.1 e}$$

First order in S

Here we first use (2.14) to obtain

$$\nabla B'\times\mathbf{k} = 0.$$

Since B' is independent of the variable normal to the plane, this indicates that B' is at most a constant. Since B' is continuous on C_e and vanishes at infinity, it must vanish everywhere.

With $B' = 0$ we then have

$$\mathbf{j}' = -\frac{(1+\lambda I^2)(\nabla\phi' + I\nabla\psi') - \kappa I(\nabla\phi' + I\nabla\psi')\times\mathbf{k}}{d}, \tag{3.3 a}$$

$$\nabla \cdot \mathbf{j}' = -(1+\lambda I^2)(\nabla^2\phi' + I\nabla^2\psi')/d = 0, \tag{3.3 b}$$

$$(\mathbf{l}_1 \cdot \nabla)\Omega' = \nabla \times (\mathbf{j}^0 \times \mathbf{k}I) = I(\mathbf{k} \cdot \nabla)\mathbf{j}^0 - I\mathbf{k}\nabla \cdot \mathbf{j}^0 = 0. \tag{3.3 c}$$

$$q',\ j'_\nu,\ \partial\phi'/\partial s \text{ are continuous on } C_e, \tag{3.3 d}$$

and

$$\Omega'_o - \Omega'_i = j'^0/l_{1\nu}, \tag{3.3 e}$$

where the subscripts o, i denote the regions outside and inside C_e, respectively.

$$\mathbf{F}' = -\iint (\mathbf{j}' \times \mathbf{k}I)\, dA = \mathbf{k} \times \iint_i \mathbf{j}'_i\, dA, \tag{3.3 f}$$

$$\mathbf{M}' = \iint I\mathbf{k}(\mathbf{r} \cdot \mathbf{j}')\, dA = \mathbf{k} \iint_i (\mathbf{r} \cdot \mathbf{j}'_i)\, dA. \tag{3.3 g}$$

First order in R_m

Here we first consider (2.16) and (2.20) which show that

$$(\mathbf{l}_1 \cdot \nabla)\Omega^a = 0,$$

$$\Omega^a_o - \Omega^a_i = 0 \quad \text{on } C_e.$$

Thus Ω^a is constant along zero-order stream lines with no jump at C_e. Since Ω^a is zero where the streamlines originate, it is zero everywhere, so

$$\boldsymbol{\Omega}^a = \nabla \times \mathbf{q}^a = 0.$$

Since we also have $\nabla \cdot \mathbf{q}^a = 0$ from (2.5 b), and since $\mathbf{q}$ is not discontinuous, $\mathbf{q}^a$ is constant everywhere. This constant must be zero to satisfy the condition (2.19 b) at infinity. Therefore $\nabla\psi^a = 0$.

Now from (2.13) one finds $\mathbf{j}^a$:

$$\mathbf{j}^a = -\frac{(1+\lambda I^2)\nabla\phi^a - \kappa I\nabla\phi^a \times \mathbf{k} + \mathbf{V}^0 B^a}{d}. \tag{3.4 a}$$

Here $\mathbf{V}^0$ is a vector which is made up entirely of zero-order quantities, and which will be defined later. It is different inside and outside the ellipse.

$$\nabla \cdot \mathbf{j}^a = -\frac{(1+\lambda I^2)\nabla^2\phi^a + \mathbf{V}^0 \cdot \nabla B^a + B^a \nabla \cdot \mathbf{V}^0}{d} = 0, \tag{3.4 b}$$

$$\nabla B^a \times \mathbf{k} = \mathbf{j}^0. \tag{3.4 c}$$

$$j^a_\nu,\ \partial\phi^a/\partial s \text{ are continuous on } C_e. \tag{3.4 d}$$

$$\mathbf{F}^a = \mathbf{k} \times \iint_i \mathbf{j}^a_i\, dA - \iint (\mathbf{j}^0 \times \mathbf{B}^a)\, dA, \tag{3.4 e}$$

$$\mathbf{M}^a = \mathbf{k} \iint_i (\mathbf{r} \cdot \mathbf{j}^a_i)\, dA - \iint \mathbf{r} \times (\mathbf{j}^0 \times \mathbf{B}^a)\, dA. \tag{3.4 f}$$

Equations (3.1), (3.3) and (3.4) describe the present problem completely to the first order in the parameters S and R_m, and their solution will be presented in the next section. Readers who wish to do so may pass on to the sections entitled Results and Discussion.

4. Solution of the perturbation equations

The solution of the perturbation equations is fairly straightforward but the algebraic details are quite lengthy. Here we shall omit most of the

algebra. Readers who are interested in the details may refer to Kemp & Petschek (1958).

The basic equations to be solved are (3.1 b), (3.3 b) and (3.4 b) for the electrostatic potentials ϕ^0, ϕ' and ϕ''. They are actually Poisson equations because in each case the terms other than the Laplacian of the potential are known. Either they are given, as in the case of ψ^0, or they are determined from zero-order quantities; ψ' is found from $\mathbf{j}^0$ through Ω' by way of (3.3 e) and B'' from $\mathbf{j}^0$ according to (3.4 c). Once the various ϕ are found the currents can be obtained from (3.1 a), (3.3 a) and (3.4 a) and then the forces and moments from (3.1 d, e), (3.3 f, g) and (3.4 e, f).

In actual practice it turns out to be easier to proceed slightly differently. The zero order and first order in S cases satisfy identical differential equations and boundary conditions, except that ψ^0 is given while ψ' must be determined, as pointed out above, from $\mathbf{j}^0$ through Ω'. Therefore, the solution of (3.1 b) and (3.3 b) as Laplace equations in $\phi + I\psi$, can be carried out simultaneously. Then the appropriate values of ψ can be inserted to complete the solution in each case, after ψ' is found from the zero-order solution. On the other hand, to find ϕ'', equation (3.4 b) is treated as a Poisson equation with $\mathbf{V}^0$ and B'' determined from zero-order quantities.

The natural coordinate system to use is an elliptic one so we introduce elliptic coordinates ξ, η by the transformation

$$z = x + iy = re^{i\theta} = \epsilon a \cosh(\xi + i\eta) = \epsilon a \cosh \zeta. \tag{4.1}$$

Here x, y are Cartesian coordinates parallel respectively to the major axis $2a$ and the minor axis $2b$ of the ellipse C_ϵ ($\xi = c$), and ϵ is the eccentricity given by

$$\epsilon^2 = 1 - h^2, \qquad h = b/a. \tag{4.2}$$

Each value of ξ defines a member of a confocal family of ellipses with foci at $x = \pm a\epsilon$. On each ellipse η is an angle running from 0 on the positive x-axis to 2π.

Since we deal with Laplace and Poisson equations we must have available solutions of Laplace's equation in elliptic coordinates. The regions inside and outside the elliptical contour C_ϵ, denoted respectively by subscripts i and o, must be treated separately. Furthermore, since the gradients of ϕ and ψ are physical quantities, they must be finite everywhere and vanish at infinity. Suitable solutions of Laplace's equation, which can be found by separation of variable in the elliptic coordinates, are

$$f_i = \alpha_o + \sum_1^\infty \alpha_m \cosh m\xi \cos m\eta + \beta_m \sinh m\xi \sin m\eta, \tag{4.3 a}$$

$$f_o = \gamma_o + \gamma_\xi \xi + \gamma_\eta \eta + \gamma_{\xi\eta} \xi\eta + \sum_1^\infty e^{-m\xi}(\gamma_m \cos m\eta + \delta_m \sin m\eta) \tag{4.3 b}$$

where α, β, γ, δ are constants.

With these solutions available it is only a matter of algebra to find ϕ in terms of ψ for the zero order and first order in S cases, while for ϕ^a some simple particular solutions must also be constructed.

Expressions for the zero order and first order in S potentials, forces and moments

As pointed out above, the zero order and first order in S equations for ϕ are the same and may be handled together. According to (3.1 b) and (3.3 b) they both satisfy

$$\nabla^2\phi + I\nabla^2\psi = 0, \tag{4.4}$$

and the boundary conditions that, on C_e, j_v and $\partial\phi/\partial s$ are continuous. In both cases, $\mathbf{j}$ is also given by the same expression, (3.1 a) and (3.3 a).

A solution to (4.4) is obtained by using (4.3 a) for $\phi_i + \psi_i$ and (4.3 b) for ϕ_o. The constants are found from the boundary conditions, and can be written in terms of the Fourier coefficients of $\partial\psi_i/\partial\eta$ on C_e. If we write

$$(\partial\psi_i/\partial\eta)_e = A_o + \sum_1^\infty A_m \cos m\eta + C_m \sin m\eta, \tag{4.5}$$

the constants are

$$\left.\begin{aligned} \gamma_\xi = \gamma_{\xi\eta} = 0, \qquad \gamma_\eta &= A_o, \\ \alpha_m &= \{A_m\kappa - C_m[(1+\lambda)\coth mc + d_i]\}/m\Delta_m \cosh mc, \\ \beta_m &= \{A_m[(1+\lambda)\tanh mc + d_i] + C_m\kappa\}/m\Delta_m \sinh mc, \\ \gamma_m e^{-mc} &= \{A_m\kappa + C_m[1+(1+\lambda)\tanh mc]\}/m\Delta_m, \\ \delta_m e^{-mc} &= \{-A_m[1+(1+\lambda)\coth mc] + C_m\kappa\}/m\Delta_m, \end{aligned}\right\} \tag{4.6}$$

where

$$\Delta_m \equiv 1 + d_i + (1+\lambda)(\tanh mc + \coth mc), \tag{4.7 a}$$

$$d_i \equiv (1+\lambda)^2 + \kappa^2. \tag{4.7 b}$$

The constants α_o and γ_o are not significant and do not enter the equations.

The current vector, both inside and outside C_e, can be found from (3.1 a) or (3.3 a) by using (4.5) and (4.3), but is too lengthy to write here. When written in Cartesian vector components it has the form of a series, each term of which is the product of an exponential function of ξ and a trigonometric function of η.

The forces and moments are obtained from (3.1 d, e) or (3.3 f, g) and require the integration of $\mathbf{j}_i\,dA$ and $\mathbf{r}\cdot\mathbf{j}_i\,dA$ over the inside of the ellipse. Because of the form of $\mathbf{j}_i$, both these integrands also involve only terms which are the product of a function of ξ and a function of η, so the integration is very simple. All but one term in each component vanishes because of the periodicity in η, and the results are

$$\mathbf{F} = -\pi a(\mathbf{x}_1 h\delta_1 - \mathbf{y}_1\gamma_1)e^{-c}, \tag{4.8 a}$$

$$\mathbf{M} = \tfrac{1}{2}\mathbf{k}\pi a^2\epsilon^2\gamma_2 e^{-2c}. \tag{4.8 b}$$

Now, in order to express $\mathbf{F}$ and $\mathbf{M}$ in terms of given parameters, it is only necessary to determine the Fourier coefficients A_m and C_m in the expansion of $(\partial\psi/\partial\eta)_e$, as indicated in (4.5).

Zero-order current, force and moment

For zero order the stream function is, of course, given as that of a uniform stream at angle α to the major axis of the ellipse:

$$\psi^0 = y\cos\alpha - x\sin\alpha = a\epsilon(\sinh\xi\sin\eta\cos\alpha - \cosh\xi\cos\eta\sin\alpha). \tag{4.9}$$

From (4.5) we see immediately that

$$A_m^0 = C_m^0 = 0, \quad m \neq 1; \qquad A_1^0 = b\cos\alpha, \qquad C_1^0 = a\sin\alpha. \tag{4.10}$$

When these are inserted into (4.6), the potential ϕ^0 is completely determined (except for an additive constant which we shall ignore) by (4.3 a) for $\phi_i^0 + \psi_i^0$ and by (4.3 b) for ϕ_o^0.

$$\phi_i^0 = \gamma_1^0 e^{-\epsilon} x/a + \delta_1^0 e^{-\epsilon} y/b, \tag{4.11 a}$$

$$\phi_o^0 = e^{-\xi}(\gamma_1^0 \cos\eta + \delta_1^0 \sin\eta). \tag{4.11 b}$$

The current is likewise found from (3.1 a) to be

$$\mathbf{j}_i^0 = \mathbf{x}_1 \gamma_1^0 e^{-\epsilon}/b + \mathbf{y}_1 \delta_1^0 e^{-\epsilon}/a \equiv j_{ix}^0 \mathbf{x}_1 + j_{iy}^0 \mathbf{y}_1, \tag{4.12 a}$$

$$\mathbf{j}_o^0 = \frac{(\mathbf{x}_1\gamma_1^0 - \mathbf{y}_1\delta_1^0)(\cos\eta - e^{-2\xi}) + (\mathbf{x}_1\delta_1^0 + \mathbf{y}_1\gamma_1^0)\sin 2\eta}{2a\,\epsilon(\sinh^2\xi + \sin^2\eta)}. \tag{4.12 b}$$

This shows that the zero-order current inside the ellipse is a constant with Cartesian components

$$j_{ix}^0 = \gamma_1^0 e^{-\epsilon}/b = [\kappa\cos\alpha + \sin\alpha(1+\lambda+h^{-1})]/\Delta_1, \tag{4.13 a}$$

$$j_{iy}^0 = \delta_1^0 e^{-\epsilon}/a = [\kappa\sin\alpha - \cos\alpha(1+\lambda+h)]/\Delta_1, \tag{4.13 b}$$

where Δ_1 is found from (4.7).

Since $\mathbf{j}_i^0$ is a constant, the calculation of the zero-order force and moment directly from (3.1 d, e) is simple:

$$\mathbf{F}^0 = (\mathbf{k} \times \mathbf{j}_i^0)\pi ab, \qquad \mathbf{M}^0 = 0. \tag{4.14}$$

These, of course, agree with (4.8). The lift and drag, normal and parallel to the stream velocity respectively, are easily found by resolving $\mathbf{j}_i^0$ along Cartesian coordinates n and l in those directions (figure 1). If we write

$$\mathbf{j}_i^0 = \mathbf{l}_1 j_{il}^0 + \mathbf{n}_1 j_{in}^0 \tag{4.15}$$

we find from (4.13) and (4.14) that

$$L^0 = \mathbf{F}^0 \cdot \mathbf{n}_1 = \pi ab j_{il}^0 = \pi ab[\kappa + \sin\alpha\cos\alpha(h^{-1} - h)]/\Delta_1, \tag{4.16 a}$$

$$D^0 = \mathbf{F}^0 \cdot \mathbf{l}_1 = -\pi ab j_{in}^0 = \pi ab[1 + \lambda + h\cos^2\alpha + h^{-1}\sin^2\alpha]/\Delta_1. \tag{4.16 b}$$

Discussion of these results is postponed to a later section.

First order in S velocity and stream function

To find the first order in S quantities one must know the stream function ψ'. This is determined by the vorticity Ω' according to (2.17 b). The vorticity is in turn determined from zero order quantities by (3.3 c, e). These equations are

$$\nabla^2\psi' = -\Omega', \qquad (\mathbf{l}_1 \cdot \nabla)\Omega' = 0, \tag{4.17 a, b}$$

$$\Omega_o' - \Omega_i' = j_v^0/l_{1v} \text{ on } C_e. \tag{4.18}$$

Equation (4.17 b) indicates that Ω' is constant along zero-order streamlines, i.e. in the l-direction, and is thus a function of n only. Equation (4.18) specifies the jump in Ω' at the ellipse caused by the discontinuity there in the applied field. The zero-order (free stream) streamlines which do not pass through the ellipse suffer no jump in vorticity, and since they come from

a region with no vorticity, they never have any. In other words, the vorticity is confined to the inside of the ellipse and to the wake. The wake is bounded by the zero-order streamlines just tangent to the ellipse. In the (l, n) coordinate system these streamlines are defined by

$$n = \pm N, \qquad N^2 = a^2(h^2\cos^2\alpha + \sin^2\alpha). \tag{4.19}$$

From (4.17) and (4.18), using (4.12 a) for $\mathbf{j}_i^0$, we find the vorticity inside the ellipse Ω_i' and in the wake Ω_w' to be

$$\Omega_i' = W_c - W_v n/\sqrt{(N^2-n^2)}, \qquad \Omega_w' = -2W_v n/\sqrt{(N^2-n^2)}, \tag{4.20 a, b}$$

where the constants are

$$W_c \equiv -a^2(h^2 j_{ix}^0\cos\alpha + j_{iy}^0\sin\alpha)/N^2, \tag{4.20 c}$$

$$W_v \equiv a^2 h(j_{ix}^0\sin\alpha - j_{iy}^0\cos\alpha)/N^2 = -a^2 h j_{in}^0/N^2. \tag{4.20 d}$$

With the vorticity known, the stream function follows by a straightforward superposition of the stream functions of elementary vortices of strength $\Omega'\,dn\,dl$:

$$\psi' = -\frac{1}{2\pi}\iint_{i+w}\Omega'(\bar{n})\log|z-\bar{z}|\;d\bar{n}d\bar{l}. \tag{4.21}$$

Here $z = x+iy$ and $|z-\bar{z}|$ is the distance between the vortex and the field point.

One convenient way to find ψ' from this formula is to first obtain $q_n' = -(\nabla\psi')_l$. The integral for $(\nabla\psi')_l$ can be converted by integration by parts and use of the divergence theorem into an integral on C_e with $(\Omega_o^i - \Omega_i')$ in the integrand. Use of (4.20) then leads to

$$(\nabla\psi')_l = \frac{a}{2\pi}\int_0^{2\pi}(hj_{ix}^0\cos\bar{\eta} + j_{iy}^0\sin\bar{\eta})\log|z-\bar{z}_e|\;d\bar{\eta}.$$

The log term can be written in elliptical coordinates and expanded in a power series in $\exp[-(\zeta+\bar{\zeta}_e)]$ and $\exp[\pm(\zeta-\bar{\zeta}_e)]$, the plus sign being used inside the ellipse and the minus sign outside. The integration on $\bar{\eta}$ is then easily performed and the result, in the (l, n) coordinates, is

$$q_{in}' = -\frac{l[j_{il}^0 - (1-h)j_{ix}^0\cos\alpha] + n[j_{in}^0 + (1-h)j_{ix}^0\sin\alpha]}{1+h}, \tag{4.22 a}$$

$$q_{on}' = -ahe^{-\xi}[j_{il}^0\cos(\eta-\alpha) + j_{in}^0\sin(\eta-\alpha)]/\epsilon. \tag{4.22 b}$$

To find ψ' we can now integrate the relation $q_n' = -\partial\psi'/\partial l$. First we work outside the ellipse. q_{on}' can be integrated with respect to l if we notice from (4.1) that

$$\frac{de^{-\zeta}}{dz} = \tfrac{1}{4}a\epsilon(2\zeta + e^{-2\zeta}), \qquad l+in = ze^{-i\alpha}. \tag{4.23}$$

This integration determines ψ_o' except for an undetermined function of n, which must be found from the vorticity relation (4.17 a), and from the boundary conditions on $q_{lo}' = \partial\psi_o'/\partial n$. This function turns out to be zero

outside the wake, but not inside it. The results for q'_o and ψ'_o are

$$q'_{ol} = ahe^{-\xi}[j^0_{il}\sin(\eta-\alpha) - j^0_{in}\cos(\eta-\alpha)]/\epsilon + \\ + \begin{cases} 0 & \text{outside the wake,} \\ -2W_v\sqrt{(N^2-n^2)} & \text{inside the wake,} \end{cases} \tag{4.24}$$

$$\psi'_o = \tfrac{1}{4}ha^2[j^0_{il}(e^{-2\xi}\cos 2\eta + 2\xi) + j^0_{in}(e^{-2\xi}\sin 2\eta - 2\eta)] + \\ + \begin{cases} 0 & \text{outside the wake.} \\ -W_v N^2\left[\sin t\cos t + t - \begin{pmatrix} \frac{1}{2}\pi \text{ for } n>0 \\ \frac{3}{2}\pi \text{ for } n<0 \end{pmatrix}\right] & \text{inside the wake.} \end{cases} \tag{4.25}$$

Here t is an angle defined by

$$n/N \equiv \sin t, \qquad 0 \leqslant t \leqslant \tfrac{1}{2}\pi \text{ for } n>0, \qquad \tfrac{3}{2}\pi \leqslant t \leqslant 2\pi \text{ for } n<0. \tag{4.26}$$

An entirely similar procedure, beginning with q'_{in}, and keeping in mind the continuity of $\mathbf{q}'$ on C_e, leads to the velocity and stream function inside the ellipse:

$$q'_{il} = l\frac{[j^0_{in} + (1-h)j^0_{ix}\sin\alpha]}{1+h} - n\frac{[W_v + j^0_{il} - (1-h)j^0_{ix}\cos\alpha]}{1+h} - W_v\sqrt{(N^2-n^2)}, \tag{4.27}$$

$$\psi'_i = \tfrac{1}{2}(nq'_{il} - lq'_{in}) - \tfrac{1}{2}W_v N^2 t + K_i \tag{4.28}$$

where K_i is a constant chosen so that $\psi'_o = \psi'_i$ on C_e. It differs for $n \lessgtr 0$.

As a check on the first order in S flow field, the velocities far from the ellipse can be found. Because Bernoulli's equation holds everywhere but in the wake the pressure can also be found far from the ellipse except in the wake. An application of the integral momentum theorem to a large circle then yields the force and moment on the fluid due to the first order in S flow field. It is found that this calculation exactly checks the zero-order force and moment. This shows the advantage of obtaining forces and moments from the body force, since to obtain them from the flow field requires a higher order calculation.

First order in S force and moment

Knowing ψ', the force and moment are found by returning to (4.8), where they are expressed in terms of γ_1, δ_1 and γ_2. To determine these constants according to (4.6), the coefficients A_m, C_m in the Fourier expansion of $\partial\psi'/\partial\eta$ on C_e must be found for $m = 1, 2$.

Since ψ' is continuous on C_e, either ψ'_o or ψ'_i may be used. When the expansion is written in the form of (4.5) we find that

$$A'_1 = -\frac{8}{3\pi}W_v Nha\cos\alpha = \left(-\frac{8}{3\pi}W_v N\right)A^0_1,$$

$$C'_1 = -\frac{8}{3\pi}W_v Na\sin\alpha = \left(-\frac{8}{3\pi}W_v N\right)C^0_1,$$

where (4.10) for the zero-order coefficients have been recalled. This

result shows that $\mathbf{F}'$ is parallel to $\mathbf{F}^0$, and proportional to it:

$$\mathbf{F}' = \left(-\frac{8}{3\pi} W_v N\right) \mathbf{F}^0 = \frac{8}{3\pi} \frac{ahj_{in}^0 \mathbf{F}^0}{\sqrt{(h^2\cos^2\alpha + \sin^2\alpha)}}. \tag{4.29}$$

The second-order coefficients, which determine the moment, are

$$A_2' = -\frac{ha^2 W_v}{1+h}(h\cos^2\alpha - \sin^2\alpha),\ C_2' = \frac{a^2}{2}\left[\frac{1+h^2}{2} W_v \sin 2\alpha - \frac{h(1-h)}{1+h} W_c\right].$$

When these are inserted into (4.6) for $\gamma_2 e^{-2\epsilon}$, and that into (4.8 b), we find that

$$\mathbf{M}' = -\mathbf{k}\frac{a^4\pi(1-h^2)}{8\Delta_2}\left\{\frac{2\kappa h}{1+h} W_v(h\cos^2\alpha - \sin^2\alpha) + \right.$$
$$\left. + [1+(1+\lambda)\tanh 2c]\left[\frac{1+h^2}{2} W_v \sin 2\alpha - \frac{h(1-h)}{1+h} W_c\right]\right\}. \tag{4.30}$$

The quantities W_v and W_c are defined in (4.20 c, d) and Δ_2 in (4.7 a). For a circle $h = 1$, and we see that $\mathbf{M}' = 0$, as required by symmetry.

First order in R_m field and potential

As has been pointed out before, to the first order in R_m there is a perturbed magnetic field, rather than a perturbed flow field as found to the first order in S. This field is related to $\mathbf{j}^0$ by (3.4 c), from which, since $\mathbf{j}_i^0$ is a constant, it is easy to see that inside C_e

$$B_i'' = -j_{iy}^0 x + j_{ix}^0 y. \tag{4.31 a}$$

Outside C_e, $\mathbf{j}_o^0 = -\nabla\phi_o^0$ according to (3.1 a) and (3.2). Using (4.11 b) for ϕ_o^0 and (4.13) for γ_1^0 and δ_1^0, we find that

$$B_o'' = e^{-\xi}(\gamma_1^0 \sin\eta - \delta_1^0 \cos\eta) = ae^{c-\xi}(hj_{ix}^0 \sin\eta - j_{iy}^0 \cos\eta). \tag{4.31 b}$$

To find the potential ϕ'' we use (3.4 b). The vector $\mathbf{V}^0$, which is obtained from the expansion of (2.13), is given by

$$\mathbf{V}^0 d \equiv (1+3\lambda I)\nabla\psi^0 + 2\lambda I\nabla\phi^0 - 2\kappa I\nabla\psi^0 \times \mathbf{k} - \kappa\nabla\phi^0 \times \mathbf{k} + 2\mathbf{j}^0 I[2\lambda(1+\lambda I^2) + \kappa^2]. \tag{4.32}$$

This is constant inside C_e since all zero-order terms have been found to be constant there. Outside C_e it is variable, but $\nabla \cdot \mathbf{V}^0 = 0$, as can be seen from the definition (4.32). Therefore, ϕ'' satisfies the Poisson equation

$$\nabla^2\phi'' = -\mathbf{V}^0 \cdot \nabla B''/(1+\lambda I^2). \tag{4.33}$$

This equation is solved both inside and outside, using (4.3) as the complementary solutions. The particular solutions are simple exponentials of 2ξ and trigonometric functions of 2η, obtained using (4.31) and (4.32) and the zero-order quantities already found. The constants in the complementary solution are determined as before by matching j_v^a and $\partial\phi''/\partial\eta$ on C_e. This results in a set of simultaneous equations whose inhomogeneous parts (which come from the right side of (4.33)), have only constant terms, and terms second harmonic in η. The determinant of the coefficients is $d_i\Delta_m$, which does not in general vanish and we conclude that only α_o^a, γ_o^a, γ_η^a and the coefficients of the second harmonic terms are non-vanishing.

The resulting expressions for ϕ^a are

$$\phi_i^a = Ka^2\epsilon^2(\cosh 2\xi + \cos 2\eta) + \alpha_2^a \cosh 2\xi \cos 2\eta + \beta_2^a \sinh 2\xi \sin 2\eta, \qquad (4.34\,a)$$

$$\phi_o^a = \tfrac{1}{8}a^2\epsilon^2(K_\xi e^{-2\xi} - K_c \cos 2\eta + K_s \sin 2\eta) + e^{-2\xi}(\gamma_2^a \cos 2\eta + \delta_2^a \sin 2\eta) + \gamma_1^a. \qquad (4.34\,b)$$

The constants K, K_c and K_s come from the right-hand side of (4.33) and are defined below (5.9). The constant K_ξ, arising from the same source, is

$$K_\xi \equiv 2(a\epsilon)^{-2}(\gamma_1^{(2)} + \delta_1^{(2)})\kappa + (a\epsilon)^{-1}(\gamma_1^{(1)} \cos\alpha - \delta_1^{(1)} \sin\alpha).$$

γ_2^a, α_2^a and β_2^a are related to A_o^a, A_2^a and C_2^a by (4.6); the latter two constants are defined below (5.9), and

$$A_o^a = \frac{(1+\lambda)ab K_c - ab(j_{ix}^0 U_y - j_{iy}^0 U_x)}{2d_i} + \frac{a^2\epsilon^2(1-h)K_\xi}{2(1+h)},$$

with U also defined below (5.9). γ_2^a and δ_2^a are given by

$$\gamma_2^a e^{-2c} = \alpha_2^a \cosh 2c + \tfrac{1}{8}a^2\epsilon^2(K + K_c),$$
$$\delta_2^a e^{-2c} = \beta_2^a \sinh 2c - \tfrac{1}{8}a^2\epsilon^2 K_s.$$

First order in R_m current, force and moment

The current is found by inserting (4.34) into (3.4a) and using (4.31) for B^a. Inside C_c the result is

$$-\mathbf{j}_i^a = K[(1+\lambda)(\mathbf{x}_1 x + \mathbf{y}_1 y) + \kappa(-\mathbf{x}_1 y + \mathbf{y}_1 x)]/2d_i + \overline{\mathbf{V}}_i^0(-j_{iy}^0 x + j_{ix}^0 y)/d_i +$$
$$+ (4/a^2\epsilon^2 d_i)\{[(1+\lambda)\alpha_2^a - \kappa\beta_2^a](\mathbf{x}_1 x - \mathbf{y}_1 y) +$$
$$+ [(1+\lambda)\beta_2^a + \kappa\alpha_2^a](\mathbf{x}_1 y + \mathbf{y}_1 x)\}. \qquad (4.35)$$

The current outside could be found also, but we will now show that the force and moment do not depend on it.

The force and moment are given by (3.4e, f). The second integral in each formula can be simplified by using the relation $\mathbf{j}^0 = \nabla \times \mathbf{B}^a$. The integrands become

$$\mathbf{j}^0 \times \mathbf{B}^a = -\tfrac{1}{2}\nabla(B^a)^2, \qquad \mathbf{r} \times (\mathbf{j}^0 \times \mathbf{B}^a) = \tfrac{1}{2}\nabla \times \mathbf{r}(B^a)^2.$$

Use of vector integral theorems for the divergence and curl then reduce the area integrals to line integrals which can easily be shown to vanish because B^a is continuous across C_c and vanishes as $\xi \to \infty$ (see (4.31b)). The formulae for force and moment therefore reduce to

$$\mathbf{F}^a = \mathbf{k} \times \iint_i \mathbf{j}_i^a \, dA, \qquad \mathbf{M}^a = \mathbf{k} \times \iint_i (\mathbf{r} \cdot \mathbf{j}_i^a) \, dA.$$

They depend only on $\mathbf{j}_i^a$, not on the outside current $\mathbf{j}_o^a$.

The integrations are very simple. Since $\mathbf{j}_i^a$ is linear in x and y, the symmetry of the ellipse indicates that

$$\mathbf{F}^a = 0. \qquad (4.36)$$

The only contributions to the moment come from x^2 and y^2 terms which

arise when $\mathbf{r}.\mathbf{j}_i^a$ is formed from (4.33). After some reduction, the result is

$$\mathbf{M}^a = \mathbf{k}\frac{a^4\pi(1-h^2)}{4}\left\{\frac{h}{2}\frac{(\bar{V}_{ix}^0 j_{iy}^0 + \bar{V}_{iy}^0 j_{ix}^0)}{d_i} + \frac{A_2^a\kappa + C_2^a[1+(1+\lambda)2h/(1+h^2)]}{\Delta_2}\right\}. \tag{4.37}$$

$\bar{\mathbf{V}}^0$, which is closely related to $\mathbf{V}^0$, is defined below (5.9). Again the moment vanishes for a circle ($h = 1$), which is required by symmetry.

5. Results

The results for force and moment to the zeroth and first order in both S and R_m are collected here for convenience of reference and discussion.

Zero order

$$F^0 = \mathbf{l}_1 D^0 + \mathbf{n}_1 L^0. \tag{5.1}$$

From (4.2), (4.7) and (4.16) the lift and drag are

$$L^0 = \pi a b j_{il}^0 = \pi a^2 h[\kappa + \tfrac{1}{2}\sin 2\alpha(h^{-1} - h)]/\Delta_1, \tag{5.2a}$$

$$D^0 = -\pi a b j_{in}^0 = \pi a^2 h[1 + \lambda + h\cos^2\alpha + h^{-1}\sin^2\alpha]/\Delta_1, \tag{5.2b}$$

where

$$\Delta_1 \equiv (1+\lambda)\frac{(1+h)^2}{h} + \lambda^2 + \kappa^2. \tag{5.3}$$

Also from (4.14) we recall that

$$\mathbf{M}^0 = 0. \tag{5.4}$$

First order in S

From (4.29) and (5.2b) the force is related to $\mathbf{F}^0$ by

$$\mathbf{F}' = \frac{8}{3\pi}\frac{ah\mathbf{F}^0 j_{in}^0}{\sqrt{(h^2\cos^2\alpha + \sin^2\alpha)}} = -\frac{8}{3\pi}\frac{ah[1+\lambda+h\cos^2\alpha+h^{-1}\sin^2\alpha]}{\sqrt{(h^2\cos^2\alpha+\sin^2\alpha)}}\mathbf{F}_0$$

$$= -\frac{8}{3\pi^2 a}\frac{\mathbf{F}^0 D^0}{\sqrt{(h^2\cos^2\alpha+\sin^2\alpha)}}. \tag{5.5}$$

From (4.30), (4.20c, d) and (4.13) the moment can be put in the form

$$\frac{\mathbf{M}'}{\mathbf{k}} = -\frac{a^4\pi(1-h)(1+h)^3}{8\Delta_1\Delta_2(1+h^2)}\left\{\frac{\sin 2\alpha}{2}\left[(1+h^2) + \frac{2h^2}{h^2\cos^2\alpha+\sin^2\alpha}\right] + \right.$$

$$+ \frac{h}{(1+h)^2}\left[(\lambda\sin 2\alpha + \kappa\cos 2\alpha)\times\right.$$

$$\left.\left.\times\left((1+h^2) + \frac{2h^2(1+\lambda)}{h^2\cos^2\alpha+\sin^2\alpha}\right) + \frac{\lambda h(1+h)^2\sin 2\alpha}{h^2\cos^2\alpha+\sin^2\alpha}\right]\right\}, \tag{5.6}$$

where

$$\Delta_2 = \frac{(1+\lambda)(1+h)^4}{2h(1+h^2)} + \lambda^2 + \kappa^2. \tag{5.7}$$

First order in R_m

From (4.36) we may recall that

$$\mathbf{F}^a = 0. \tag{5.8}$$

The moment is too lengthy to write out in one expression. From (4.37) it is

$$\frac{\mathbf{M}^a}{\mathbf{k}} = \frac{\pi a^4(1-h^2)}{4}\left\{\frac{h}{2}\frac{\bar{\Gamma}^0_{ix}j^0_{iy}+\bar{\Gamma}^0_{iy}j^0_{ix}}{(1+\lambda)^2+\kappa^2}+\frac{A^a_2\kappa+C^a_2[1+(1+\lambda)2h/(1+h^2)]}{\Delta_2}\right\}, \tag{5.9}$$

where

$$A^a_2 = \frac{a^2(h^2j^0_{ix}U_x - j^0_{iy}U_y)-\frac{1}{2}\kappa a^2\epsilon^2K}{2(1+\lambda)^2+2\kappa^2}+\frac{a^2\epsilon^2K_s}{4},$$

$$C^a_2 = \frac{a^2h(j^0_{iy}U_x+j^0_{ix}U_y)}{2(1+\lambda)^2+2\kappa^2}+\frac{a^2\epsilon^2(K+K_c)}{4},$$

$$\mathbf{U} = [(1+\lambda)^2+\kappa^2]\bar{\mathbf{V}}^0_o-\bar{\mathbf{V}}^0_i,$$

$$\bar{\mathbf{V}} = [(1+\lambda I^2)^2+\kappa^2]^{-1}\{(1+3\lambda I)\nabla\psi^0+2\lambda I\nabla\phi^0-2\kappa I\nabla\psi^0\times\mathbf{k}-$$
$$-\kappa\nabla\phi^0\times\mathbf{k}+2\mathbf{j}^0I[2\lambda(1+\lambda I^2)+\kappa^2]\},$$

$$K_c = (a\epsilon)^{-1}(\delta^0_1\sin\alpha-\gamma^0_1\cos\alpha), \qquad K_s = (a\epsilon)^{-1}(\delta^0_1\cos\alpha+\gamma^0_1\sin\alpha),$$

$$K = -\bar{\mathbf{V}}^0_i\cdot\mathbf{k}\times\mathbf{j}^0_i/(1+\lambda),$$

$$\frac{\gamma^0_1e^{-c}}{b} = \frac{\kappa\cos\alpha+\sin\alpha[1+\lambda+h^{-1}]}{\Delta_1}, \qquad \frac{\delta^0_1e^{-c}}{a} = \frac{\kappa\sin\alpha-\cos\alpha[1+\lambda+h]}{\Delta_1},$$

$$\nabla\phi^0_i = \mathbf{x}_1(\gamma^0_1e^{-c}/a)+\mathbf{y}_1(\delta^0_1e^{-c}/b), \qquad \nabla\psi^0 = -\mathbf{x}_1\sin\alpha+\mathbf{y}_1\cos\alpha,$$

$$\mathbf{j}^0_i = \mathbf{x}_1j^0_{ix}+\mathbf{y}_1j^0_{iy} = \mathbf{x}_1(\gamma^0_1e^{-c}/b)+\mathbf{y}_1(\delta^0_1e^{-c}/a).$$

For the special case of $\kappa=\lambda=0$, $\mathbf{M}^a$ reduces to the following very simple expression

$$\frac{\mathbf{M}^a}{\mathbf{k}} = \frac{\pi}{8}\frac{a^4h^2(1-h)}{1+h}\sin 2\alpha. \tag{5.10}$$

6. Discussion

The problem that has been considered basically contains six parameters; the interaction parameter S, the magnetic Reynolds number R_m, the Hall coefficient κ, the ion slip coefficient λ, the ratio of minor to major axis of the ellipse h, and the angle of attack α. Since the analysis has been carried out as a perturbation in S and R_m, the results for each order, as given in the previous section, are functions of the four parameters κ, λ, h and α. Discussion of these four-parameter functions is, necessarily, limited to consideration of certain limiting cases.

Zero order

To the zero order the gas current distribution and the resulting forces are computed from the undisturbed flow and magnetic field. Since to this order the hydrodynamic properties of the fluid do not enter, the zero-order solutions are not restricted to incompressible flows.

As may be seen from (4.12a) both the magnitude and the direction of the gas current inside the ellipse are independent of position. While this is true for all values of the parameters κ, λ, h and α, it cannot be

generalized to all closed contours, but seems to be a property peculiar to ellipses. It can easily be demonstrated, for example, that it would not hold for a rectangular cross-section.

The fact that the zero-order moment vanishes for all ellipses follows directly from the fact that the current and, therefore, the body forces on the fluid are uniform throughout the ellipse.

Let us consider first the special case of high densities where κ and λ are both zero and discuss the force on ellipses one of whose axes is parallel to the flow ($\alpha = 0$ or $\frac{1}{2}\pi$). Equation (5.2a) shows that the lift is zero, and equation (5.2b) may be written in the dimensional form

$$D^{0*} = \sigma q^0 B^{0^2} \pi a^* b^* \left(\frac{H}{1+H}\right), \tag{6.1}$$

where H is the ratio of the lengths of the axes perpendicular and parallel to the stream; i.e.,

$$H = h \text{ for } \alpha = 0, \qquad H = h^{-1} \text{ for } \alpha = \tfrac{1}{2}\pi.$$

The factor preceding the bracket is the drag the ellipse would have if there were no electric field to impede the current flow, i.e. if the current in the ellipse were $\sigma q^0 B^0$. The factor in brackets is then the reduction in drag due to the fact that an electric field is required to close the current loops outside the ellipse. In other words, it is a measure of the electrical impedance seen by the e.m.f. which is generated inside the ellipse as a result of the motion of the gas through the magnetic field. For ellipses of fixed area the drag increases monotonically as the length of the axis perpendicular to the stream increases.

The case of general angle of attack for $\kappa = \lambda = 0$ may be considered as the superposition of flows parallel and perpendicular to the major axis. Since the problem has been linearized, the total force is the vector sum of the forces resulting from the component flows. Because the drag per unit velocity is larger for the flow perpendicular to the major axis than it is for the flow parallel to it, the total force will not be a pure drag force but will also have a lift component.

In figures 2 and 3 the drag and lift for ellipses of different fineness ratios h have been plotted as a function of angle of attack from (5.2). The perimeter P has been used as the representative length $\mathscr{L}$ in this plot, so that the forces are compared for ellipses of the same perimeter. This choice was motivated by the fact that for a given magnetic field and a given mass of copper in the solenoid the joule dissipation required in the copper is a function only of the perimeter. On this basis, in addition to the factor due to the change in impedance with shape discussed above, the drag decreases as the ellipse becomes thinner because the area decreases.

The lift is zero for a circle because of symmetry, as mentioned above, and also zero for a very fine ellipse because the area goes to zero. It has a maximum for a fineness ratio of about 0·3. The ratio of lift to drag becomes infinite for infinitely thin ellipses at small angles of attack. At this point,

of course, both the lift and the drag themselves approach zero. For a reasonable fineness ratio the lift-drag ratio is not large. For example, for a fineness ratio greater than 0·2 the lift is less than the drag at all angles of attack.

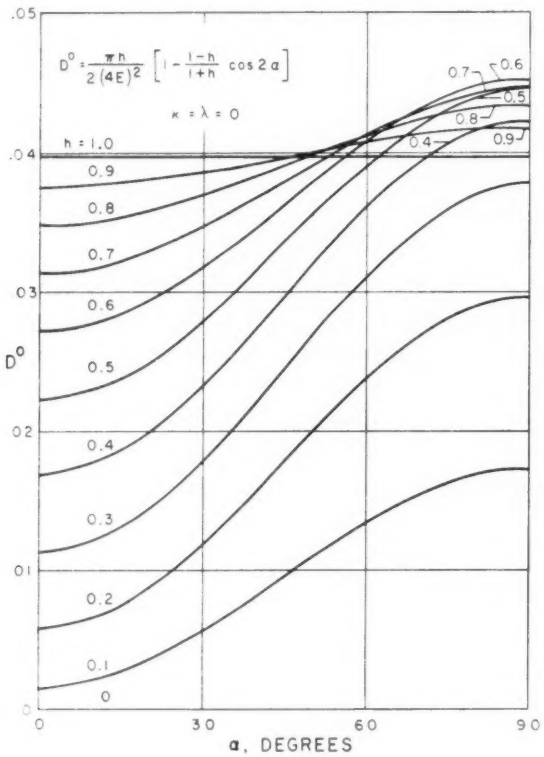

Figure 2. Non-dimensional zero-order drag $D^0 = D^{0*}/\sigma q^0 P^2 (B^0)^2$ (based on perimeter, $\mathscr{P} = P$) *vs* angle of attack α for varying fineness ratio h; plotted from equation (5.2 b) with Hall and ion slip coefficients κ and λ equal to zero. E is the complete elliptic integral of the second kind.

In order to describe the effect of the Hall and ion slip coefficients κ and λ let us consider first a circular solenoid, $h = 1$. The Hall coefficient tends to produce a current in the stream direction. The cross product of this current with the magnetic field produces a lift even for a circle. Since the sign of the Hall current is independent of the sign of the magnetic field, the sign of the lift will depend on the sign of the magnetic field. Lift and drag have been plotted as a function of κ in figure 4 from (5.2). In drawing

this graph we have assumed that

$$\lambda = \kappa^2/500, \tag{6.2}$$

which is a limiting case of (A 5).

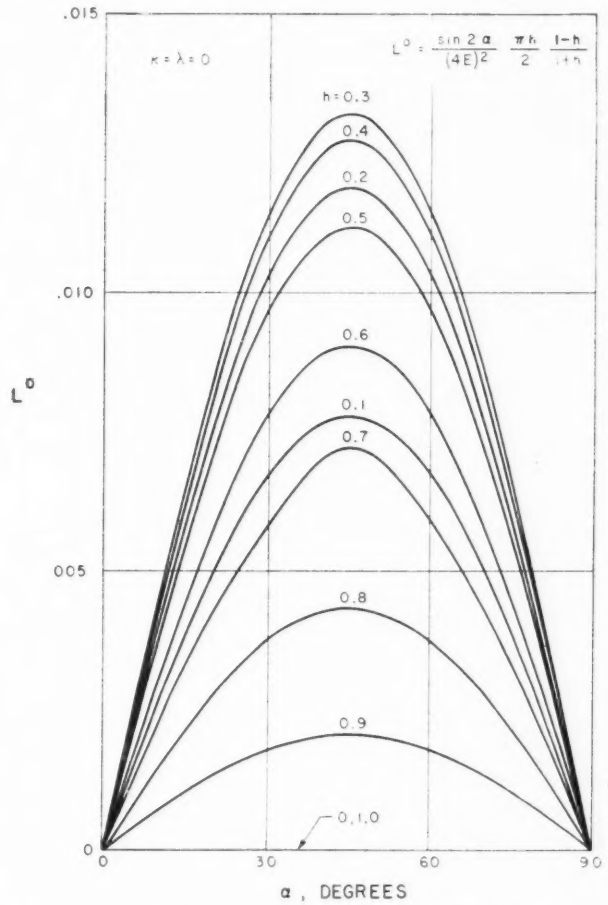

Figure 3. Non-dimensional zero-order lift $L^0 = L^{0*}/\sigma q^0 P^2 B^{0^2}$ (based on perimeter, $\mathscr{L} = P$) *vs* angle of attack α for varying fineness ratio h; plotted from equation (5.2 a) with Hall and ion slip coefficients κ and λ equal to zero. E is the complete elliptic integral of the second kind.

As κ increases from zero the lift initially increases and then decreases. However, both the drag and the total force decrease monotonically. Lift-drag ratios up to 7·9 can be obtained, but these large ratios occur when the total force has been reduced by almost a factor of ten compared with the case $\kappa = 0$.

As can be seen by looking at the general formula for zero-order drag (5.2b) the reduction in drag associated with κ depends on the geometry. It becomes less significant for flat ellipses. This reduction can probably also be made less significant by the use of electrodes whose potentials are adjusted to inhibit the flow of the Hall current. Non-uniform conductivity in the flow field, which would be encountered in an actual flight case, might also tend to produce a similar effect.

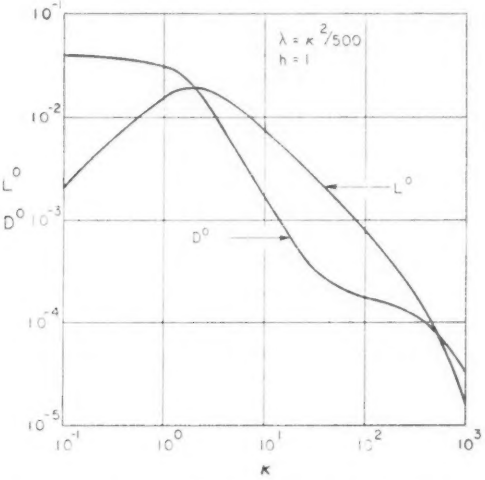

Figure 4. Non-dimensional zero-order lift L^0 and D^0 *vs* Hall coefficient κ for a circle, $h = 1$; plotted from (5.2a, b) with ion slip coefficient $\lambda = \kappa^2/500$.

It is instructive to examine two limiting values of κ and λ for general ellipses. Equation (6.2) shows that κ can be large compared with unity while λ is still small. This case will be approximated by $\kappa \to \infty$, $\lambda = 0$. In the second case examined, both $\kappa \to \infty$, $\lambda \to \infty$.

In the first case, the lift is much larger than the drag. The dimensional form of the lift may be obtained from (5.2a) as

$$L^{0*} = \frac{\sigma q^0 B^{0^2} \pi a^* b^*}{\kappa} = (N_I e q^0) B^0 \pi a^* b^*. \tag{6.3}$$

In order to obtain (6.3), equations (A2b) and (2.8a) have been used to define κ. Since the current inside the ellipse was shown to be constant, the force is the product of this current, the (constant) magnetic field, and the area. Thus, the term in parentheses in (6.3) must be the current. In order to produce this current the difference between the ion and electron velocities must be q^0. For $\lambda = 0$, (A1b) shows that the ion velocity is equal to the gas velocity q^0. The mean electron velocity must therefore be zero inside the ellipse. This is physically reasonable since, for κ large, the electrons make tight spirals around the magnetic field lines. When the

electron suffers a collision the centre of the spiral is moved by something less than the radius of the spiral. Since in this region the radius of the spiral is small and collisions are relatively infrequent, the electrons are practically stationary in the magnetic field. We may conclude that in the limit of κ large but λ still small the current may be approximated by assuming that in the magnetic field the electrons are stationary and the ions move with the gas velocity.

In the limit of both κ and λ large the drag becomes the dominant force. Using equations (A 2c) and (2.8b), we find that the expression for zero-order drag becomes

$$D^{0*} = \frac{\sigma q^0 B^{0^2} \pi a^* b^*}{\lambda} = (N_I N_N \epsilon_{IN} q^0) \pi a^* b^*. \tag{6.4}$$

From the definition of ϵ_{IN}, the term in parentheses is the frictional force due to collisions between ions and neutrals when their relative velocity is q^0. In this case, then, the ions are held almost stationary in the magnetic field. It should be noted that in this limit the drag becomes independent of the magnetic field strength.

When the ion slip term is significant, the ion velocity is appreciably less inside than outside the ellipse. The assumption of uniform conductivity, which we have used throughout, implies that the ion concentration is uniform in space. In order to satisfy the continuity equation for the ions under these two conditions, a large portion of the ions entering the ellipse must recombine with electrons near the boundary. Also, where the streamlines leave the ellipse a corresponding number of ions must be produced. If the rates of ionization and recombination are sufficiently rapid, this requirement can be satisfied. The rapid rate of ionization would maintain thermal equilibrium everywhere. The uniform temperature which is implied by the assumption of incompressible flow then assures uniform degree of ionization. However, since ion slip occurs at low densities, the rate of recombination may not be sufficiently rapid to give thermal equilibrium everywhere. In this case the degree of ionization inside the ellipse would be greater than outside. Equation (6.4) would then suggest that the drag would be higher than one might expect assuming a uniform degree of ionization. The reduction in drag due to ion slip may, therefore, not be as large as the present calculations indicate, if the rates of ion recombination are not fast enough.

First order in S

To the first order in S we have calculated first the modified flow field and then the resulting forces and moments. The perturbation velocity perpendicular to the free stream velocity is given in (4.22a). The parallel component inside and outside the ellipse is given in (4.27) and (4.24). As was mentioned previously, for a circle the external flow outside the wake may be represented by a point source and vortex at the origin.

The gas pressure may be computed by substituting the first-order velocity and zero-order current and magnetic field into the momentum

equation (2.5 a). It is interesting to note that in general the pressure gradient inside the ellipse is a constant, and its component in the free stream direction is negative. For a circle this pressure gradient is equal to one-half the zero-order magnetic force. For an ellipse, it is more complicated and is not in general parallel to the magnetic force.

The first-order forces (5.5) are of opposite sign to the zero-order forces. The fact that the forces must be reduced by the first-order terms is obvious since the flow velocity in the ellipse is reduced by the magnetic field. It is interesting to note, however, that the calculation shows that the first-order force is exactly anti-parallel to the zero-order force.

The magnitude of the first-order force may be used as a crude indication of the range of validity of the perturbation procedure. The ratio of first to zero-order forces is, from (5.5),

$$\frac{\mathbf{F}'S}{\mathbf{F}^0} = -\frac{8}{3\pi^2}\left(h^2\cos^2\alpha+\sin^2\alpha\right)^{-1/2}\frac{D^0S}{a}$$

$$= -\frac{8}{3\pi^2}\left(h^2\sin^2\alpha+\cos^2\alpha\right)^{-1/2}\left(\frac{D^{0*}}{a^*\rho q^{0*}}\right). \quad (6.5)$$

The term in parentheses may be interpreted as a drag coefficient based on the major axis. If we take the square root as about unity, the first order in S produces about a 25% correction when the zero-order drag coefficient is unity. One would therefore expect that the terms which have been calculated are insufficient beyond this point. It should be remembered that when κ and λ are not zero the drag coefficient may be small for fairly large values of S. The first-order terms become comparable with the zero-order terms only when the drag coefficient becomes comparable with unity, not when S becomes comparable with unity.

The moment, which vanished to the zero order for ellipses, appears in the first-order approximation. In figure 5 the moment for $\kappa = \lambda = 0$, has been plotted from (5.6). The moment has been plotted in terms of the non-dimensional moment arm $M'^*/F^{0*}\mathscr{L}$ divided by the zero-order drag coefficient $2SD^0$. The plot therefore compares the moment arm for different ellipses with the same drag. It will be noted that the moment is zero at angles of attack of both 0° (major axis parallel to free stream) and 90° (minor axis parallel to free stream). At 0° the neutral point is unstable, so that the ellipse would orient itself at the other neutral point with the major axis perpendicular to the free stream. The sign of this moment may be explained crudely by noting that the flow through the downstream parts of the ellipse has already been decelerated somewhat in the magnetic field. The flow velocity is then higher in the upstream part of the ellipse and therefore the forces are larger there. A small angle between the major axis and the free stream direction therefore produces a moment which tends to increase the angle of attack.

For general κ and λ the moments become quite complex. One may to some extent regard the Hall effect as introducing another angle into the

problem, the angle between the current and the electric field in a coordinate system moving with the gas. The introduction of this angle tends to change the angle of attack for a given moment. In order to illustrate this effect the stable angle of attack for an ellipse with $h = \frac{1}{3}$ has been plotted in figure 6 as a function of κ. This was calculated numerically from (5.6), and (6.2) was used to relate κ and λ. It will be seen that for κ both very

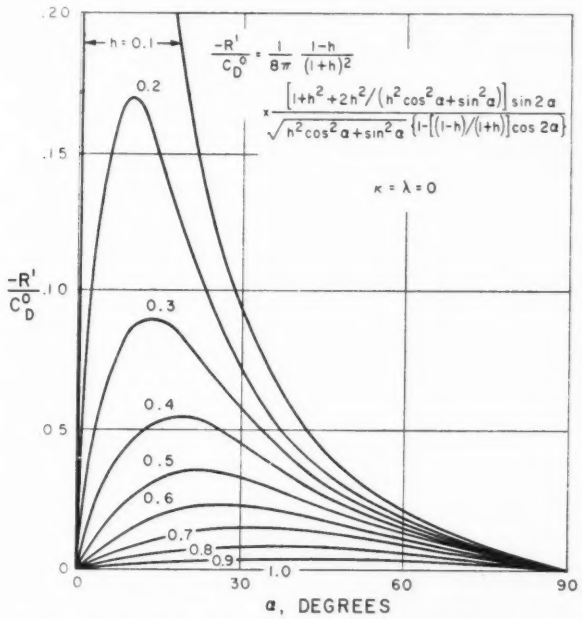

Figure 5. Non-dimensional first-order in S moment arm $R' = M'/\mathscr{L}F^0$ divided by zero-order drag coefficient $C^0 = D^0/\frac{1}{2}\rho^0 q^{0^2}\mathscr{L} = 2SD^0$ *vs* angle of attack α for varying fineness ratio h. Plotted from equations (5.6) and (5.2 b) with Hall and ion slip coefficients κ and λ equal to zero.

small and very large the stable angle is 90°. For intermediate values the stable angle is reduced to almost 45°. In the limit $\kappa \to \infty$ and $\lambda = 0$ the stable angle would be 45°. For small values of κ the stable angle depends on the ellipticity. However, for large κ the curves for different ellipses approach one another asymptotically.

First order in R_m

The first-order calculations in R_m principally determine the changes in the magnetic field caused by the flow. The change in field is given by (4.31 a) and (4.31 b). As a result of the uniform zero order current (4.12 a) inside the ellipse the field inside varies linearly with position, the field

strength increasing toward the downstream side. For κ and λ zero the magnitude of the field change across the ellipse is roughly R_m times the zero-order field. In this case the perturbed field is small compared with the applied field for R_m less than unity. For κ and λ not zero the current and therefore the field change is reduced and the ratio of perturbed to applied fields remains small to larger values of R_m.

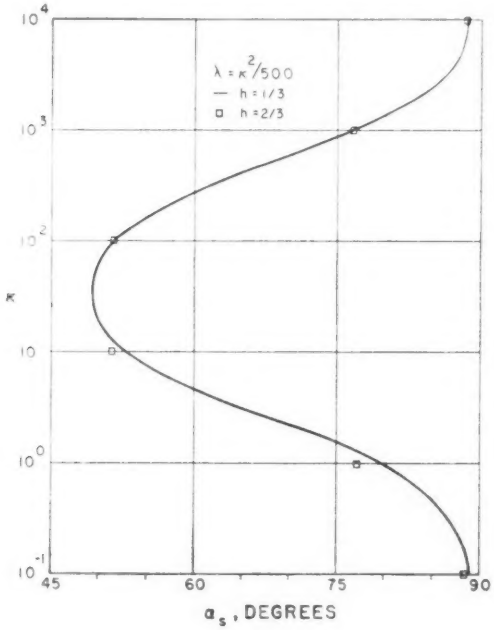

Figure 6. Angle of attack α_s at which ellipse has zero moment to the first order in S, and is stable with respect to that moment, *vs* Hall coefficient κ for two fineness ratios $h = \frac{1}{3}, \frac{2}{3}$. Plotted from equation (5.6) with ion slip coefficient $\lambda = \kappa^2/500$.

The fact that the field variation is linear immediately implies that the first-order force is zero (5.8). The increase in force on the downstream side of the ellipse due to the increased magnetic field is exactly balanced to this order by the reduced force on the upstream side.

The moments to this order for $\kappa = \lambda = 0$ have been plotted in figure 7, from (5.9). The shape and magnitude are very similar to that for the first order terms in S. The sign of this moment is, however, opposite to that of $\mathbf{M}'$. Therefore, for R_m somewhat larger than S the stable angle of attack for the ellipse is 0°. This may be seen qualitatively from the argument above that the force on the downstream end is larger than on the upstream end.

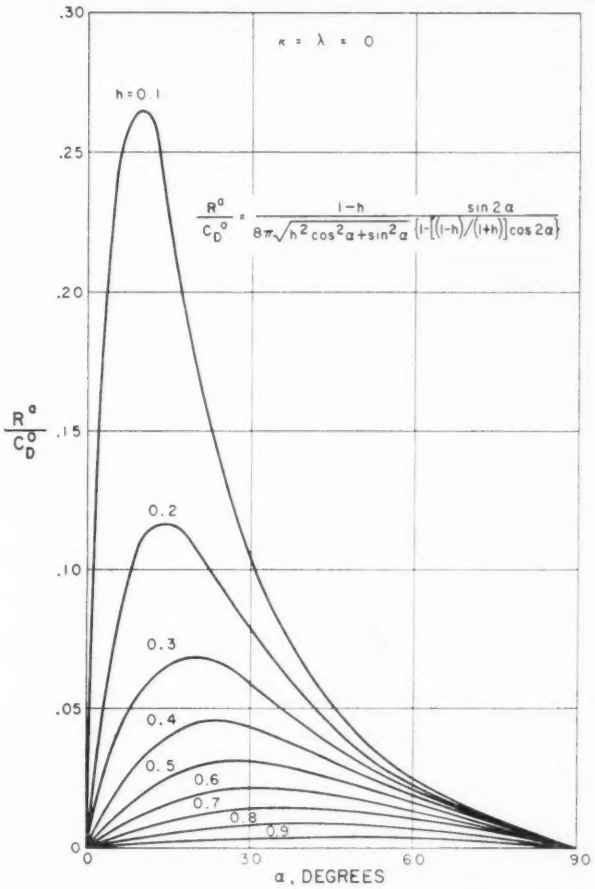

Figure 7. Non-dimensional first-order in R_m moment arm $R^a = M^{a*}/\mathscr{L}F^0$ divided by zero-order drag coefficient $C^0 = D^0/\frac{1}{2}\rho q^{0^2}\mathscr{L} = 2SD^0$ *vs* angle of attack α for varying fineness ratio h. Plotted from equations (5.10) and (5.2 b) with Hall and ion slip coefficients κ and λ equal to zero.

Concluding remarks

This analysis has been carried out as a step toward the solution of the more complicated situation which exists in hypersonic flight. Further work in this direction is presently under way at the AVCO Research Laboratory. Dr Frank Fishman is considering theoretically the corresponding perturbation problem for supersonic flow and Mr John Lothrop has begun an experimental investigation of the supersonic case utilizing a shock tube.

This work was sponsored by the U.S. Air Force, Air Research Development Command, partly under Contract AF 04(645)-18 with the Ballistic Missile Division and partly under Contract AF 49(638)-61 with the Office of Scientific Research.

Appendix A. Generalized Ohm's law

The electrical conductivity of a partially ionized gas in the presence of a magnetic field has been calculated by Schluter (1950, 1951). A review of this work with some extensions and some algebraic corrections is given by Finkelnburg & Maecker (1956). Very briefly Schluter's approach consists of considering the separate momentum equations of the component gases, i.e. neutrals, ions, and electrons. These equations include, in addition to the acceleration, pressure gradient, and electromagnetic force terms, a frictional type of force arising from collisions between different components of the gas. This frictional force is proportional to the difference in mean velocity of the components. These three momentum equations may be combined to give the overall gas momentum equation (2.1a) and in addition the mean velocities of the ions and electrons may be determined in terms of the local flow properties and their gradients. Instead of using the electron velocity explicitly it is more convenient to use the difference between electron and ion velocity, which is essentially the current.

The result (equations (51.17) and (51.18) in Finkelnburg & Maecker (1956) for the case of arbitrary degree of ionization of the gas is quite complex. However, for the special case of very small degrees of ionization where the partial pressures of the ions and electrons may be neglected the equations for current and ion velocity may be reduced to the form

$$\mathbf{j}^* = \sigma(\mathbf{E}^* + \mathbf{q}_I^* \times \mathbf{B}^* - \kappa^* \mathbf{j}^* \times \mathbf{B}^*), \tag{A 1a}$$

$$\mathbf{q}_I^* = \mathbf{q}^* + \lambda^* \mathbf{j}^* \times \mathbf{B}^*, \tag{A 1b}$$

where $\mathbf{q}_I^*$ is the mean ion velocity, and σ, κ^* and λ^* are coefficients which describe the gas conductivity. In terms of kinetic theory parameters

$$\sigma = \frac{N_I}{N_N} \frac{e^2}{\epsilon_{EN} + N_I \epsilon_{IE}/N_N}, \tag{A 2a}$$

$$\kappa^* = 1/N_I e, \tag{A 2b}$$

$$\lambda^* = 1/N_I N_N \epsilon_{IN}, \tag{A 2c}$$

where the subscripts N, I, and E refer to neutrals, ions, and electrons, respectively, N is the number density of particles, e is the absolute value of the electronic charge and ϵ_{jk} is a coefficient which describes the frictional force between species and is given by

$$\epsilon_{jk} = \frac{8}{3} \sqrt{\left(\frac{2}{\pi} kT \frac{m_j m_k}{m_j + m_k} \right)} Q_{jk} \tag{A 3}$$

where k is Boltzmann's constant, T is the temperature, m is the particle mass and Q_{jk} is the elastic collision cross-section.

The reduction of the general equations to the form given in (A 1) is not completely straightforward since it involves neglecting terms with gradients of the dynamic pressure of the ions. In the case being considered the discontinuous change in magnetic field produces a discontinuous change in ion velocity according to (A 1 b). In the immediate vicinity of this discontinuity the above equations are therefore not valid. The width of this region would, however, be of the order of one mean free path and, therefore, very small compared with the characteristic dimensions of the solenoid. Furthermore the total force due to the current resulting from the terms which have been dropped cannot be larger than the dynamic pressure of the ions. The equations (A 1) are, therefore, valid everywhere except in the immediate vicinity of the discontinuity in magnetic field and the discrepancies there do not produce significant effects on the flow field as a whole.

The generalized Ohm's law given in (2.3) may be obtained by direct substitution of (A 1 b) in (A 1 a). The physical significance of the coefficients is, however, more easily described in terms of the equations (A 1). By considering the case of zero magnetic field strength it is clear that σ is the electrical conductivity in the absence of a magnetic field. From (A 1 b) it may be seen that the coefficient, λ^*, determines the magnitude of the slip velocity of the ions relative to the neutrals. The term involving κ^* gives rise to a current which is not parallel to the electric field when observed from a coordinate system moving with the ion velocity. Using terminology carried over from solid state physics this current is usually referred to as a Hall current.

Using (A 2) and (A 3) it can easily be shown that the non-dimensional Hall coefficient κ, given by (2.8 a), is the product of the angular frequency at which the electrons spiral around the magnetic field lines and the mean free time between collisions of electrons with ions or neutrals. In other words the Hall coefficient is 2π times the average number of revolutions an electron experiences between collisions. The magnitude of the Hall coefficient depends, of course, on the physical conditions being considered. However, to obtain an estimate of the magnitude we will consider the case where the magnetic pressure $B^{0^2}/2\mu$ is equal to the gas pressure p^*. This condition is equivalent to taking both S/R_m and $p^*/\rho q^{0^2}$ of order unity. Using this condition and further assuming that the degree of ionization is so low that the second term in the denominator of equation (A 2 a) is negligible and taking $Q_{EN} = 1 \times 10^{-15}$ cm^2 one finds

$$\kappa \doteq 0{\cdot}2\sqrt{(\rho_{SL}/\rho)} \tag{A 4}$$

where ρ_{SL} is the sea-level density of air. From the above formula it is clear that the Hall currents must be considered in the density regions that are of interest for high speed flight applications of magneto-hydrodynamics.

The ion slip coefficient λ may be expressed in terms of the Hall coefficient as follows:

$$\lambda = \frac{\epsilon_{EN}}{\epsilon_{IN}}\left(1 + \frac{N_I}{N_N}\frac{\epsilon_{IE}}{\epsilon_{EN}}\right)\kappa^2 \doteq \frac{\kappa^2}{500}\left(1 + \frac{N_I}{N_N}\frac{\epsilon_{IE}}{\epsilon_{EN}}\right) \tag{A 5}$$

where the masses of the ions and neutrals are taken as the molecular weight of N_2 and it is assumed that $Q_{IN}/Q_{EN} = 3$. As pointed out by Patrick (1956), under typical flight conditions $\epsilon_{IE}/\epsilon_{EN}$ is of the order of 500. For degrees of ionization less than 2×10^{-3} the term in brackets may therefore be taken as unity.

References

Cowling, T. G. 1953 Solar Electrodynamics, article in *The Sun*, p. 533. University of Chicago Press.

Finkelnburg, W. & Maecker, H. 1956 Elektrische Bögen und Thermisches Plasma, article in *Handbuch der Physik*, Band XXII, p.325. Springer-Verlag.

Kantrowitz, A. R. 1955 A Survey of Physical Phenomena Occurring in Flight at Extreme Speeds. *Proceedings of the Conference on High Speed Aeronautics held at Polytechnic Institute of Brooklyn.*

Kemp, N. H. & Petschek, H. E. 1958 Two-dimensional incompressible flow across an elliptical solenoid, *AVCO Research Lab. Res. Rep.* no. 26.

Lamb, L. & Lin, S. C. 1957 Electrical Conductivity of Thermally Ionized Air Produced in a Shock Tube, *J. App. Phys.* **28,** 754–759.

Patrick, R. M. 1956 Magnetohydrodynamics of Compressible Fluids. Ph.D. thesis, Cornell University.

Rosa, R. 1956 Part I. Shock Wave Spectroscopy. Part II. Engineering Magnetohydrodynamics. Ph.D. thesis, Cornell University.

Schluter, A. 1950 Dynamik des Plasmas, *Z. Naturforschg.*, **5a,** 72.

Schluter, A. 1951 Dynamik des Plasmas, *Z. Naturforschg.*, **6a,** 73.

Influence of diaphragm opening time on shock-tube flows

By DONALD R. WHITE

General Electric Research Laboratory, Schenectady, New York

(*Received* 13 *May* 1958)

SUMMARY

Shock waves generated in a shock tube by use of hydrogen or helium as a driver gas and air, nitrogen, oxygen or argon as a driven gas have higher velocities than predicted by simple theory when sufficiently large diaphragm pressure ratios are used. Expected shock-tube performance curves have been constructed using the equilibrium Hugoniot for the driven gas, both for the usual model of shock tube flow, which assumes instantaneous diaphragm removal, and for a suggested model based on a finite rupture time for the diaphragm. Agreement between experiment and the latter model is in general good, and the differences are qualitatively accounted for by the pressure waves expected to result from mixing between driver and driven gases at the contact surface. These waves may be either compression or expansion waves, depending on the relative heat capacities of the two gases. The maximum shock strength observed as a shock goes down the tube was found to occur at a distance from the diaphragm which increases with the shock strength, and the strongest shocks were found to be still accelerating at the end of a 42 ft. long shock tube of $3\frac{1}{2}$ in. square cross-section. Diaphragm breaking time has been measured and found to be consistent with the observations on the shock formation distance.

1. INTRODUCTION

A number of investigators have shown that calculations of expected shock-tube performance based upon the usual ideal model of shock-tube flow (i.e. no attenuation, instantaneous diaphragm removal, and one-dimensional flow) agree satisfactorily with experiment, the observed shock being slightly weaker than predicted for the given initial conditions. Even the effect of a change in area at the diaphragm section has been shown to be amenable to a one-dimensional treatment (Alpher & White 1958). Most of the reported comparisons between expected and observed shock-tube performance, however, have concerned relatively weak shocks generated by diaphragm pressure ratios less than $z \equiv p_4/p_1 = 10^3$ (for example, Bleakney, Weimer & Fletcher 1949). With a z of the order of 10^4, shocks stronger than predicted were observed and reported without comment by Yoler (1954) and Rabinowicz (1957). One might expect that the greater

velocity, temperature and pressure ratios encountered as stronger shock waves are generated would cause greater departures from the expected performance, and that study of these departures might illuminate the nature of real shock-tube flows.

Previous investigators have demonstrated photographically (Geiger & Mautz 1949; Glass, Martin & Patterson 1953) that the process by which a diaphragm actually ruptures involves formation of a small opening near the centre, followed by the outward tearing of the material and the folding back of the leaves so formed. The effective cross-sectional area of the shock tube at the diaphragm location therefore increases gradually with time instead of attaining its maximum value instantaneously as assumed in the usual ideal analysis. The effective piston velocity pushing on the driven gas increases with the degree of opening of the diaphragm. Since each positive increment in this piston velocity sends out a compression wave, the gradual opening will generate a train of compression waves which must overtake each other to form a shock wave. Further, the high velocity jet which issues from the first hole in the diaphragm generates a high degree of turbulence as it penetrates the driven gas; and as the contact zone between the driver and driven gases moves down the tube, the initially gross mixing proceeds toward mixing on a microscopic scale. These two processes resulting from the gradual diaphragm removal, generation of a large amplitude steepening compression wave and the mixing of the driver and driven gases, will be examined more closely to determine what observable effects might be expected to result.

2. Theory

Formation of a shock from a compression wave

To estimate the result of a finite but unspecified opening time for the diaphragm, consider that an unsteady isentropic compression wave is first formed in the driven gas, and that the pressure profile of this compression wave then steepens as it progresses down the tube so that a shock wave is formed. Since the gas velocity is not the same behind a shock wave as behind a compression wave having the same pressure ratio, a third reflected wave is required to match the boundary conditions as the shock is formed. It is readily shown that this third wave must be an upstream-facing expansion wave, and that the transmitted shock wave has a lower pressure ratio than does the original compression. To determine the expected shock-tube performance as a function of the diaphragm pressure ratio, the pressure and velocity of the expanded driver gas (p_3, u_3) will be equated to the pressure and velocity behind the compression wave (p_c, u_c); and then the strength shock (p_2/p_1 or u_2/a_1) resulting from the steepening of this compression wave will be determined. This model of the shock-tube flow is displayed in the (p, x, t)-diagram of figure 1. Since further wave reflections and interactions are not taken into account, the strength computed on this basis must represent a transient condition. The shock strength

should approach that predicted from the usual model (neglecting losses) as the effects of the starting process disappear.

For simplicity in the analysis required to determine the shock formed from a given compression wave, consider that the individual elements of the compression all overtake the leading edge at the same point in the tube, resulting in a transmitted shock and a reflected expansion fan as shown in figure 1 and the insert of figure 2. Let the state of the gas in

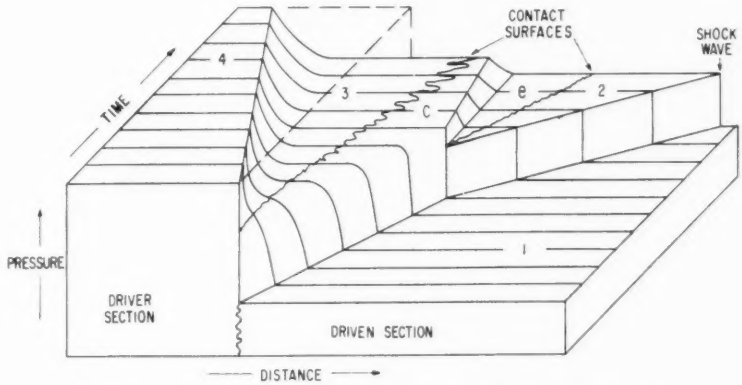

Figure 1. Suggested model of shock-tube flows as depicted by a (p, x, t)-diagram.

the various regions be indicated by the suffixes 1, 2, c, and e. In figure 2, for $\gamma_1 = 1{\cdot}4$, the curve labelled 'isentropic compression' represents the locus of states which may be reached through an isentropic unsteady compression wave from the initial state (p_1, $u_1 = 0$) assuming ideal gas properties. Similarly, the curves labelled 'shock states' represent the locus of states (p_2, u_2) which may be reached from the initial state through a shock wave, assuming ideal gas properties or equilibrium air, as indicated. From any selected state (p_c/p_1) on the compression curve, the locus of states which may be reached through a backward-facing unsteady isentropic expansion wave (again assuming ideal gas properties) may be constructed as has been done to obtain the dashed lines labelled 'expansions'. The intersection of such an expansion curve with the shock curve determines that gas state which can satisfy the boundary conditions $p_e = p_2$ and $u_e = u_2$, and hence defines the shock which will result from the steepening of the initial compression.

When the driver and driven gases have been selected, and the sound velocities a_1 and a_4 and specific heat ratios γ_1 and γ_4 are known, then from the velocity ratio u_c/a_1 behind the selected compression wave p_c/p_1, the value of u_3/a_4 is determined by the requirement that the velocities be matched across the contact surface, $u_3 = u_c$. From u_3/a_4 the expansion pressure ratio p_4/p_3 for the driver gas is found, assuming as usual that $u_4 = 0$. The

diaphragm pressure ratio is then determined from $(p_4/p_3)(p_c/p_1) = z$. The procedure for obtaining the expected shock-tube performance curve based on the ideal model with instantaneous diaphragm removal is well known.

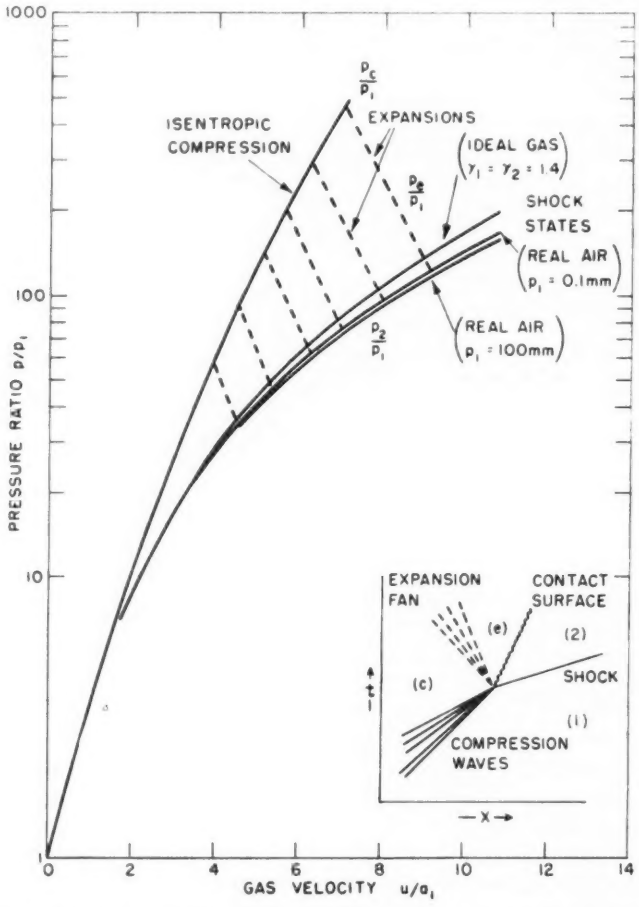

Figure 2. A graphical method for determination of the strength of the shock wave formed by steepening of an isentropic compression wave; $\gamma_1 = 1{\cdot}4$.

For the large diaphragm pressure ratios considered here, the gases cannot in general be considered ideal for either model of the shock-tube flow. Equilibrium shock Hugoniots for the shocked gases were used and were obtained from the following sources: for air, Gilmore (1955); for nitrogen and oxygen, Alpher & Greyber (1958); and for argon, Bond (1954) and unpublished calculations supplied by AVCO Research

Laboratory. In addition, hydrogen used as a driver gas expands to such low temperatures that changes in the degree of excitation of its internal degrees of freedom must be considered (Huber 1958). It may be noted that use of the equilibrium isentrope (Hilsenrath 1955) for the hydrogen expansion results in a decrease by about one Mach number in the predicted shock strengths for $z \sim 10^6$, this decrease being greater for the ideal model because of the larger expansion ratio.

Expected performance curves for the various gas combinations are given in figures 3 to 7, both for the ideal model and for the 'formation-from-compression' model for a shock tube with an area reduction of 1·51 across the diaphragm section. The method of Alpher & White (1958) is useful when equilibrium gas properties are to be incorporated.

It is characteristic of the flow processes associated with this formation-from-compression model that the initial rate of extraction of energy from the driver gas is lower than that rate obtained using the ideal model. That is, for a given diaphragm pressure ratio the driver gas expands through a smaller pressure ratio and acquires a lower velocity. Yet in some instances a stronger shock is predicted. This seeming contradiction is associated with the transient nature of the flow being analysed. We have considered in this model an isentropic compression wave whose leading edge propagates at the velocity of sound a_1 in the low pressure gas. Although energy has been extracted from the driver at a lower rate, up to the point where the shock forms this energy has gone isentropically into a quantity of gas proportional to a_1, whereas in the ideal model the energy goes anisentropically into a quantity of gas proportional to the product of the shock Mach number and a_1. When the transmitted shock forms from this compression, it is maintained both by the energy still being taken from the driver gas through the first expansion wave (state 4 to state 3) and by the additional energy extracted from the isentropically compressed driven gas through the second upstream-facing expansion wave (state c to state e). This region of driven gas which has undergone an isentropic compression acts in a sense as an energy accumulator, feeding energy back to generate transiently a shock wave stronger than can be maintained by the energy being taken from the driver gas alone.

This formation-from-compression model can be only an approximation, of course, because moderately strong shocks are found relatively near the diaphragm even when the maximum strength occurs much further down the tube. Since the entropy rise across a shock wave is proportional to the cube of the shock strength, however, this isentropic model should be a reasonable approximation even if, for example, a series of weaker shocks overtake each other to form a strong shock.

Mixing of gases in the contact region

It is clear that during every shock-tube experiment the driver and driven gases mix to some extent. While the magnitude of such mixing must be influenced by many factors, including the gases used and the shock strength,

a jagged opening projecting into the tube (the breaking diaphragm) would in particular promote mixing. While a quantitative prediction of the effect of such mixing on the shock strength cannot be made, nevertheless the direction of the effect may be determined.

In those experiments where the driver and driven gases have different heat capacities, this mixing if considered to be carried forward at constant pressure will be accompanied by a change in volume, since the gases will generally be at different temperatures. While this change in volume is taking place, there is effectively a velocity gradient across the region of mixing resulting in unequal velocities for the regions of uniform flow on either side. To indicate the direction and possible magnitude of this change in volume, consider on either side of an ideal contact surface two equal volumes $\frac{1}{2}V$ containing n_a moles of gas a at temperature T_a and n_b moles of gas b at T_b, respectively. Let $N = T_a/T_b = n_b/n_a$. The change in volume after mixing has been completed at constant pressure is obtained from

$$1 + \frac{\Delta V}{V} = \frac{1+N}{2}\left(\frac{1 + C_{p_a}/C_{p_b}}{N + C_{p_a}/C_{p_b}}\right),$$

and for $N \gg 1$, this becomes $\frac{1}{2}(1 + C_{p_a}/C_{p_b})$.

Considering only shock-tube experiments where the driver and driven gases are initially at the same temperature (not combustion driving), a region of the flow which includes the contact zone would be expected to undergo a volume increase from the mixing of a monatomic driver gas and a diatomic driven gas. Conversely, a volume decrease would be expected when the heat capacity of the driven gas is smaller than that of the driver gas. This mixing can be considered to affect the shock strength either through generation of pressure waves or through a change in the effective piston velocity. To give a numerical example, in a shock tube of constant bore, a diaphragm pressure ratio of 10^4 between helium and air would produce on an ideal basis a Mach 7 shock. The temperature of the expanded helium would be 38° K, and that of the shocked air 3140° K. This yields $N = 83$, and $\Delta V/V = 0{\cdot}194$. The limiting value for large diaphragm pressure ratios for these gases is $\Delta V/V = 0{\cdot}20$.

The effect on the shock wave cannot be determined quantitatively, since one does not know either the extent of the mixing region or the rapidity with which mixing approaches completion; and hence neither the magnitude of the compression waves nor the difference in flow velocity across the contact zone is known. It may further be pointed out that with the stronger shock waves the excitation of further internal degrees of freedom of the shocked gas results in a still greater heat capacity, and hence a greater value for the strong shock limit of $\Delta V/V$. Wray (1956) has reported observations on strong shock waves ($M_s \sim 8$) generated in fluorine by use of helium as a shock-tube driver gas. Fluorine is largely dissociated under these conditions and hence has a large heat capacity. He observed the shock velocity first to decrease with increasing distance from the diaphragm, reach a minimum, and then increase to the end of the tube.

Effect of diaphragm opening time on formation distance

The expected effect of the diaphragm opening time upon the formation distance may also be estimated by use of a simple model. Assume first that in a shock tube of constant bore the flow at any time is that predicted by use of the ideal model, i.e. with instantaneous diaphragm removal. Let the gas combination and the diaphragm pressure ratio be given, and further assume ideal-gas behaviour for both driver and driven gases. Then one determines the distance travelled by the shock wave at the time it is overtaken by a sound wave originating from the diaphragm location at some given time after the flow was initiated. This distance becomes relevant if one assumes that the maximum shock strength occurs as a result of the last compression sent out as the diaphragm is fully removed.

Proceeding downstream from the diaphragm location, the flow may be divided into three regimes, an upstream-facing, isentropic unsteady expansion wave, a region of uniform flow of expanded driver gas, and a region of uniform flow of shocked gas. The velocity of propagation of a sound wave will be the sum of the fluid velocity and the local velocity of sound. Assume for simplicity that the average velocity of propagation through the unsteady expansion wave is the mean of the velocities at the diaphragm location and at the foot of the expansion wave. All flow velocities, local sound velocities and propagation velocities may be readily calculated on this basis. A consequence of the highly idealized model utilized is that the distance travelled by the shock will be directly proportional to the time after flow initiation at which the signal is sent out. Representative results are given in table 1.

Gases	Diaphragm pressure ratio	Shock Mach number	Formation distance per 100 microseconds effective diaphragm opening time
He/N_2	2500	6	6·5 ft.
H_2/N_2	2500	8·8	8·3 ft.
H_2/N_2	334	6	3·3 ft.

Table 1. Estimation of formation distance for finite opening time of diaphragm.

It may be noted from table 1 that, for the same shock strength, the shock should form in only half the distance with a hydrogen driver as compared with a helium driver. For the same diaphragm pressure ratio, the formation distance with the hydrogen driver is only 30% greater. The use of a combustion driver would further shorten the formation distance for a given shock strength, because of the higher temperature and hence higher propagation velocity through the expanded driver gases.

3. Experiments

Apparatus and procedure

These data were obtained in the 3·25 in. square shock tube at the General Electric Research Laboratory. The driver section of this tube is of 4·5 in. inside diameter and 6·5 ft. long, and the driven section is 3·25 in. square and 42 ft. long. Most of the diaphragms used in these experiments were made of type 302 stainless steel, 0·018 in. thick, scored in the form of an X by a milling cutter with a 0·010 in. radius tip. The groove depth was generally 0·008 or 0·009 in., and the breaking pressures varied from 15 to 30 atm. The unsupported diameter was 4·5 in.

For most of these experiments the initial pressure in the driver section was between 0·040 and 10 mm of mercury, and was recorded as the average of the readings of two McLeod gauges or, for the higher pressures, a precision Bourdon gauge. A calibrated Bourdon gauge was used to read the driver gas pressure as it was slowly increased to the point of rupture of the diaphragm. From these readings the pressure ratio across the diaphragm was obtained as the independent variable.

The arrival of the shock wave at each of up to twelve stations along the tube caused a signal to be displayed on a cathode-ray oscilloscope which was tracing a raster pattern at the rate of 20 microseconds/cm. A photographic record of the trace permitted determination of the variation of shock velocity with distance from the diaphragm. The transducers employed in the tube were thin-film heat gauges, ionization gauges, or pressure gauges of our own design, depending upon the conditions of the experiment; and they were typically 32·6 in. apart.

The average shock Mach number was computed for the interval between each pair of shock detection stations, and the maximum of this set of values plotted against the diaphragm pressure ratio.

Shock tube performance curves

Experimental shock-tube performance data together with predicted curves are shown in figure 3 for helium/nitrogen and hydrogen/nitrogen, and in figure 4 for helium/argon and hydrogen/argon. The tendency for the experimental points to follow the formation-from-compression curve is clear, and in fact shocks stronger than predicted by the ideal model are noted for all gas combinations. For the case of helium/nitrogen in figure 3, as well as helium/oxygen in figure 5 and helium/air in figures 6 and 7, the shock strengths exceed even the stronger of the two predicted curves. These gas combinations are such that one would expect the contact zone mixing to enhance the shock strength. For hydrogen/argon, where the mixing would be expected to attenuate the shock, the experimental points are somewhat weaker relative to the compression-formation curve than are the hydrogen/nitrogen data. For helium/argon and hydrogen/nitrogen, mixing should have no effect to the extent that further excitation of internal degrees of freedom may be neglected.

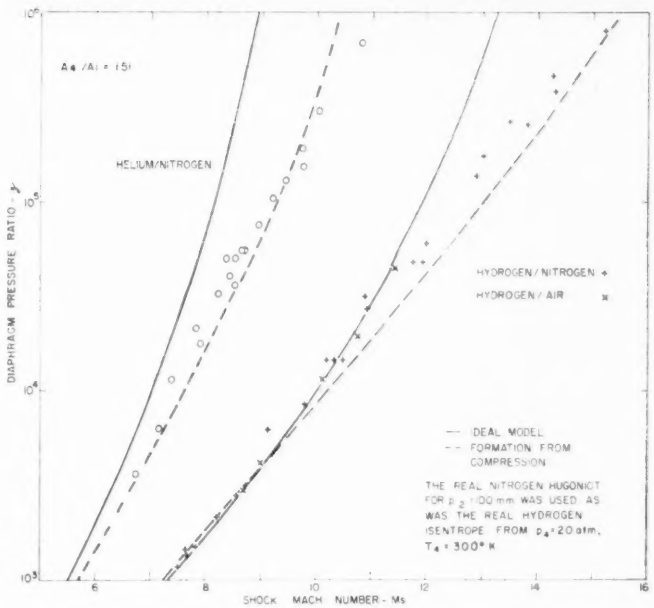
A4 /A1 = 151
HELIUM/NITROGEN
HYDROGEN/NITROGEN +
HYDROGEN/AIR ×
— IDEAL MODEL
-- FORMATION FROM COMPRESSION
THE REAL NITROGEN HUGONIOT FOR p1 = 100 mm WAS USED AS WAS THE REAL HYDROGEN ISENTROPE FROM p4 = 20 atm, T4 = 300° K
DIAPHRAGM PRESSURE RATIO - p4/p1
SHOCK MACH NUMBER - Ms

Figure 3. Observed and predicted shock-tube performance for helium/nitrogen and hydrogen/nitrogen. Experimental points indicate the maximum strength observed in an experiment. Compression waves due to contact zone mixing would enhance the shock strength for helium/nitrogen.

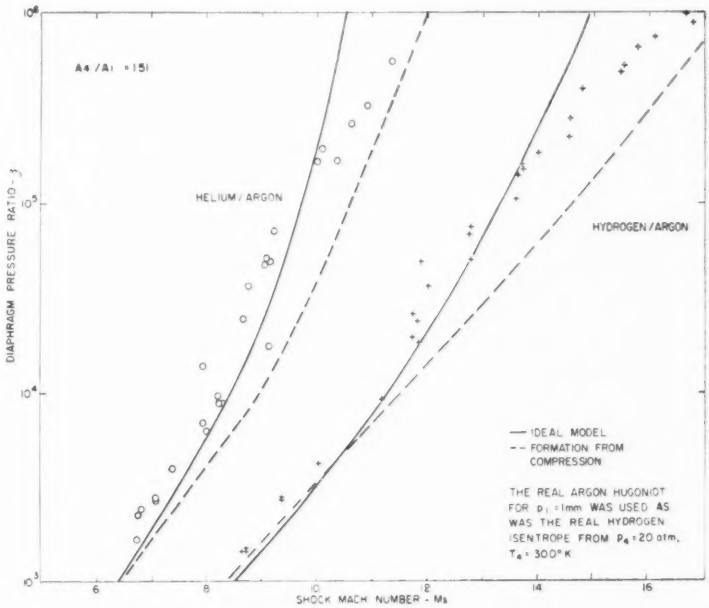
A4 /A1 = 151
HELIUM/ARGON
HYDROGEN/ARGON
— IDEAL MODEL
-- FORMATION FROM COMPRESSION
THE REAL ARGON HUGONIOT FOR p1 = 1mm WAS USED AS WAS THE REAL HYDROGEN ISENTROPE FROM p4 = 20 atm, T4 = 300° K
DIAPHRAGM PRESSURE RATIO - p4/p1
SHOCK MACH NUMBER - Ms

Figure 4. Observed and predicted shock-tube performance for helium/argon and hydrogen/argon. Expansion waves due to contact zone mixing would weaken the shock in hydrogen/argon experiments.

A set of experiments was run with helium/oxygen to determine whether significant differences could be found relative to helium/nitrogen. For the strongest shocks ($M_s \sim 10$), the dissociation of the oxygen is significant whereas it is still negligible for nitrogen; and the heat capacity, and hence the effect of mixing with the helium, would be greater for oxygen than for nitrogen. The data are given in figure 5. Comparison with the helium/nitrogen results given in figure 3 shows that the helium/oxygen shocks appear to be somewhat stronger.

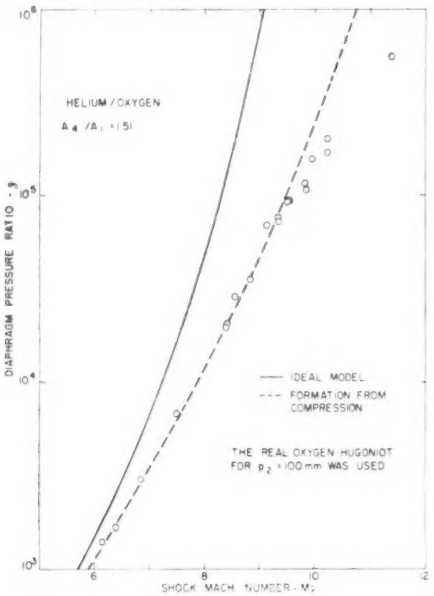

Figure 5. Observed and predicted shock-tube performance for helium/oxygen.

The data shown in figure 6 were obtained in connection with work on the effect of an area ratio across the diaphragm section (Alpher & White 1958). These experiments show that the incremental shock strength due to a change in the area ratio across the diaphragm section is adequately predicted by a theory based on the ideal model even though the actual shock strength may be appreciably greater than predicted.

Use of the equilibrium rather than the ideal-gas Hugoniot for the shocked gas results in the prediction of a weaker shock for a given diaphragm pressure ratio. Expected performance curves have been computed both on the basis of an ideal gas and of a real gas, and the comparison with experiment is shown in figure 7 for helium/air. The rather striking agreement with the real-gas compression-formation curve is probably partially fortuitous, in

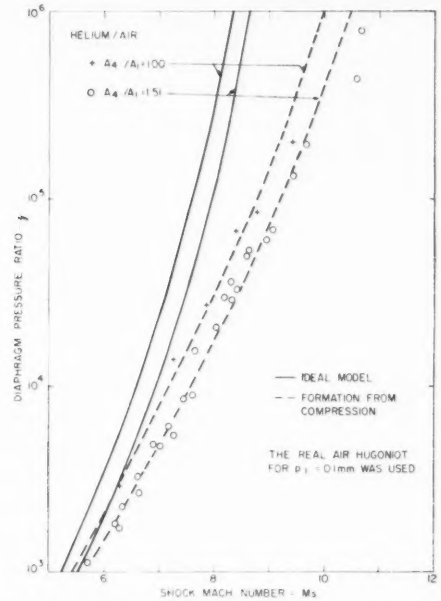
HELIUM / AIR
+ A4 /A1 =100
O A4 /A1 =151
IDEAL MODEL
FORMATION FROM COMPRESSION
THE REAL AIR HUGONIOT FOR p1 = 01mm WAS USED
DIAPHRAGM PRESSURE RATIO
SHOCK MACH NUMBER = Ms

Figure 6. The effect of an area ratio across the diaphragm section upon the maximum shock strength observed.

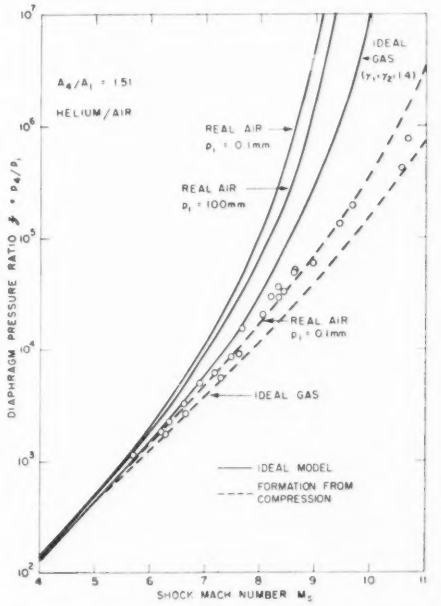

Figure 7. Comparison of experimental shock-tube performance with predicted performances based upon various assumptions.

the sense that apparently the enhancement effects of mixing approximately balanced the attenuation mechanisms which must always be present.

In each of figures 3 to 7, the shock strengths observed for the largest diaphragm pressure ratios represent a lower bound on the maximum which could have occurred in the experiments, since the shock was still accelerating at the end of the tube where the recorded strength was measured.

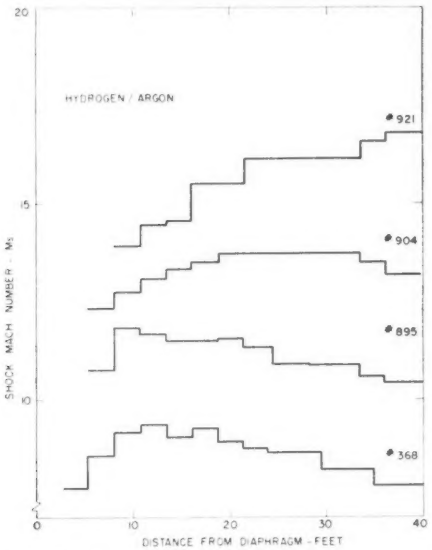

Figure 8. Typical records of shock strength at various distances from the diaphragm in the $3\frac{1}{4}$-in. square shock tube. The horizontal lines indicate the average velocity of the shock wave over the corresponding distance. For the largest diaphragm pressure ratios the shock is still accelerating at the end of the tube.

Further indication of the relative magnitudes of the mixing and formation-from-compression effects may be noted from the shock velocity records. In the hydrogen/argon experiments, for example, in addition to the losses due to the interaction between the shocked gas and the wall, the mixing at the contact surface would, for the weaker shocks, cause the shock to decelerate. The attenuating effect of mixing would decrease, however, for the stronger shocks when the hydrogen is cooled to the point that its heat capacity approaches that of a monatomic gas, and when the ionization of the argon greatly increases its heat capacity. Representative data showing the variation of shock strength with distance along the tube are given in figure 8. The horizontal lines indicate the average velocity of the shock over the corresponding distance, and do not imply that the actual shock velocity varied in a stepwise fashion. For the larger diaphragm pressure ratios, the shock wave is observed to accelerate for the full length of the tube, emphasizing the dominant role played by these non-ideal processes.

From such velocity records the distance along the tube required for realization of the maximum shock strength has been determined. This distance is plotted *vs* shock Mach number in figure 9, and *vs* diaphragm

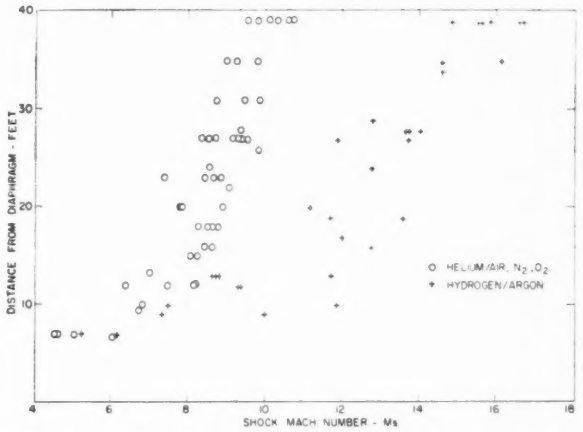

Figure 9. Shock-formation distance as a function of shock Mach number in the $3\frac{1}{4}$-in. square shock tube. Points for helium/argon and hydrogen/nitrogen generally lie between the helium/nitrogen and the hydrogen/argon values.

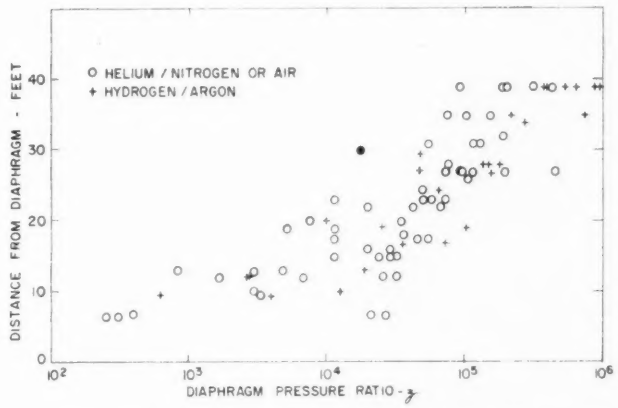

Figure 10. Shock-formation distance as a function of diaphragm pressure ratio in the $3\frac{1}{4}$-in. square shock tube, Points for helium/argon and hydrogen/nitrogen are similarly distributed. The solid point was obtained by loading each of the four leaves of the scored diaphragm with 6·2 gm of solder.

pressure ratio in figure 10. The curves probably apply only to this particular tube and to these diaphragms, and should be used only qualitatively in estimating the expected performance of other shock tubes.

Diaphragm opening time

To determine experimentally the time required for the leaves of the diaphragm to fold back to the full open position, the transmission of light through the diaphragm section was measured as a function of time. A light source was mounted near a $\frac{3}{8}$ in. window in a blind flange at the end of the driven section, 42 ft. from the diaphragm. A barium titanate pressure transducer was mounted in the driver chamber wall near the diaphragm section and responded to the metal vibration as the diaphragm first began to break under the gradually increasing pressure, producing a signal to trigger a cathode-ray oscillograph. A photomultiplier viewing the side wall of the driven chamber observed the variation with time of the intensity of the scattered light and displayed it on the oscillograph.

The diaphragms used in these experiments took about 600 microseconds to open fully. The initial rate of opening was low however, since the light intensity recorded had reached less than 10% of its final value after 200 microseconds. This slow initial rate of opening was also characteristic of both 0·010 in. and 0·035 in. thick diaphragms, which took somewhat shorter and longer times respectively to open fully.

These measurements of formation distance and diaphragm opening times are considered to be consistent with the highly simplified analysis previously described, since the many approximations involved preclude other than qualitative interpretation of the results. For example, a convergence at the diaphragm section would tend to shorten the formation distance because of the higher temperature of the expanded driver gas, and attenuating effects would do likewise by inhibiting attainment of the maximum possible shock strength.

However, one may conclude that an opening time of several hundred microseconds should result in an appreciable formation distance for the larger diaphragm pressure ratios, and that this distance should be more nearly independent of diaphragm pressure ratio than of shock Mach number as various gases are used. This is observed in figures 9 and 10.

Shock attenuation

Since these stronger-than-predicted shock waves (as in helium/nitrogen) exist only transiently, successive wave interactions may be expected to reduce the shock strength. Mixing in the contact zone may either have no effect or act to enhance or reduce the shock strength, depending upon the gases employed. Therefore, these two effects associated with the starting of the shock tube flow may both strengthen and 'attenuate' the shock at different times in the same experiment. Interpretation of attenuation data from strong-shock experiments in terms of energy loss mechanisms must be done carefully, since these other adiabatic processes may also cause the shock strength to vary with time.

4. Conclusions

The finite time required for removal of the diaphragm can result in an appreciable modification of the shock-tube flow for the case of the larger diaphragm pressure ratios. For a monatomic driver/diatomic driven gas combination, this opening time can cause generation of a shock significantly stronger than predicted by the usual model. An analysis based upon the formation first of a compression wave, then of a shock wave, agrees with experiment. The mixing of the driver and driven gas in the contact zone may also modify the shock strength, either strengthening or weakening it according to the relative heat capacities of the gases used. Observed shock deceleration may result partially from these adiabatic processes of mixing and wave interactions, as well as from attenuating effects of energy losses to the wall.

The shock-tube starting process can occupy a significant portion of the length of the tube. In these experiments, for the largest diaphragm pressure ratios ($z \sim 10^6$) the shock was still accelerating 40 ft. from the diaphragm.

The one-dimensional analysis of Alpher & White (1958) successfully predicts the shock enhancement due to area ratio at the diaphragm, even for the larger diaphragm pressure ratios where the actual shock strength may not be predicted by use of the ideal model.

In experiments employing combustion driving, approximately equivalent performance curves are computed from the ideal model, whether hydrogen or helium is employed as a diluent. The processes discussed here, however, might cause one or the other to be advantageous in a particular experiment.

This research was supported by the Ballistic Missile Division of the United States Air Force under contract AF-04-(645)-24. A preliminary account of the work was given at the annual meeting of the American Physical Society in New York, January 1957.

References

Alpher, R. A. & Greyber, H. D. 1958 *General Electric Research Lab., Schenectady, Rep.* no. 58–RL–1915.

Alpher, R. A. & White, D. R. 1958 *J. Fluid Mech.* **3,** 457.

Bleakney, W., Weimer, D. K. & Fletcher, C. H. 1949 *Rev. Sci. Inst.* **20,** 807.

Bond, J. W. 1954 *Los Alamos Scientific Lab. Rep.* no. LA–1693.

Geiger, F. W. & Mautz, C. W. 1949 *University of Michigan, Engr. Res. Inst. Rep., Proj.* M 720–4.

Gilmore, F. R. 1955 *Rand Corporation Rep.* no. RM–1543.

Glass, I. I., Martin, W. & Patterson, G. N. 1953 *Institute of Aerophysics, University of Toronto, UTIA Rep.* no. 2.

Hilsenrath, J. 1955 *Nat. Bur. Stand., Wash., Circular* no. 564.

Huber, P. W. 1958 *J. Aero. Sci.* **25,** 269.

Rabinowicz, J. 1957 *California Institute of Technology, Guggenheim Aeronautical Lab., Hypersonic Wind Tunnel Project, Mem.* no. 38.

Wray, K. L. 1956 Ph.D. Thesis, Brown University.

Yoler, Y. A. 1954 *California Institute of Technology, Guggenheim Aeronautical Lab., Hypersonic Wind Tunnel Project, Mem.* no. 18.

A modified tangent-gas approximation for two-dimensional steady flow

By G. POWER and P. SMITH
Department of Mathematics, University of Nottingham

(*Received* 30 *May* 1958)

SUMMARY

A set of two-dimensional subsonic flows past certain cylinders is obtained using hodograph methods, in which the true pressure-volume relationship is replaced by various straight-line approximations. It is found that the approximation obtained by a least-squares method possibly gives best results. Comparison is made with values obtained by using the von Kármán-Tsien approximation and also with results obtained by the variational approach of Lush & Cherry (1956).

1. INTRODUCTION

There are a number of ways available for finding the approximate steady two-dimensional flow past a fixed cylinder. One such method is the tangent-gas method proposed by Chaplygin and later extended by Tsien, which uses a tangent to the curve, pressure (p) *vs* volume (v), as a representation of the true relationship. The significance of this device is that the hodograph equations can be reduced to the Cauchy-Riemann differential equations. Demtchenko (1932) considered a tangent at the point on the curve corresponding to the stagnation conditions, and as a result his theory can only be applied, with any accuracy, to flows with speeds up to about one-half sonic speed. Tsien (1939), on von Kármán's suggestion, took the tangent at the point corresponding to conditions at infinity, assuming uniform flow there, and thus succeeded in extending the range of accuracy. These cases are only two examples of a set of flows obtainable by taking a tangent at each point of the (p, v)-curve, or, more precisely, a series of straight-line approximations to the curve within the significant limits for the particular problem.

A method is suggested for finding the particular line which possibly will yield the best results, and comparison is made with the accurate values obtained by Lush & Cherry (1956), using a variational method, for the adiabatic flow past a circular cylinder.

2. EQUATIONS OF MOTION

Assume

$$p = a - b^2 v \tag{1}$$

as the straight-line approximation to the (p, v)-curve, which for illustration may be taken to be the adiabatic relation

$$pv^{\gamma} = 1.$$

(For convenience the stagnation pressure and density are taken as unity.) Since $v = 1/\rho$ (ρ representing fluid density), Bernoulli's theorem immediately yields

$$q^2 = b^2(v^2 - 1), \tag{2}$$

where q represents fluid speed such that $v = 1$ when $q = 0$.

If ϕ represents the velocity potential and ψ the stream function, the hodograph equations are

$$\phi_q = q\frac{d}{dq}\left(\frac{1}{q\rho}\right)\psi_\theta, \qquad \phi_\theta = \left(\frac{q}{\rho}\right)\psi_q, \tag{3}$$

where θ is the angle the fluid velocity makes with a fixed direction.

Equations (3) can be reduced immediately to the Cauchy-Riemann differential equations

$$\phi_\omega = -\psi_\theta, \qquad \phi_\theta = \psi_\omega, \tag{4}$$

by using (2), and setting

$$\begin{aligned}\omega &= \int (\rho/q)\,dq \\ &= \log[Bq/\{b + (b^2+q^2)^{1/2}\}],\end{aligned} \tag{5}$$

where B is an arbitrary constant.

From (4), $\phi + i\psi$ must be an analytic function of $\omega - i\theta$, that is to say,

$$W = \phi + i\psi = f(\bar{\sigma}),$$

with $\sigma = \omega + i\theta$ and the over-bar representing a complex conjugate.

If x, y represent coordinates in the plane of flow, then quite simply

$$dz = q^{-1}e^{i\theta}(d\phi + i\rho^{-1}\,d\psi), \qquad z = x + iy,$$

and, in particular, on a profile given by $\psi =$ constant,

$$dz = q^{-1}e^{i\theta}\,dW. \tag{6}$$

Now the function $f(\bar{\sigma})$ will represent the flow of an incompressible fluid in a certain ζ-plane, so that

$$\frac{dW}{d\zeta} = Qe^{-i\theta}, \qquad Q = Ce^{\omega},$$

where C is an arbitrary constant and Q, θ are respectively the magnitude and angle of inclination of the velocity vector of the incompressible fluid in the ζ-plane. Equation (5) shows that

$$Q = 2bq/\{b + (b^2+q^2)^{1/2}\}, \tag{7}$$

if the condition $Q \to q$ as $q \to 0$ is assumed, so that

$$q = 4b^2Q/(4b^2 - Q^2). \tag{8}$$

Assume the flow in the ζ-plane to be uniform and parallel at infinity, and write $W = Q_\infty G(\zeta)$, Q_∞ being the fluid speed at infinity; then

$$Q^2 = Q_\infty^2 \frac{dG}{d\zeta}\frac{d\bar{G}}{d\bar{\zeta}},$$

and from (6) and (8),

$$z = \zeta - \frac{Q_\infty^2}{4b^2} \int \left(\frac{d\overline{G}}{d\overline{\zeta}}\right)^2 d\overline{\zeta}, \tag{9}$$

since $dG = d\overline{G}$ along the profile $\psi =$ constant.

3. Pressure and density

Let the straight line (1) be parallel to the tangent to the curve $pv^\gamma = 1$ at the point (p_1, v_1). Then

$$\left(\frac{dp}{dv}\right)_1 = \left(\frac{dp}{d\rho}\frac{d\rho}{dv}\right)_1 = -c_1^2 \rho_1^2,$$

where c_1 is the local sonic speed. This linear assumption yields

$$c^2 = \frac{dp}{d\rho} = \frac{b^2}{\rho^2},$$

so that

$$b^2 = c^2\rho^2 = c_1^2 \rho_1^2. \tag{10}$$

Equation (2) now gives

$$\rho^2 = 1 - M^2, \tag{11}$$

where $M = q/c$ is the Mach number. This means that the density and pressure are given very simply in terms of M, and as $\rho = 0$ when $M = 1$, it appears that (11) will probably not be a good approximation near the critical velocity.

It seems a reasonable assumption therefore to find only the fluid speed by this approximation method, and to use the correct adiabatic relations

$$p = \left(1 - \frac{\gamma - 1}{2\gamma} q^2\right)^{\gamma/(\gamma-1)}, \qquad \rho = \left(1 - \frac{\gamma - 1}{2\gamma} q^2\right)^{1/(\gamma-1)}, \tag{12}$$

for pressure and density once q has been determined.

4. Best approximation when $\gamma = 1{\cdot}4$

Obviously a set of flows can be constructed by taking values of b to correspond to tangents at various points on the (p, v)-curve between the stagnation and critical conditions. Such a set has been calculated by taking tangents at points on the curve corresponding to Mach numbers 0, 0·1, 0·2, ..., 1·0, and applied in each case to uniform flow past a circular cylinder of unit radius in the ζ-plane, so that

$$G(\zeta) = \zeta + 1/\zeta.$$

The Mach number at infinity in the z-plane is taken to be $M_\infty = 0{\cdot}35$, and since

$$q^2 = \gamma M^2 / \{1 + \tfrac{1}{2}(\gamma - 1) M^2\},$$

$q_\infty = 0{\cdot}4091$, when γ has the value 1·4.

Table 1 shows the thickness ratio of the corresponding cylinder in the z-plane, also the ratio $q_{\max}/q_\infty$, $q_{\max}$ being the maximum speed on the profile, which occurs at the points where thickness is greatest. An inspection of this table shows that although thickness ratio increases with M_∞

q_{max}/q_∞ increases even more quickly, so that it is reasonable to suppose that for any given thickness ratio, the value of q_{max}/q_∞ is too small if the tangent corresponding to $M = 0$ is taken and too large if the tangent corresponding to $M = 1$ is used. The problem is now to select the 'best' tangent, or in effect the best value of b^2, since only the slope of the

M	b^2	Q_∞	Thickness ratio	q_{max}/q_∞
0	1·400	0·3975	1·041	2·191
0·1	1·383	0·3974	1·041	2·194
0·2	1·334	0·3970	1·042	2·201
0·3	1·257	0·3964	1·045	2·215
0·4	1·144	0·3953	1·050	2·239
0·5	1·044	0·3941	1·055	2·262
0·6	0·9224	0·3921	1·062	2·300
0·7	0·7989	0·3894	1·072	2·351
0·8	0·6797	0·3865	1·086	2·423
0·9	0·5798	0·3832	1·101	2·508
1·0	0·4687	0·3779	1·127	2·663

Table 1. Thickness ratio and q_{max}/q_∞ for various tangent approximations with $\gamma = 1{\cdot}4$.

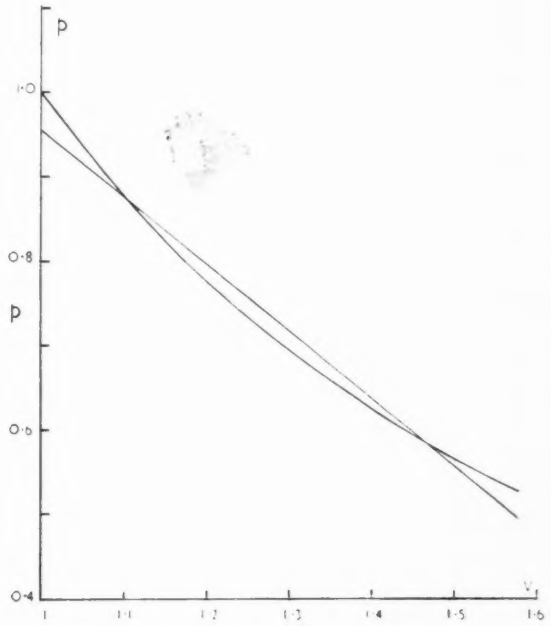

Figure 1. Approximation to (p, v)-curve.

straight-line approximation occurs in the results. Tsien (1939) chose the tangent at the point on the (p, v)-curve corresponding to the conditions at infinity, and it appears that the speeds obtained by this assumption are too small. It is suggested here that the value of b^2 should be taken to correspond to the best straight-line fit to the (p, v)-curve, found, say, by the method of least squares, between the significant limits for the particular problem under consideration. For example, it is found by using the least-squares method over 11 points between the stagnation and critical points, that the best straight-line fit over this range corresponds to $a = 1{\cdot}7544$, $b^2 = 0{\cdot}7982$. This is shown in figure 1.

5. Circular cylinder

In order to test the accuracy of this method, the compressible flow, uniform at infinity, past a circular cylinder of thickness ratio unity is considered, and comparison made with the accurate results obtained by Lush & Cherry (1956).

t	x	y	q/q_∞	$(x^2+y^2)^{1/2}$
0	4·325	0	0	4·325
10	4·247	0·811	0·3424	4·324
20	4·022	1·590	0·6846	4·325
30	3·661	2·298	1·0231	4·322
40	3·191	2·915	1·3516	4·322
50	2·643	3·423	1·6589	4·325
60	2·028	3·820	1·9271	4·325
70	1·370	4·103	2·1378	4·326
80	0·692	4·270	2·2766	4·326
90	0	4·325	2·3181	4·325

Table 2. Coordinates and fluid speed for a nearly circular cylinder at $M_\infty = 0{\cdot}4$.

To obtain such a flow in the z-plane, the uniform flow past an elliptic cylinder in the incompressible plane is considered, represented by

$$G(\zeta) = \zeta' + \alpha^2/\zeta',$$

where $\zeta = \zeta' + 1/\zeta'$; the profile is given by $\zeta' = \alpha e^{it}$. This is substituted in (9), from which it is found on integrating and separating into real and imaginary parts,

$$\left.\begin{aligned} x &= \left(\alpha + \frac{1}{\alpha}\right)\cos t - \lambda\left[\alpha(1+\alpha^2)\cos t + \tfrac{1}{4}(\alpha^2-1)^2 \log\left\{\frac{(\alpha^2-1)^2 + 4\alpha^2\sin^2 t}{(\alpha^2 + 2\alpha\cos t + 1)^2}\right\}\right] \\ y &= \left(\alpha - \frac{1}{\alpha}\right)\sin t + \lambda\left[\alpha(1-\alpha^2)\sin t + \tfrac{1}{2}(\alpha^2-1)^2 \tan^{-1}\left\{\frac{2\alpha\sin t}{\alpha^2-1}\right\}\right] \end{aligned}\right\} \tag{13}$$

with $$\lambda = Q_\infty^2/4b^2.$$

The semi-axes of the resulting cylinder can be found by setting t equal to 0 and $\frac{1}{2}\pi$ in (13), and the ratio of these gives the thickness ratio δ as

$$\delta = \left(\frac{\alpha^2-1}{\alpha^2+1}\right)\left\{\frac{1+\lambda\left[-\alpha^2+\frac{1}{2}\alpha(\alpha^2-1)\tan^{-1}\left(\frac{2\alpha}{\alpha^2-1}\right)\right]}{1-\lambda\left[\alpha^2+\frac{1}{2}\alpha(\alpha^2-1)\left(\frac{\alpha^2-1}{\alpha^2+1}\right)\log\left(\frac{\alpha-1}{\alpha+1}\right)\right]}\right\}. \quad (14)$$

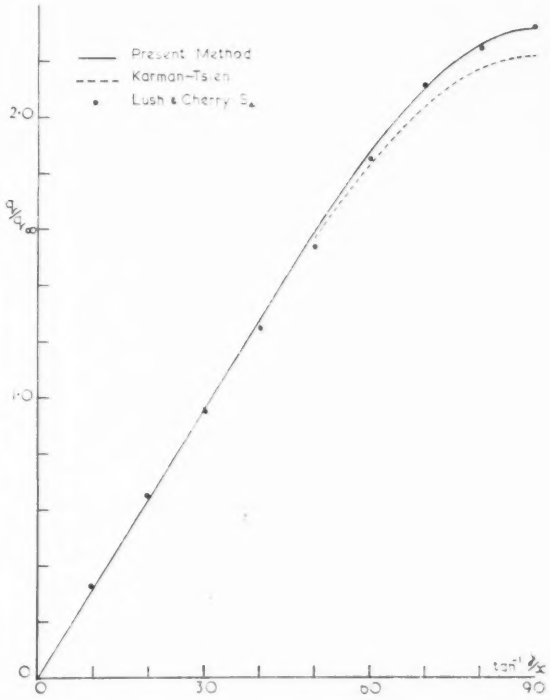

Figure 2. q/q_∞ plotted against $\tan^{-1}(y/x)$ for circular profile at $M_\infty = 0{\cdot}4$. Comparison is shown with the von Kármán-Tsien approximation and Lush & Cherry's S_4 result.

If now $M_\infty = 0{\cdot}4$, then $q_\infty = 0{\cdot}4659$, $Q_\infty = 0{\cdot}4380$, and, by employing the best straight-line fit previously found with $b^2 = 0{\cdot}7982$, λ takes the value 0·0601. Using this value of λ, it is found that when $\alpha^2 = 24{\cdot}00$, $\delta = 1$ to four significant figures. Table 2 shows coordinates, calculated from (13), and fluid speeds on the profile for various values of t. This table shows that the profile is almost circular, the error in radius being nowhere greater than 0·1%.

Figure 2 shows the graph of q/q_∞ plotted against $\tan^{-1}(y/x)$. From this an interesting comparison can be made with the results obtained by Lush & Cherry, and in particular with their S_4 approximation. Comparison is also made with a similar approach using the von Kármán-Tsien method. Agreement with Lush & Cherry is extremely good, although it must be observed that they use $\gamma = 1{\cdot}405$.

It would therefore appear that by this means of approximation a very accurate result can be obtained, at least for flow past cylinders with elliptic-type cross-section. Unfortunately there are very few solutions that are known to be sufficiently accurate for further comparison to be made.

One of the authors (P. S.) wishes to acknowledge the receipt of a maintenance grant from the Department of Scientific and Industrial Research.

References

Demtchenko, B. 1932 *Comptes Rendus* **194**, 1218.

Lush, P. E. & Cherry, T. M. 1956 *Quart. J. Mech. Appl. Math.* **9**, 6.

Tsien, H. S. 1939 *J. Aero. Sci.* **6**, 399.

Surface waves on water of non-uniform depth

By JOSEPH B. KELLER
Institute of Mathematical Sciences, New York University

(*Received* 20 *March* 1958)

1. Introduction

Gravity waves occur on the surface of a liquid such as water, and the manner in which they propagate depends upon its depth. Although this dependence is described in principle by the equations of the 'exact linear theory' of surface waves, these equations have not been solved except in some special cases. Therefore, oceanographers have been unable to use the theory to describe surface wave propagation in water whose depth varies in a general way. Instead they have employed a simplified geometrical optics theory for this purpose (see, for example, Sverdrup & Munk (1944)). It has been used very successfully, and consequently various attempts, only partially successful, have been made to deduce it from the exact linear theory. It is the purpose of this article to present a derivation which appears to be satisfactory and which also yields corrections to the geometrical optics theory.

The present derivation is based upon an asymptotic solution of the equations of the exact linear theory for periodic waves in water of arbitrary non-uniform depth. The solution is asymptotic in the sense that the depth and wavelength must be small compared to the horizontal scale length of the bottom contour. Our solution is formal since we do not prove its asymptotic character. Therefore, it is significant that the first term agrees exactly with the asymptotic form of the solution for waves in water with a uniformly sloping bottom, as the bottom slope tends to zero. This asymptotic form was deduced by Friedrichs (1948). The accuracy of our result is indicated by the fact that for a bottom slope angle of 6°, the asymptotic form agrees very well with the exact solution at all points beyond one wavelength from the shore (see Stoker 1947).

Previously Lowell (1949) has shown that in shallow water the geometrical optics theory follows from the linear shallow-water theory. The latter is a simplified form of the exact linear theory which applies when the depth is small compared to the wavelength. The significance of this restriction is not clear, in view of the fact that Lowell's derivation depends upon letting the wavelength tend to zero. Our derivation seems to clarify this point since we require the depth to tend to zero in a fixed ratio to the wavelength, while the horizontal scale of the bottom contour is constant. We could have obtained the same results by keeping the depth and wavelength constant while permitting the horizontal scale length of the bottom contour to become infinite.

A previous attempt by the present author to derive the geometrical optics theory from the exact linear theory was based upon an asymptotic solution obtained by requiring the wavelength alone to tend to zero. The resulting geometrical optics theory was independent of the depth. That result can be explained by noting that waves disturb the water only within a few wavelengths of the surface. As the wavelength tends to zero, the wave motion is confined to a vanishingly thin layer near the surface, so the waves do not 'feel' the bottom. This derivation, which may be useful for other purposes, is contained in Appendix I.

We will now describe the geometrical optics theory to which we have already referred. In this theory a propagation velocity is defined at each point P of the surface. This velocity is just that which waves of the given period would have in water having uniform depth equal to that at P. By using this propagation velocity and employing Fermat's principle of optics, rays can be defined. It is assumed that surface waves propagate along these rays. The variation of the amplitude of these waves along a ray is then determined by using the principle of conservation of energy. In its optical form this principle states that the flux of energy is the same at all cross-sections of a tube of rays. In the present case a tube is bounded by two neighbouring rays. The energy flux is proportional to the square of the amplitude of the waves and to the distance between the rays. It is assumed that at each point P the proportionality factor, which depends upon the depth, is the same as for plane waves in water of uniform depth equal to the depth at P. From these assumptions the variations of amplitude along a ray can be determined. This amplitude variation has been studied by Miche (1944).

2. Formulation of the problem

We consider the periodic irrotational motion of an inviscid incompressible liquid bounded below by the rigid surface $Y = -H(x,z)$ and bounded above by an unknown free surface. In the absence of motion the free surface is the plane $Y = 0$; when motion of angular frequency ω occurs, it is $Y = \mathscr{R}\{e^{i\omega t}\eta(x,z)\}$. Here t denotes the time, η is the complex amplitude of the surface wave motion, and the positive Y-axis points vertically upward. In the exact linear theory of surface waves, the wave amplitude η is given by

$$\eta(x,z) = (i\omega/g)\Phi(x,0,z). \tag{1}$$

Here $\Phi(x, Y, z)$ is the velocity potential of the fluid motion, and g is the acceleration of gravity.

The velocity potential satisfies the following conditions (see Stoker 1947)

$$\Delta\Phi = 0 \quad \text{in} \quad 0 \geqslant Y \geqslant -H(x,z), \tag{2}$$

$$\Phi_Y = \beta\Phi \quad \text{on} \quad Y = 0 \qquad (\beta = \omega^2/g), \tag{3}$$

$$\Phi_Y + H_x\Phi_x + H_z\Phi_z = 0 \quad \text{on} \quad Y = -H(x,z). \tag{4}$$

Furthermore, Φ satisfies other conditions which we will consider later.

We now introduce the new quantities y, h and ϕ defined by

$$y = \beta Y, \qquad h = \beta H, \qquad \phi(x,y,z) = \Phi(x,Y,z). \tag{5}$$

In terms of these quantities, (2), (3) and (4) become

$$\beta^2\phi_{yy} + \phi_{xx} + \phi_{zz} = 0 \quad \text{in} \quad 0 \geqslant y \geqslant -h(x,z), \tag{6}$$

$$\phi_y = \phi \quad \text{on} \quad y = 0, \tag{7}$$

$$\beta^2\phi_y + h_x\phi_x + h_z\phi_z = 0 \quad \text{on} \quad y = -h(x,z). \tag{8}$$

The problem we consider is that of finding solutions ϕ of (6), (7) and (8) for large values of β.

As the first step towards finding solutions, we introduce three unknown functions $k(x,z)$, $S(x,z)$ and $A(x,y,z,\beta)$. Without loss of generality we may express ϕ in terms of these functions by the relation

$$\phi = A\cosh[k(y+h)]e^{i\beta S}. \tag{9}$$

Next we insert (9) into (6), (7) and (8). These equations then become the following, in which $\alpha \equiv k(y+h)$ and $\nabla \equiv (\partial/\partial x, \partial/\partial z)$:

$$\beta^2[\{k^2 - (\nabla S)^2\}A\cosh\alpha + A_{yy}\cosh\alpha + 2kA_y\sinh\alpha] +$$
$$+ i\beta[(\nabla^2 S)A\cosh\alpha + 2\nabla S\,.\,\nabla(A\cosh\alpha)] + \nabla^2(A\cosh\alpha) = 0; \tag{10}$$

$$A_y\cosh kh + kA\sinh kh = A\cosh kh \qquad y = 0; \tag{11}$$

$$\beta^2 A_y + i\beta A\nabla h\,.\,\nabla S + \nabla h\,.\,\nabla A = 0 \qquad y = -h. \tag{12}$$

We now want solutions of (10), (11) and (12) for large β which represent waves travelling on the surface.

3. Solution of the problem

To solve (10), (11) and (12), we assume that, for large β, A has an asymptotic expansion of the form

$$A \sim A_0(x,z) + \sum_{n=1}^{\infty} A_n(x,y,z)/(i\beta)^n. \tag{13}$$

Then we insert (13) into (10), assuming that termwise differentiation is correct. When we equate coefficients of each power of β, we obtain the following equations:

$$(\nabla S)^2 = k^2; \tag{14}$$

$$(A_1)_{yy}\cosh\alpha + 2k(A_1)_y\sinh\alpha = 2\nabla S\,.\,\nabla(A_0\cosh\alpha) + A_0\cosh\alpha\nabla^2 S; \tag{15}$$

$$(A_n)_{yy}\cosh\alpha + 2k(A_n)_y\sinh\alpha = 2\nabla S\,.\,\nabla(A_{n-1}\cosh\alpha) + A_{n-1}\cosh\alpha\nabla^2 S +$$
$$+ \nabla^2(A_{n-2}\cosh\alpha) \qquad (n \geqslant 2). \tag{16}$$

In a similar way, we obtain from (11) the equations

$$k\tanh kh = 1, \tag{17}$$

$$(A_n)_y = 0 \qquad y = 0 \qquad (n \geqslant 1). \tag{18}$$

Finally, from (12), we obtain

$$(A_1)_y = A_0\nabla h\,.\,\nabla S \qquad y = -h, \tag{19}$$

$$(A_n)_y = A_{n-1}\nabla h\,.\,\nabla S + \nabla h\,.\,\nabla A_{n-2} \qquad y = -h \qquad (n \geqslant 2). \tag{20}$$

Let us now examine the equations (14) to (20) which must be satisfied by k, S and the A_n. Equation (17) is a transcendental equation which determines $k(x,z)$ in terms of the known depth $h(x,z)$. This is the same equation that occurs in the case of uniform depth and its solution is well known. Once k is known, (14) is the eiconal equation of geometrical optics for S. If the value of S is prescribed at each point of any given curve, the solution S can be found by means of the characteristics of (14). These characteristics are just the optical rays in a medium of refractive index k, and the surfaces $S = \text{const.}$ are the corresponding wave-fronts. In terms of these rays the directional derivative $\nabla S \cdot \nabla f$, which appears in (15) and (16) is just $k(df/d\tau)$ where τ measures arc-length along a ray.

Next let us consider the amplitudes A_n which satisfy (15) and (16). These equations can be simplified by means of the identity

$$(A_n)_{yy}\cosh\alpha + 2k(A_n)_y \sinh\alpha = (\cosh\alpha)^{-1}[(A_n)_y \cosh^2\alpha]_y. \tag{21}$$

Now (21) is inserted into (15), which becomes

$$[(A_1)_y \cosh^2\alpha]_y = (2\nabla S\cdot\nabla A_0 + A_0\nabla^2 S)\cosh^2\alpha + A_0\nabla S\cdot\nabla\cosh^2\alpha. \tag{22}$$

Now we integrate (22) from zero to y, noting that, by (18), $(A_1)_y = 0$ at $y = 0$. Thus (22) yields

$$(A_1)_y\cosh^2\alpha = (2\nabla S\cdot\nabla A_0 + A_0\nabla^2 S + A_0\nabla S\cdot\nabla)\int_0^y \cosh^2\alpha\, dy. \tag{23}$$

The integral in (23) is given by

$$\int_0^y \cosh^2 k(y+h)\,dy = \tfrac{1}{2}k^{-1}\times \\ \times[\sinh k(y+h)\cosh k(y+h) - \sinh kh\cosh kh] + \tfrac{1}{2}y. \tag{24}$$

We now use (24) in (23) and obtain

$$(A_1)_y\cosh^2\alpha = \tfrac{1}{2}(2\nabla S\cdot\nabla A_0 + A_0\nabla^2 S + A_0\nabla S\cdot\nabla)\times \\ \times\{k^{-1}[\sinh\alpha\cosh\alpha - \sinh kh\cosh kh] + y\}. \tag{25}$$

From (25) we can calculate A_1 up to an additive function of x and z, once A_0 is known. The method which we will now use to find A_0 will also determine this additive function. For that purpose the equation (16) for $n = 2$ would have to be examined.

To find A_0 we set $y = -h$ in (25). Then we can eliminate $(A_1)_y$ by means of (19). In this way we obtain the following equation for A_0:

$$2A_0\nabla h\cdot\nabla S = -(2\nabla S\cdot\nabla A_0 + A_0\nabla^2 S)(\sinh^2 kh + h) + A_0\nabla S\cdot(\nabla h - \nabla\sinh^2 kh). \tag{26}$$

This can be written as

$$\nabla S\cdot\nabla[A_0^2(\sinh^2 kh + h)] + [A_0^2(\sinh^2 kh + h)]\nabla^2 S = 0. \tag{27}$$

Since $\nabla S\cdot\nabla = k(d/d\tau)$, (27) is an ordinary differential equation along a ray. Its solution is

$$A_0^2(\sinh^2 kh + h) = [A_0^2(\sinh^2 kh + h)]_{\tau_0}\exp\left\{-\int_{\tau_0}^{\tau} k^{-1}\nabla^2 S\, d\tau\right\}. \tag{28}$$

Luneberg (1944) has shown that the exponential in (28) is given by

$$\exp\left\{-\int_{\tau_0}^{\tau} k^{-1}\nabla^2 S\, d\tau\right\} = \frac{k(\tau_0)}{k(\tau)}\,\frac{d\sigma(\tau_0)}{d\sigma(\tau)}. \tag{29}$$

In (19), $d\sigma(\tau_0)/d\sigma(\tau)$ is the ratio of the width of a narrow strip of rays at τ_0 to its width at τ, or rather the limit of this ratio as the width tends to zero. When (29) is used in (28), the equation for the variation of A_0 along a ray finally becomes

$$A_0^2(\sinh^2 kh + h)k\, d\sigma = \text{const.} \tag{30}$$

Equation (30) has a simple physical interpretation. Except for a constant factor, the left side of (30) is the energy flux per length $d\sigma$ of a plane wave in water of uniform depth h. Thus (30) expresses the fact that the energy flux is constant along a tube of rays.

4. Conclusion

Let us now summarize our results. The wave amplitude η is given by (1), the potential is given by (9), k is given by (17), S is determined by the eiconal equation (14), and A_0 is determined by (30). This yields the leading term in the solution for large β. It conforms with all the principles of the geometrical optics theory and thus provides a derivation of that theory. Additional terms are given by the A_n, which satisfy (16) and the boundary conditions (18) and (20).

In Appendix II our result is compared with the asymptotic form of the exact solution for plane waves normally incident on a uniformly sloping beach. That asymptotic form is obtained from the work of Friedrichs (1948). It agrees exactly with our result.

Our result is not valid at caustics of the ray system since $d\sigma$ is zero on them, and then (30) shows that A_0 is infinite. A method for obtaining the correct finite result at and near caustics was given by Kay & Keller (1954). At a shore line where $h = 0$, our result also fails because it yields an infinite value for A_0. In this case the solution for the uniformly sloping beach given by Peters (1952) can be used near the shoreline to yield the correct result there. Both of the exceptions just described are instances of 'boundary layers' in which the asymptotic behaviour of the solution is different from that outside these layers.

Appendix I. Another asymptotic solution

We will try to solve (2), (3) and (4) for Φ by writing

$$\Phi = ue^{i\beta S}. \tag{A 1}$$

In terms of u and S, (2) and (3) become

$$\beta^2(\nabla S)^2 u - i\beta[2\nabla S.\nabla u + u\nabla^2 S] + \nabla^2 u = 0, \tag{A 2}$$

$$i\beta S_y u + u_y = \beta u \qquad y = 0. \tag{A 3}$$

Here ∇ is the three-dimensional gradient and $y = Y$ is used for notational convenience. We now assume that u has the asymptotic expansion

$$u \sim \sum_{j=1}^{\infty} u_j(x,y,z)/(i\beta)^j. \tag{A 4}$$

Upon inserting (A 4) into (A 2) and equating coefficients of β, we obtain

$$(\nabla S)^2 = 0, \tag{A 5}$$

$$2\nabla S \cdot \nabla u_j + u_j \nabla^2 S = -\nabla^2 u_{j-1} \qquad j \geqslant 0, \quad u_{-1} \equiv 0. \tag{A 6}$$

Similarly from (A 3) we obtain

$$iS_y = 1 \qquad y = 0, \tag{A 7}$$

$$(u_j)_y = 0 \qquad y = 0, \qquad j \geqslant 0. \tag{A 8}$$

From (A 5) we conclude that S is complex, so we write

$$S = R + iI; \tag{A 9}$$

where R and I are real. Now (A 5) yields the two equations

$$\nabla R \cdot \nabla I = 0, \qquad (\nabla R)^2 = (\nabla I)^2. \tag{A 10), (A 11}$$

Equation (A 10) shows that the wave-fronts $R = \text{const.}$ are orthogonal to the surfaces $I = \text{const.}$, which are essentially surfaces of constant amplitude. This is common in evanescent waves.

When (A 9) is used in (A 7), there results

$$R_y = 0, \qquad I_y = -1, \qquad y = 0. \tag{A 12}$$

To satisfy (A 10) and (A 12), we assume

$$I = -y, \qquad R = R(x,z). \tag{A 13), (A 14}$$

Then (A 11) yields the eiconal equation for R

$$(\nabla R)^2 = 1. \tag{A 15}$$

To solve (A 6) with $j = 0$ for u_0, we assume that u_0 is real. Then (A 6) implies that $u_0 = u_0(x,z)$, and that

$$2\nabla R \cdot \nabla u_0 + u_0 \nabla^2 R = 0. \tag{A 16}$$

As before, (A 16) is an ordinary differential equation along a ray. Its solution is

$$u_0(\tau) = u_0(\tau_0)[d\sigma(\tau_0)/d\sigma(\tau)]^{1/2}. \tag{A 17}$$

From (A 15) it follows that the rays are straight lines, and along any ray $R = R(\tau_0) + \tau$. Then $d\sigma(\tau_0)/d\sigma(\tau) = (\rho + \tau_0)/(\rho + \tau)$, where ρ denotes the radius of curvature of the wave-front at τ_0.

Upon collecting our results, we find

$$\Phi \sim A\tau^{-1/2} e^{i\beta\tau + \beta y}. \tag{A 18}$$

In writing (A 18) we have collected the factors independent of τ into the factor A and shifted the origin of τ so that $\rho + \tau$ becomes τ. In other words, we now measure τ from the centre of curvature of the wave-front—i.e. from the caustic—on each ray. The result (A 18) does indeed conform to the principles of geometrical optics, but the index of refraction to which

it corresponds is unity. The waves travel with the velocity $\omega/\beta = g/\omega$, which is the velocity of waves of frequency ω in water of infinite depth. This was explained in the Introduction.

In constructing the solution (A 18) the condition (4) at the bottom was ignored and the result in (A 18) does not satisfy it. It is also impossible to satisfy this condition by including additional terms of the sum (A 4). Therefore, the present expansion applies in water of infinite depth, when condition (4) is absent. When the depth is finite we must modify the expression (A 1) by including another term of the same form, which we may think of as arising by reflection of the original term from the bottom. This reflected term must be so chosen that the two terms together satisfy condition (4) at the bottom. But then the reflected term violates the condition (3) at the top, which the first term alone satisfies. We therefore add another term, reflected from the top, to remedy this, then another reflected from the bottom, etc.

On the basis of these considerations, we assume that Φ has the following asymptotic expansion

$$\Phi \sim \sum_{n=0}^{\infty} \exp(i\beta S_n)\beta^{[n/2]} \sum_{j=0}^{\infty} u_{nj}/(i\beta)^j . \tag{A 19}$$

Here $[n/2]$ denotes the greatest integer not exceeding $n/2$, and the S_n and u_n are functions of x, y and z. The terms with $n = 0$ are those considered before. By proceeding as before we can obtain equations for all the new terms. It appears that at $y = 0$ all the S_n with $n \geqslant 1$ will have positive real parts which depend upon the depth. Therefore they will all be of exponentially lower order in β than the terms with $n = 0$ which we considered before. Therefore, our previous result will still determine the surface shape or wave pattern.

Appendix II. Comparison with an exact solution

Friedrichs (1948) has obtained the asymptotic form of the exact solution for waves on a sloping beach as the slope angle tends to zero. He considered only points on the top surface $y = 0$. However, it can be seen that his equation (16) also holds for $y < 0$ provided that x is replaced by $x + iy$ in (12). If we then treat y as small compared to x, we obtain

$$\lambda(x+iy) = \lambda(x) + i\omega y\lambda'(x) + \dots ,$$

and

$$k[\lambda(x+iy)] = k[\lambda(x)] + i\omega y/\lambda(x) + \dots .$$

When these results are inserted into his (16) and a typographical error in the second exponent is corrected, (16) becomes

$$\begin{aligned} X_2^P(x,y,t) = &-(1-\lambda)A(\lambda)\exp[i(\omega^{-1}k + t + \tfrac{1}{4}\pi) - y/\lambda] - \\ &-(1+\lambda)A(\lambda)\exp[-i(\omega^{-1}k + t + \tfrac{1}{4}\pi) + y/\lambda] + \dots . \end{aligned}$$

Then the real potential function ϕ is given by

$$\begin{aligned} \phi = \mathscr{R}\{X_2^P\} &= -A(\lambda)[(1-\lambda)e^{-y/\lambda} + (1+\lambda)e^{y/\lambda}]\cos(\omega^{-1}k + t + \tfrac{1}{4}\pi) \\ &= -2A(\lambda)[\cosh(y/\lambda) + \lambda\sinh(y/\lambda)]\cos(\omega^{-1}k + t + \tfrac{1}{4}\pi). \end{aligned}$$

Now we reintroduce dimensional variables by replacing x by βx, t by σt (σ is the angular frequency and $\beta = \sigma^2/g$) and we define the depth $h = \beta\omega x$ (ω is the slope of the bottom). We also introduce $k' = \lambda^{-1}$. Then (12) becomes $k' \tanh k'h = 1$. Now ϕ is given by

$$\phi = -2A(\lambda)\frac{\cosh[k'(y+h)]}{\cosh k'h}\cos(\omega^{-1}k + \sigma t + \tfrac{1}{4}\pi).$$

From the definition of $A(\lambda)$, it follows that $A(\lambda) = A_0 \cosh k'h$, where A_0 is given by our equation (30). Thus, ϕ finally becomes

$$\phi = -2A_0 \cosh[k'(y+h)]\cos(\omega^{-1}k + \sigma t + \tfrac{1}{4}\pi).$$

This is exactly the sum of two expressions of the form (9) given by our asymptotic solution.

This paper represents results obtained under the sponsorship of the Office of Naval Research, Contract Nonr–285(06).

References

Friedrichs, K. O. 1948 Water waves on a shallow sloping beach, *Comm. Pure Appl. Math.* **1,** 109–134.

Kay, I. & Keller, J. B. 1954 Asymptotic evaluation of the field at a caustic, *J. Appl. Phys.* **25,** 876–883.

Lowell, S. C. 1949 The propagation of waves in shallow water, *Comm. Pure Appl. Math.* **2,** 275–291.

Luneburg, R. K. 1944 Mathematical theory of optics, Brown University Lecture Notes.

Miche, A. 1944 Mouvements ondulatoires de la mer en profondeur constante ou décroissante, *Annales des ponts et chaussées* **14,** 131–164, 270–292, 369–406.

Peters, A. S. 1952 Water waves over sloping beaches, *Comm. Pure Appl. Math.* **5,** 87–108.

Stoker, J. J. 1947 Surface waves in water of variable depth, *Quart. Appl. Math.* **5,** 1–54.

Sverdrup, H. U. & Munk, W. H. 1944 *Breakers and surf, U.S. Navy Department, Hydrographic Office, Publ.* no. 234.

Effects of compressibility on a laminar wall jet

By N. RILEY
Department of Mathematics, University of Manchester

(*Received* 8 *May* 1958)

SUMMARY

The effects of compressibility on a radial laminar wall jet are investigated. On the assumption that the coefficient of viscosity is proportional to the temperature, it is shown that a similarity solution for the velocity distribution exists, which is expressible directly in terms of the corresponding solution for an incompressible wall jet. For arbitrary Prandtl number the energy equation is studied in detail and solutions are obtained for a variety of temperature conditions.

1. INTRODUCTION

The term 'wall jet' was introduced by Glauert (1956) to describe the flow due to a jet of air spreading out over a plane surface, either radially or in two dimensions. With compressibility neglected, Glauert studied the velocity distribution in a wall jet for both laminar and fully turbulent flow, and for laminar flow found an exact solution of the boundary-layer equations in the form of a similarity solution. This solution should be asymptotically approached whatever the initial form of the jet near the axis.

The present paper considers the influence of compressibility on a laminar radial wall jet. The effects of viscous dissipation, wall temperature conditions and of the initial temperature of the fluid in the wall jet are analysed. Some of the results of this study have been briefly referred to by Glauert (1957).

Glauert (1956) proved that, in an incompressible wall jet, the 'flux of exterior momentum flux' is constant; this forms the basic starting point of his theory. It is here shown how this result can be generalized to compressible flow, the flux of exterior momentum flux being constant when the viscosity is proportional to the temperature.

In the boundary-layer equations of momentum, continuity and energy, the stream function may be conveniently chosen as independent variable in place of the coordinate normal to the wall. This transformation was first used for incompressible flow by von Mises (1927) and later by von Kármán & Tsien (1938) for compressible flow. Under the simplifying assumption that the viscosity is proportional to the temperature, it is possible to solve the momentum and energy equations independently, the momentum equation becoming identical with the corresponding equation for incompressible flow, and the same solution being applicable. The interpretation of the results in terms of geometrical coordinates differs,

and is fully investigated. In particular it is shown that the skin friction has the same value as in the corresponding incompressible flow.

Still retaining the simple viscosity–temperature law, but imposing no restrictions on the Prandtl number, solutions of the energy equation are obtained. These solutions describe the effects of viscous heating, wall temperature and initial jet temperature on the velocity and temperature profiles, both when there is no heat transfer across the wall and when the wall is maintained at a constant temperature. If the assumption that the Prandtl number is unity is made, the well-known Crocco relation between the temperature and the velocity provides a particular solution of the energy equation, being a special form of the solutions obtained in the more general analysis. When a more accurate viscosity–temperature law is assumed it is possible to develop solutions of the momentum and energy equations in series form, though the details are not set out here.

In practice, wall jets will almost always be turbulent. No attempt is made in this paper to extend Glauert's analysis for turbulent flow, since it is not easy to predict how the eddy viscosity and diffusivity will vary with temperature. However, the general nature of the changes in the velocity profiles in the laminar case may perhaps serve as an indication of the sort of modifications to be expected for turbulent compressible flow.

Glauert (1956) shows that there is a close analogy between wall jets in two and three dimensions, the same velocity profile occurring in each case. Similarly all the results obtained here, with simple changes, become applicable to compressible plane wall jets.

2. Equations of motion

On the boundary-layer approximation, the momentum, continuity and energy equations governing a compressible, laminar, radial wall jet flowing over a plane wall are

$$\rho u \frac{\partial u}{\partial x} + \rho v \frac{\partial u}{\partial y} = \frac{\partial}{\partial y}\left(\mu \frac{\partial u}{\partial y}\right), \tag{2.1}$$

$$\frac{\partial}{\partial x}(\rho x u) + \frac{\partial}{\partial y}(\rho x v) = 0, \tag{2.2}$$

$$\rho u \frac{\partial T}{\partial x} + \rho v \frac{\partial T}{\partial y} = \frac{1}{\sigma}\frac{\partial}{\partial y}\left(\mu \frac{\partial T}{\partial y}\right) + \frac{\mu}{C_p}\left(\frac{\partial u}{\partial y}\right)^2. \tag{2.3}$$

The boundary conditions are $u = v = 0$ at $y = 0$; $u \to 0$, $T \to T_\infty$ as $y \to \infty$, together with a condition on T at $y = 0$, $x = 0$.

Here x and y denote distances along and normal to the wall, x being measured from the jet axis, u and v the corresponding velocity components, ρ the density, T the temperature and μ the coefficient of viscosity. The specific heat at constant pressure C_p and the Prandtl number σ are assumed constant. The subscript ∞ is used to denote values at $y = \infty$. On the boundary-layer approximation the pressure is uniform everywhere and hence the equation of state implies that

$$\rho T = \text{const.} \tag{2.4}$$

For an incompressible wall jet, Glauert established an integral relation which he interpreted as saying that the flux of exterior momentum flux is constant. We can follow the same procedure as Glauert to obtain a corresponding result for compressible flow. Multiply equation (2.1) by x and integrate with respect to y between the limits y and ∞, using the condition that $u \to 0$ as $y \to \infty$; then, since

$$\int_y^\infty \rho x v \frac{\partial u}{\partial y}\, dy = [\rho x v u]_y^\infty - \int_y^\infty u \frac{\partial}{\partial y}(\rho x v)\, dy$$

$$= -\rho x v u + \int_y^\infty u \frac{\partial}{\partial x}(\rho x u)\, dy$$

using (2.2), we have

$$\frac{\partial}{\partial x}\int_y^\infty (\rho x u^2)\, dy - \rho x v u + x\mu \frac{\partial u}{\partial y} = 0. \tag{2.5}$$

Multiplying (2.5) by $\rho x u$ and integrating with respect to y between the limits 0 and ∞, we have

$$\frac{\partial}{\partial x}\int_0^\infty \rho x u \left\{\int_y^\infty \rho x u^2\, dy\right\} dy - \int_0^\infty \frac{\partial}{\partial x}(\rho x u)\left\{\int_y^\infty \rho x u^2\, dy\right\} dy -$$

$$- \int_0^\infty \rho^2 x^2 v u^2\, dy + \int_0^\infty \rho\mu x^2 u \frac{\partial u}{\partial y}\, dy = 0. \tag{2.6}$$

From the continuity equation, the second term of (2.6) is

$$\left[\rho x v \int_y^\infty \rho x u^2\, dy\right]_0^\infty + \int_0^\infty \rho^2 x^2 v u^2\, dy.$$

Now at $y = 0$, $u = v = 0$, therefore equation (2.6) reduces to

$$\frac{\partial}{\partial x}\int_0^\infty \rho x u \left\{\int_y^\infty \rho x u^2\, dy\right\} dy + \int_0^\infty \rho\mu x^2 u \frac{\partial u}{\partial y}\, dy = 0. \tag{2.7}$$

For incompressible flow, where ρ and μ are constants, the second term of (2.7) is zero. For compressible flow it will vanish only in certain circumstances. In particular it will do so if $\rho\mu$ is a function of the velocity u, or is constant. In these cases (2.7) reduces to

$$\int_0^\infty \rho x u \left\{\int_y^\infty \rho x u^2\, dy\right\} dy = F, \tag{2.8}$$

where the constant F is the flux of exterior momentum flux. It may be noted, that as defined here, the constant F differs by a factor ρ^2 from the definition used by Glauert (1956).

The continuity equation (2.2) implies the existence of a stream function ψ such that

$$\left.\begin{aligned} \rho x u &= \frac{\partial \psi}{\partial y}, \\ \rho x v &= -\frac{\partial \psi}{\partial x}. \end{aligned}\right\} \tag{2.9}$$

Following von Mises, we now take x and ψ as the independent variables,

and hence write

$$\left.\begin{aligned}\left(\frac{\partial}{\partial x}\right)_y &= \left(\frac{\partial}{\partial x}\right)_\psi - \rho v x\left(\frac{\partial}{\partial \psi}\right)_x,\\ \left(\frac{\partial}{\partial y}\right)_x &= \rho u x\left(\frac{\partial}{\partial \psi}\right)_x.\end{aligned}\right\} \tag{2.10}$$

Substituting (2.10) into the momentum and energy equations (2.1) and (2.3) we have

$$\frac{\partial u}{\partial x} = x^2\frac{\partial}{\partial \psi}\left(\rho\mu u\frac{\partial u}{\partial \psi}\right), \tag{2.11}$$

$$\frac{\partial T}{\partial x} = \frac{x^2}{\sigma}\frac{\partial}{\partial \psi}\left(\rho\mu u\frac{\partial T}{\partial \psi}\right) + \frac{\rho\mu x^2 u}{C_p}\left(\frac{\partial u}{\partial \psi}\right)^2. \tag{2.12}$$

On introducing dimensionless variables by writing

$$\left.\begin{aligned} u &= U\bar{u}, & x &= \nu_\infty \bar{x}/U, & \psi &= \rho_\infty \nu_\infty^2 \bar{\psi}/U,\\ \rho &= \rho_\infty \bar{\rho}, & \mu &= \mu_\infty \bar{\mu}, & T &= T_\infty \bar{T},\end{aligned}\right\} \tag{2.13}$$

where U is an arbitrary constant velocity and ν the kinematic viscosity, we find that equations (2.11) and (2.12) become

$$\frac{\partial \bar{u}}{\partial \bar{x}} = \bar{x}^2\frac{\partial}{\partial \bar{\psi}}\left(\bar{\rho}\bar{\mu}\bar{u}\frac{\partial \bar{u}}{\partial \bar{\psi}}\right), \tag{2.14}$$

$$\frac{\partial \bar{T}}{\partial \bar{x}} = \frac{\bar{x}^2}{\sigma}\frac{\partial}{\partial \bar{\psi}}\left(\bar{\rho}\bar{\mu}\bar{u}\frac{\partial \bar{T}}{\partial \bar{\psi}}\right) + \frac{U^2}{C_p T_\infty}\bar{\rho}\bar{\mu}\bar{x}^2\bar{u}\left(\frac{\partial \bar{u}}{\partial \bar{\psi}}\right)^2. \tag{2.15}$$

Since ρT is constant by (2.4) ,we have, if $\mu \propto T$, $\rho\mu = \text{const.} = \rho_\infty \mu_\infty$ or

$$\bar{\rho}\bar{\mu} = 1. \tag{2.16}$$

Using (2.16) we see that equations (2.14) and (2.15) become

$$\frac{\partial \bar{u}}{\partial \bar{x}} = \bar{x}^2\frac{\partial}{\partial \bar{\psi}}\left(\bar{u}\frac{\partial \bar{u}}{\partial \bar{\psi}}\right), \tag{2.17}$$

$$\frac{\partial \bar{T}}{\partial \bar{x}} = \frac{\bar{x}^2}{\sigma}\frac{\partial}{\partial \bar{\psi}}\left(\bar{u}\frac{\partial \bar{T}}{\partial \bar{\psi}}\right) + \frac{U^2}{C_p T_\infty}\bar{x}^2\bar{u}\left(\frac{\partial \bar{u}}{\partial \bar{\psi}}\right)^2. \tag{2.18}$$

3. Velocity distribution

The density $\bar{\rho}$, and hence the temperature $\bar{T}$, does not appear explicitly in the momentum equation (2.17), and so (2.17) may be solved independently of the energy equation (2.18). Moreover a particular solution of equation (2.17) must be the similarity solution, obtained by Glauert (1956), of the corresponding incompressible equation, that is

$$\bar{u} = \tfrac{3}{4}f'(\eta)\bar{x}^{-3/2}, \tag{3.1}$$

where

$$f(\eta) = \bar{\psi}\bar{x}^{-3/4} \tag{3.2}$$

and $f(\eta)$ satisfies the equation

$$\left.\begin{aligned} f''' + ff'' + 2f'^2 &= 0,\\ f(0) = f'(0) = 0, \qquad f(\infty) &= 1.\end{aligned}\right\} \tag{3.3}$$

The boundary condition at the outer edge of the wall jet only requires $f'(\infty) = 0$, but writing $f(\infty) = 1$ involves no loss of generality, since the velocity U in (2.13) remains arbitrary. Glauert obtained the solution of equation (3.3) in the form

$$f = g^2, \qquad \eta = \log \frac{\sqrt{(1+g+g^2)}}{(1-g)} + \sqrt{3} \tan^{-1} \frac{\sqrt{3}g}{(2+g)}. \tag{3.4}$$

More recently, Glauert (1957) has shown that

$$\bar{u} = \tfrac{3}{4} f'(\eta)(\bar{x}^3 + l^3)^{-1/2}, \tag{3.5}$$

where

$$f(\eta) = \bar{\psi}(\bar{x}^3 + l^3)^{-1/4}, \tag{3.6}$$

is also a solution of the momentum equation (2.17), l being an arbitrary constant length. Since the velocity given by equation (3.5) remains finite as $\bar{x} \to 0$, this solution may have some significance even near the axis. We shall make use of this latter solution of the momentum equation.

Although the velocity function $f'(\eta)$ is the same in the incompressible and compressible problems, the interpretation of the variable η differs. Connection of η with the physical variable y can be made as follows. Using (2.9) and (2.13)

$$y = \int_0^{\psi} \frac{d\psi}{\rho x u} = \frac{\nu_\infty}{U} \int_0^{\bar{\psi}} \frac{\rho_\infty}{\rho \bar{u} \bar{x}} d\bar{\psi}. \tag{3.7}$$

Substituting $\rho_\infty/\rho = \bar{T}$ and introducing $\bar{u}$ and η according to equations (3.5) and (3.6) we obtain, from equation (3.7)

$$y = \left(\frac{U(x^3 + l^3)^3}{\nu_\infty x^4} \right)^{1/4} \frac{4}{3} \int_0^{\eta} \bar{T}\, d\eta. \tag{3.8}$$

Thus, in order to obtain the velocity in terms of the physical variable y, we see that the temperature distribution throughout the wall jet must be known. The temperature distribution will be the subject of §4. The skin friction is independent of the temperature distribution when $\mu \propto T$, since it is given by

$$\tau_w = \left(\mu \frac{\partial u}{\partial y} \right)_{y=0} = \frac{9}{16} \mu_\infty f''(0) \left(\frac{\nu_\infty x^4}{U(x^3 + l^3)^5} \right)^{1/4} \tag{3.9}$$

which has the same value as for incompressible flow.

The arbitrary velocity U may be expressed in terms of the flux of exterior momentum flux F defined by equation (2.8). Substituting the values of (3.5) and (3.8), we obtain

$$F = \frac{3}{40} \frac{\nu_\infty^4 \rho_\infty^2}{U}. \tag{3.10}$$

Proceeding exactly as in the corresponding incompressible case, if the wall jet is the result of a free jet impinging on a flat plate, a rough estimate of the magnitude of F may be obtained from the conditions in the free jet as

$$F = \tfrac{1}{2} \times (\text{typical velocity}) \times (\text{mass flow/radian})^2. \tag{3.11}$$

The constant length l can be estimated by equating the maximum velocity at $x = 0$, given by (3.5), to the maximum velocity in the impinging jet.

Alternatively, if the wall jet is formed by fluid flowing out radially, with uniform velocity U_0 and temperature T_0, from beneath a circular disc of radius a and at a distance h from the wall, then equation (2.8) may be evaluated at $x = a$ to give

$$F = \frac{U_0^3 h^2 a^2}{2T_0^2}. \tag{3.12}$$

In this case l can be estimated by requiring the maximum velocity at $x = a$, given by (3.5), to be U_0.

4. Temperature distribution

In order to determine the temperature distribution, the energy equation (2.3) must be solved for T. When the Prandtl number σ is unity, a particular solution of (2.3) is the Crocco relation

$$T + \frac{u^2}{2C_p} = A + Bu, \tag{4.1}$$

where A and B are constants. Since $u \to 0$ as $y \to \infty$, A must have the value T_∞. The value of B depends on the degree of heating in the initial jet. In particular the solution with $B = 0$ will be appropriate for a jet issuing from a reservoir of fluid maintained at the same temperature, T_∞, as the fluid outside the wall jet. In this case the heat transfer across the wall is seen to be zero. If we suppose the wall jet to be formed by fluid flowing out uniformly from beneath a circular disc as in § 3, then equation (4.1) can be evaluated at $x = a$, giving

$$B = \frac{T_0 + \frac{1}{2}(\gamma - 1)M_0^2 - 1}{U_0} \cdot T_\infty, \tag{4.2}$$

where γ is the ratio of the specific heats and $M_0 = U_0/a_\infty$, a_∞ being the velocity of sound outside the wall jet.

We shall now seek solutions of the energy equation for arbitrary Prandtl number. The simple solutions, for Prandtl number unity, given by (4.1) occur as special cases of these more general solutions.

When the assumption $\mu \propto T$ is made, the energy equation takes the form given in equation (2.18), a linear equation for T. Since $\tilde{u}(\bar{x}, \eta)$ is known, it is convenient to change the independent variables again from $(\bar{x}, \bar{\psi})$ to $(\bar{x}, \eta)$, where η is defined by equation (3.6). To do this we have the transformation formulae

$$\left.\begin{aligned} \left(\frac{\partial}{\partial \bar{x}}\right)_{\bar{\psi}} &= \left(\frac{\partial}{\partial \bar{x}}\right)_{\eta} - \frac{3}{4}\frac{f}{f'}\frac{\bar{x}^2}{(\bar{x}^3 + l^3)}\left(\frac{\partial}{\partial \eta}\right)_{\bar{x}}, \\ \left(\frac{\partial}{\partial \bar{\psi}}\right)_{\bar{x}} &= \frac{1}{f'(\bar{x}^3 + l^3)^{1/4}}\left(\frac{\partial}{\partial \eta}\right)_{\bar{x}}. \end{aligned}\right\} \tag{4.3}$$

Substituting for $\tilde{u}$ from equation (3.5) the final form of the energy equation (2.3) is

$$\frac{\partial^2 T}{\partial \eta^2} - \sigma\left(\frac{4}{3}\frac{(\bar{x}^3 + l^3)}{\bar{x}^2} f' \frac{\partial T}{\partial \bar{x}} - f\frac{\partial T}{\partial \eta}\right) = -\sigma \frac{9}{16}\frac{U^2}{C_p T_\infty}\frac{f''^2}{(\bar{x}^3 + l^3)}. \tag{4.4}$$

This equation (4.4) is the form in which we shall study the energy equation. A boundary condition at the wall, $\eta = 0$, must be specified. We shall consider only the two cases of a perfectly conducting wall, over which the temperature is maintained at a constant value, and of a thermally insulated wall, at which the heat transfer is zero. The outer boundary condition is $\bar{T} = 1$. A condition at $\bar{x} = 0$ must also be specified. This is related to the temperature of the initial jet. When the solution for $\bar{T}$ has been found, the correspondence between η and the physical variable y may be obtained from equation (3.8).

A particular integral of equation (4.4) may be found in the form

$$\bar{T} = 1 + C_0(\bar{x}^3 + l^3)^{-1}\theta_0(\eta). \tag{4.5}$$

Equation (4.4) also has an infinity of complementary functions of the form

$$\bar{T}_n = C_n(\bar{x}^3 + l^3)^{-\alpha}\theta_n(\eta), \tag{4.6}$$

where θ_n satisfies the equation

$$\theta_n'' + \sigma(f\theta_n' + 4\alpha f'\theta_n) = 0. \tag{4.7}$$

By adding to the particular integral (4.5) suitable complementary functions of the type (4.6), the temperature conditions we wish to be able to prescribe can be satisfied.

The effects of viscous heating, wall temperature and initial heating will be discussed separately, and the solutions appropriate for both the required conditions at $\eta = 0$ will be determined.

Viscous heating

Let us first examine the temperature distribution due to viscous heating in the wall jet. As we have seen, we require a solution of equation (4.4) in the form (4.5), where, if we choose

$$C_0 = -\frac{9}{16}\frac{U^2}{C_p T_\infty}, \tag{4.8}$$

the equation to be satisfied by $\theta_0(\eta)$ is

$$\theta_0'' + \sigma(f\theta_0' + 4f'\theta_0) = \sigma f''^2, \tag{4.9}$$

where

$$\left.\begin{array}{lll} & \theta_0(\infty) = 0 & \\ \text{and either} & \theta_0(0) = 0 & \text{for constant wall temperature } T_\infty, \\ \text{or} & \theta_0'(0) = 0 & \text{for a thermally insulated wall.} \end{array}\right\} \tag{4.10}$$

When $\sigma = 1$, $\theta_0(\eta) = \frac{1}{2}f'^2(\eta)$ satisfies all the conditions (4.10), a result indicated by (4.1). For arbitrary σ, no solution of equation (4.9) has been found in closed terms. The equation has been integrated numerically for $\sigma = 0{\cdot}72$, the value appropriate for air.

When the wall jet is flowing over a thermally insulated wall, the wall temperature is, from equations (4.5) and (4.8)

$$\bar{T}_w = 1 - \frac{9}{16}\frac{U^2}{C_p T_\infty}\frac{\theta_0(0)}{(\bar{x}^3 + l^3)}. \tag{4.11}$$

The numerical integration gave $\theta_0(0) = 0{\cdot}0060$.

When the wall is maintained at a constant temperature T_∞, the rate at which heat is transferred across the wall, per unit area, is

$$Q_w = -\left(\lambda \frac{\partial T}{\partial y}\right)_{y=0} \tag{4.12}$$

$$= \frac{27}{64}\lambda_\infty \left(\frac{\nu_\infty^{13} x^4}{U^5 (x^3 + l^3)^7 C_p^4}\right)^{1/4} \theta_0'(0), \tag{4.13}$$

using equations (3.8), (4.5) and (4.8), where λ is the thermal conductivity. The numerical integration gave $\theta_0'(0) = 0{\cdot}0036$.

If $(T - T_\infty)/T_\infty \gg$ (Mach number)^2 at all points in the wall jet, then the effects of viscous heating may be neglected and the particular integral (4.5) may be taken as $\bar{T} = 1$.

Wall heating

To describe the effects on the temperature distribution of maintaining the wall at a constant temperature $T_w \neq T_\infty$, we require a complementary function (4.6) with $\alpha = 0$. Thus

$$\bar{T}_1 = (\bar{T}_w - 1)\theta_1(\eta), \tag{4.14}$$

where

$$\left.\begin{aligned} \theta_1(0) &= 1, \\ \theta_1(\infty) &= 0. \end{aligned}\right\} \tag{4.15}$$

The required solution of equation (4.7) is immediately obtained as

$$\theta_1(\eta) = \int_\eta^\infty \exp\left\{-\sigma \int_0^\eta f\, d\eta\right\} d\eta \Big/ \int_0^\infty \exp\left\{-\sigma \int_0^\eta f\, d\eta\right\} d\eta. \tag{4.16}$$

As shown by Glauert (1956), $f = g^2$, where $g' = \frac{1}{3}(1 - g^3)$, and hence

$$-\int_0^\eta f\, d\eta = \log(1 - g^3), \tag{4.17}$$

and equation (4.16) may be written

$$\theta_1 = \int_g^1 (1 - g^3)^{\sigma - 1}\, dg \Big/ \int_0^1 (1 - g^3)^{\sigma - 1}\, dg. \tag{4.18}$$

When $\sigma = 1$ this reduces to

$$\theta_1 = (1 - g). \tag{4.19}$$

When $\sigma \neq 1$, θ_1 may be represented as an incomplete beta function by writing $(1 - g^3) = t$ in equation (4.18), which then becomes

$$\theta_1 = \int_0^t t^{\sigma - 1}(1 - t)^{-2/3}\, dt \Big/ \int_0^1 t^{\sigma - 1}(1 - t)^{-2/3}\, dt$$

$$= B_t(\sigma, \tfrac{1}{3})/B(\sigma, \tfrac{1}{3}). \tag{4.20}$$

The contribution to the rate at which heat is transferred across the wall, per unit area, is given by

$$q_w = -\tfrac{3}{4}\lambda_\infty (T_w - T_\infty)\left(\frac{\nu_\infty x^4}{U(x^3 + l^3)^3}\right)^{1/4} \theta_1'(0), \tag{4.21}$$

from equations (3.8), (4.12) and (4.14). Expressing the beta function in terms of Γ functions, we find that $\theta_1'(0) = -0{\cdot}2861$.

Initial heating

When the jet is heated initially, we require another complementary function of the form (4.6),

$$\bar{T}_2 = C_2(\bar{x}^3 + l^3)^{-\alpha}\theta_2(\eta) \tag{4.22}$$

where $\theta_2(\eta)$ satisfies equation (4.7). The boundary conditions are

$$\theta_2(\infty) = 0 \tag{4.23}$$

and either $\theta_2(0) = 0$ for constant wall temperature, (4.24)

or $\theta_2'(0) = 0$ for a thermally insulated wall. (4.25)

The determination of α is an eigenvalue problem. We shall consider first the case of a thermally insulated wall. Integrating equation (4.7) with respect to η between the limits 0 and η, and using (3.3) and (4.25) we have

$$\theta_2' + \sigma\left\{\theta_2 f + (4\alpha - 1)\int_0^\eta f'\theta_2\, d\eta\right\} = 0. \tag{4.26}$$

On letting $\eta \to \infty$, equation (4.26) becomes, from (4.23),

$$(4\alpha - 1)\int_0^\infty f'\theta_2\, d\eta = 0. \tag{4.27}$$

Unless the integral in (4.27) is zero, which on physical grounds is unlikely, this shows that $\alpha = \frac{1}{4}$. With this value of α, equation (4.7) may be integrated in closed terms, using the result (4.17), to give

$$\theta_2 = (1 - g^3)^\sigma. \tag{4.28}$$

It follows that the contribution to the wall temperature is

$$\bar{T}_{2w} = C_2(\bar{x}^3 + l^3)^{-1/4}. \tag{4.29}$$

The value of the constant C_2, which depends on the initial conditions in the jet, is discussed later.

For a wall maintained at constant temperature, it may be verified that the solution of (4.7) satisfying the boundary conditions (4.23) and (4.24) is given by

$$\alpha = \frac{(3\sigma + 1)}{8\sigma}, \tag{4.30}$$

$$\theta_2 = g(1 - g^3)^\sigma. \tag{4.31}$$

When $\sigma = 1$, these equations become $\alpha = \frac{1}{2}$, $\theta_2 = \frac{3}{2}f'$, in accord with the term Bu in equation (4.1). The contribution to the rate at which heat is transferred across the wall, per unit area, is given by

$$q_w = -\tfrac{3}{4}\lambda_\infty T_\infty C_2\left[\left(\frac{\nu_\infty}{U}\right)^{(11\sigma+3)/2\sigma}\frac{x^4}{(x^3 + l^3)^{(9\sigma+1)/2\sigma}}\right]^{1/4}\theta_2'(0), \tag{4.32}$$

from equations (3.8), (4.12) and (4.22), where, from (4.31), $\theta_2'(0) = \frac{1}{3}$.

An estimate of the constant C_2 may be obtained as follows. The maximum values of θ_2 are 1 in equation (4.28), and 0·4740 in equation (4.31), when $\sigma = 0{\cdot}72$. Hence, by requiring the maximum temperature at $\bar{x} = 0$

(or $\bar{x} = \bar{a}$ when the jet flows from beneath a circular disc) to be the excess of total temperature at this point in the physical flow, the value of C_2 may be roughly determined.

Since the equation (4.4) is linear, we may construct a solution which is any linear combination of the solutions obtained above, and thus we are able to deal with a wall jet of arbitrary Mach number, wall temperature and initial heating. When the wall is maintained at constant temperature we require (4.5), (4.14) and (4.22), the total rate at which heat is transferred across the wall, per unit area, being given by a combination of (4.13), (4.21) and (4.32). For a thermally insulated wall (4.5) and (4.22) are the appropriate solutions, the wall temperature being given by a combination of (4.11) and (4.29).

5. Results

The results obtained in § 3 and § 4 are presented in figures 1–5. Figure 1 shows the velocity function $f'(\eta)$ whilst figures 2–5 show the temperature distribution across the jet and the resulting dependence of the geometrical distance y on η for all the cases considered above. This dependence of y on η is given directly by equation (3.8) when the temperature distribution is known. Since the velocity u is a function of the mass flux ψ, a decrease

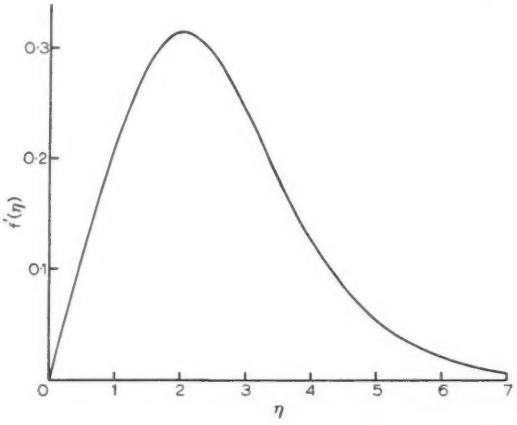

Figure 1. The velocity function $f'(\eta)$.

of ρ (corresponding to an increase of T) causes a physical broadening of the wall jet, and an increase of ρ causes a narrowing. The broadening or narrowing occurs most where $|T - T_\infty|$ is greatest. Since, in general, the temperature distribution across the wall jet changes as the jet develops, it follows that even for our similarity solution the geometrical form of the velocity profile is not independent of x, as it is in the corresponding incompressible flow.

The effect of viscous heating is shown in figure 2 where the temperature distributions across the wall jet, for a thermally insulated wall and for a wall maintained at constant temperature T_∞, are given from equation (4.5). The simple Crocco relation for $\sigma = 1$, given by equation (4.1) with $B = 0$, is included for comparison. In this case the total energy in the wall jet is constant, so the effect of a decrease in velocity is exactly balanced by an

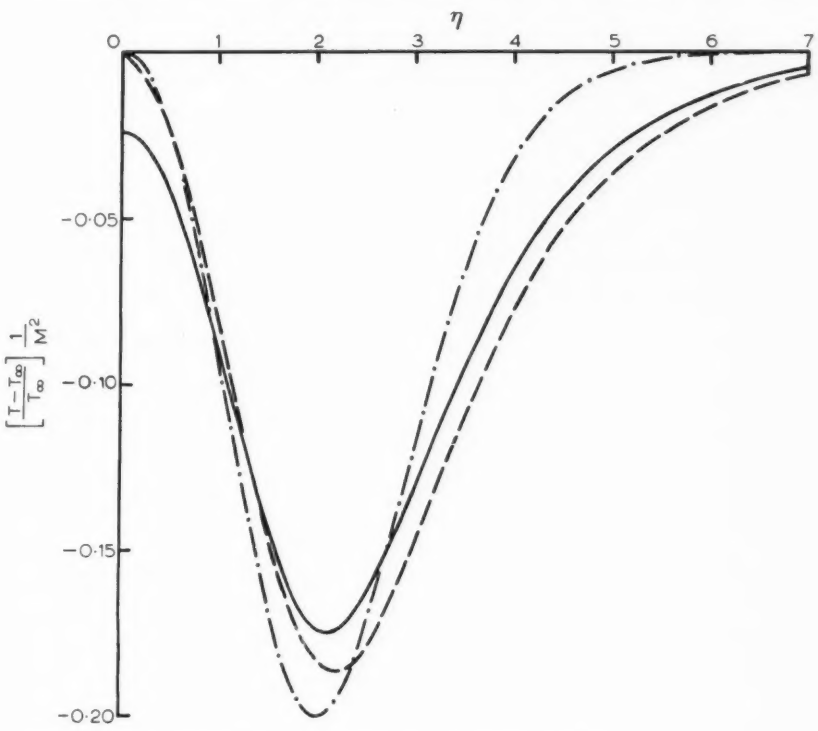

Figure 2. The temperature distribution due to viscous heating;
———— thermally insulated wall,
— — — — wall maintained at constant temperature T_∞,
—·—·—·— Crocco solution for $\sigma = 1$.

increase in temperature. When the wall is maintained at a temperature T_∞ there is no heat transfer across the wall and hence both conditions at the wall are satisfied together. For $\sigma = 0{\cdot}72$ this energy balance is not maintained, and a solution for each of the wall conditions is required; qualitatively, however, the results are similar to the case $\sigma = 1$. Figure 3 shows how the wall jet is narrowed in the region of higher velocity, in comparison with the profile at low Mach number. The Mach number M is here defined as the ratio of the maximum velocity across the wall jet to the velocity of sound outside the wall jet.

When the wall is maintained at a constant temperature $T_w \neq T_\infty$, the contributions to the temperature distribution and to the variation of y with η are as shown in figure 4. These results were obtained by numerically integrating equation (4.20) for the value $\sigma = 0{\cdot}72$. As we might expect, the temperature increment is greatest near the wall, gradually falling to zero with increasing distance from the wall.

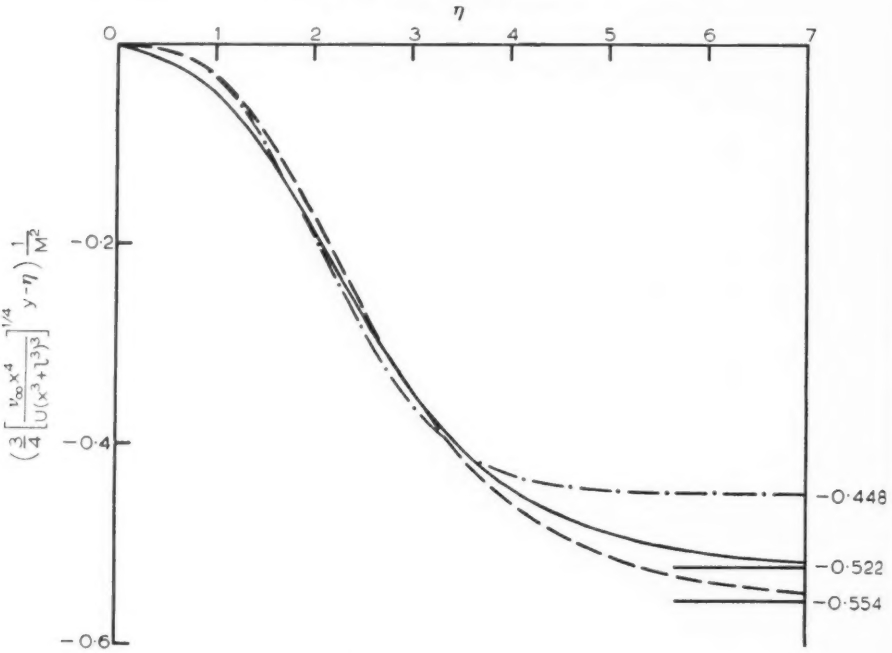

Figure 3. The variation of y with η due to viscous heating;
———— thermally insulated wall,
— — — — — wall maintained at constant temperature T_∞,
—·—·—·— Crocco solution for $\sigma = 1$.

Figure 5 depicts the contribution to the temperature distribution and to the variation of y with η when heat is added initially to the jet, for the two cases of a thermally insulated wall and a perfectly conducting wall. For a thermally insulated wall the effects of the added heat are similar to those shown in figure 4, though the variation with distance from the axis is different. For a perfectly conducting wall, the effects of the added heat are mainly confined to the faster moving regions of the wall jet.

As we have seen in § 4, when a hot wall jet flows at high speeds over a heated wall, the temperature distribution can be obtained by taking a suitable linear combination of the distributions that have been considered above. Similarly, we see from equation (3.8) that to obtain the total variation of y with η we need the same combination of the appropriate distributions shown

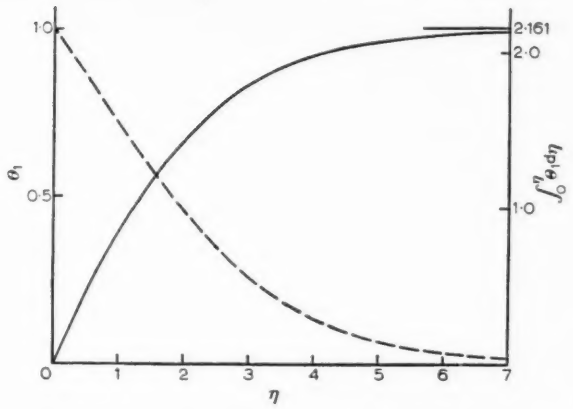

Figure 4. Contributions to the temperature distribution (θ_1 — — — —), and to the variation of y with $\eta\left(\int_0^\eta \theta_1\, d\eta \text{ ————}\right)$, when the wall is maintained at constant temperature $T_w \neq T_\infty$.

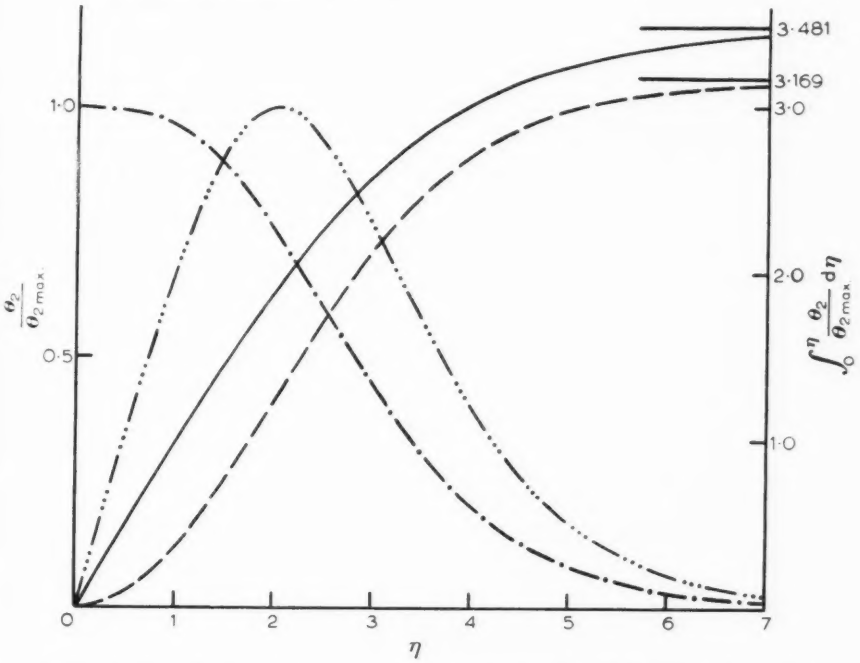

Figure 5. Contributions to the temperature distribution ($\theta_2/\theta_{2\max}$) and to the variation of y with $\eta\left(\int_0^\eta \theta_2/\theta_{2\max}\, d\eta\right)$, when heat is added to the jet initially;
—·—·—·—, ———— for a thermally insulated wall respectively,
—···—···—, — — — — and for constant wall temperature respectively.

in figures 3–5, the total increment in y being the sum of the increments of y in the separate distributions. As the distance from the axis of the jet increases, the Mach number decreases and the added heat is diffused away until their effects on the temperature eventually become negligible. We see from equation (4.5) that the effects of viscous heating, which fall off like $(x^3+l^3)^{-1}$, decrease faster than the effects of added heat which, from (4.22), behave like $(x^3+l^3)^{-\alpha}$, where $\alpha = 0{\cdot}25$ for a thermally insulated wall, and $\alpha = 0{\cdot}548$ for a perfectly conducting wall when $\sigma = 0{\cdot}72$. However, the effect of a wall temperature $T_w \neq T_\infty$ does not decay with increasing x. As a result the form of the velocity profile changes as the wall jet develops, and only when the effects of viscous heating and added heat have become negligible is geometrical similarity achieved, the final velocity profile being the incompressible one unless the wall is maintained at a temperature different from T_∞.

The author is indebted to Mr M. B. Glauert for suggesting this problem and for his encouragement at all times, also to the Department of Scientific and Industrial Research for a maintenance grant whilst this work was being carried out.

References

Glauert, M. B. 1956 *J. Fluid Mech.* **1**, 625.

Glauert, M. B. 1957 *Symposium uber Grenzschichtforschung*, edited by H. Görtler. Springer-Verlag.

Kármán, Th. von & Tsien, H. S. 1938 *J. Aero. Sci.* **5**, 227.

Mises, R. von 1927 *Z. angew. Math. Mech.* **7**, 425.

A two-dimensional air intake in a sonic stream

By L. E. FRAENKEL
Aeronautics Department, Imperial College, London

(*Received* 20 *March* 1958)

SUMMARY

In this paper transonic small-disturbance theory is applied to a simplified model of the flow near the front of a ducted body. The body is assumed to consist simply of two parallel flat plates which extend from the inlet station to infinity downstream. The velocity far upstream is sonic, and the velocity far downstream in the duct, which is assumed to be known, is slightly subsonic. Air is therefore 'spilled' around the intake edges. An analytic solution is found for the resulting flow field up to the 'limiting Mach wave', and asymptotic solutions are found for the supersonic flow and for the shock wave far from, and near, the intake edges. The pressure distribution along the outside walls is then known at both ends, and its computation is completed by an empirical procedure. Distributions of pressure along the centre-line and along the inside and outside walls are shown. These results may be used to compute the drag of sharp-edged intakes with a very small frontal area.

1. INTRODUCTION

Under most flight conditions, the intakes of high-speed aircraft 'spill' air: that is, the mass-flow requirement of the engine is such that the entering stream-tube of air has a cross-sectional area, far upstream, which is smaller than the area of the hole at the front of the body. As a result, air is diverted around the intake edge, and at high subsonic and at all supersonic flight speeds the flow field is of mixed type (see figure 1). In the subsonic case there are regions of supersonic flow near the edge and, possibly, further back along the external wall of the intake. In the supersonic case there is a subsonic region which is bounded by the bow shock wave, by a sonic surface from this shock to the intake edge, and by the walls of the duct. As far as the external flow is concerned, the outer wall of the intake acts somewhat like the upper surface of an aerofoil, increasing spillage corresponding roughly to increasing incidence. These mixed intake flows have been the subject of considerable experimental work, and various empirical theories have been developed to predict the effect of spillage on the drag of aircraft, but (as far as the writer is aware) nothing approaching a theoretical description of the flow field has been developed.

In the present paper we study the simplest possible example of such a flow. The intake is assumed to be two-dimensional and to consist simply

of two parallel, semi-infinite, flat plates. Alternatively, the upper half of this configuration may be interpreted as a simplified model of one of the side intakes found on some aircraft. The final velocity in the duct (which in practice is known from the air mass flow of the engine) is assumed to be only slightly less than that in the free stream, so that perturbations from a uniform stream are small, except in the neighbourhood of the intake edge. If the free-stream Mach number is near one, transonic small-disturbance theory may then be applied, and the central problem, in which the free stream is sonic, is considered here.

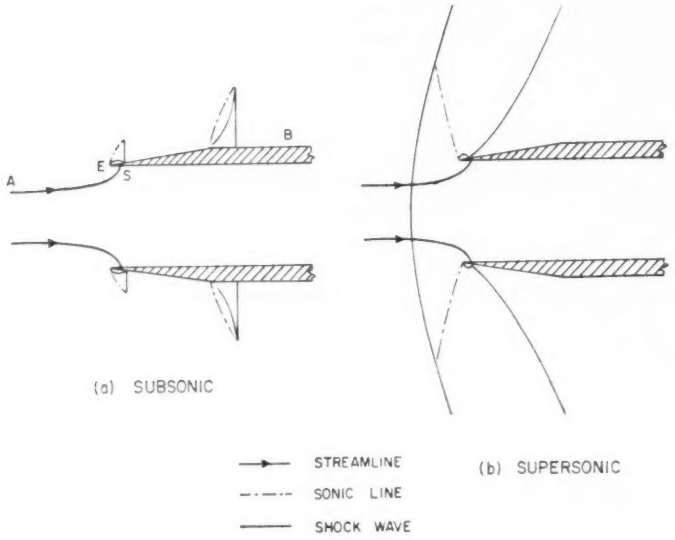

Figure 1.

It is usual in intake work to use a definition of drag which for plane flow becomes

$$D = 2\int (P-P_0)\,dY,$$

where P_0 denotes the pressure in the free stream, and the integral is taken over the entire length of the dividing streamline, $ASEB$ in figure 1. This definition is consistent with the usual definition of engine thrust. It is natural to consider the drag as the sum of two parts: (i) the 'pre-entry drag', which is the contribution of the upstream part, AS, of the dividing streamline, and can be calculated from the known change in momentum and pressure of the internal flow; and (ii) the 'cowl drag', which in the case of a flat-plate intake is simply the force on the edge E. In incompressible flow theory these two drags precisely cancel each other, as might be expected, regardless of whether exact or small-disturbance theory is used. In the

present transonic problem, however, the singularity in velocity at the edge is rather weak, and the edge force is found to be zero. Both in incompressible and in transonic flow, the edge flow has, of course, the same character as that at the leading edge of a lifting flat plate, for which the transonic solution has been found by Guderley (1954). Hence the result of zero edge force, which was not discussed by Guderley, applies to that problem also.

Some further information about cowl drag can also be obtained from the present model. Consider a wedge intake (that is, a two-dimensional intake of the type shown in figure 1) in a sonic stream. For moderate wedge angles the flow up to the 'limiting Mach wave' (figure 2 (*a*)) is the same as that past a flat-plate intake. (The significance of the limiting Mach wave will become clear from what follows.) Further, if the wedge angle is of even smaller order than the slope of the dividing streamline ahead of the intake, then the dominant part of the pressure acting on the wedge face is that on the outer wall of the flat-plate intake. Hence for such slender-wedge intakes a first approximation to the (negative) cowl drag can be found from the present solution.

2. The equations of transonic flow

Let X, Y be Cartesian coordinates such that a free stream of near-sonic velocity U_0 and of Mach number M_0 flows in the direction of increasing X. Let the velocity at a point in the field be (U_0+U_0U', U_0V'). The fluid is assumed to be a perfect gas whose specific-heat ratio is γ. Then for small disturbances the equations of transonic flow may be written

$$\left.\begin{aligned}(1-M_0^2-\Gamma U')U'_X+V'_Y=0, \qquad (\Gamma=(\gamma+1)M_0^2),\\ U'_Y-V'_X=0,\end{aligned}\right\} \tag{2.1}$$

where subscripts denote partial derivatives, and where we have adopted Spreiter's (1954) version of these equations. In order to work with variables whose magnitude is $O(1)$, and to express the equations in canonical form, we introduce a small parameter δ, such that $V' \sim O(\delta)$, and a length L, representative of the lateral extent of the field, and make the transformation

$$\left.\begin{aligned}X=L(\delta\Gamma)^{1/3}x, \qquad & Y=Ly,\\ U'=(1-M_0^2)\Gamma^{-1}+\delta^{2/3}\Gamma^{-1/3}u(x,y), \qquad & V'=\delta\, v(x,y).\end{aligned}\right\} \tag{2.2}$$

Then equations (2.1) become

$$\left.\begin{aligned}-uu_x+v_y=0,\\ u_y-v_x=0,\end{aligned}\right\} \tag{2.3}$$

with the boundary condition

$$u\to(M_0^2-1)(\delta\Gamma)^{-2/3}=K, \quad v\to 0, \quad \text{as } x,y\to\infty.$$

Here K is the transonic similarity parameter.

If the roles of the independent and dependent variables are now interchanged, equations (2.3) become

$$x_u - uy_v = 0,$$
$$x_v - y_u = 0,$$

so that the Legendre contact potential, $\chi = \int (x\,du + y\,dv)$, satisfies the Tricomi equation

$$\chi_{uu} - u\chi_{vv} = 0. \tag{2.4}$$

The characteristic curves of this equation are $v = \frac{2}{3}u^{3/2} + \text{constant}$, $(u > 0)$: hence we introduce the variables $\zeta = \frac{2}{3}u^{3/2}$ in the hyperbolic half-plane, and $w = -u$, $z = \frac{2}{3}w^{3/2}$ in the elliptic half-plane. Then the equation becomes

$$\chi_{\zeta\zeta} + \frac{1}{3\zeta}\chi_\zeta - \chi_{vv} = 0, \qquad \chi_{zz} + \frac{1}{3z}\chi_z + \chi_{vv} = 0. \tag{2.5}$$

Two types of elementary solution of this equation, and the relations between them, are discussed in Appendix I.

To the lowest order, the stream function is $\Psi = \int \rho_0 U_0\,dY$, so that $y\,(= \chi_v)$ may be taken constant on streamlines. The variable y also satisfies the Tricomi equation.

3. Solution of the intake problem up to the limiting Mach wave

Figure 2 shows qualitatively the physical and hodograph planes of the present problem. The origin of coordinates is taken at the intake edge, and the length L in (2.2) is taken as half the distance between the two flat plates. The final velocity in the duct being U_1, we define δ by

$$\delta^{2/3}\Gamma^{-1/3} = \frac{U_0 - U_1}{U_0}. \tag{3.1}$$

By continuity, the overall change in width of the entering streamtube is then $O(\delta^{1/3})$, and this occurs essentially over an X-length of $O(\delta^{1/3})$, so that the slope of the dividing streamline is $O(\delta)$.

The physical and hodograph fields may be described as follows. The origin in the physical plane maps to infinity in the hodograph plane, and vice versa. The most important streamline is the dividing streamline, $y = 0$. As this approaches the stagnation point, S, it has positive slope $(v > 0)$ and the velocity is reduced $(w > 0)$. At S $(x = 0, y = 0, w = \infty, v = 0$ on the approximate theory) the dividing streamline branches; one part, $y = 0-$, running along the inner wall SI, while the other, $y = 0+$, expands at infinite velocity about the edge E. In fact it overexpands, as do all the external streamlines, and ultimately attains negative slope $(v < 0)$. Recompression and the return to zero slope occur first through a shock, and then continuously. The shock corresponds to a jump in position in the hodograph plane, along the appropriate shock polar, and the subsequent flow maps on to a second sheet of the hodograph, which is here shown superposed on the first.

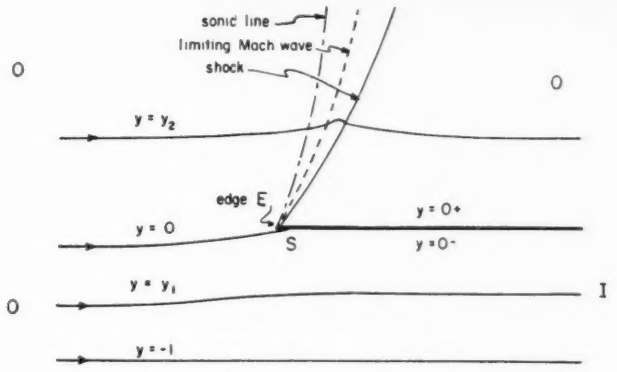

(a) PHYSICAL PLANE

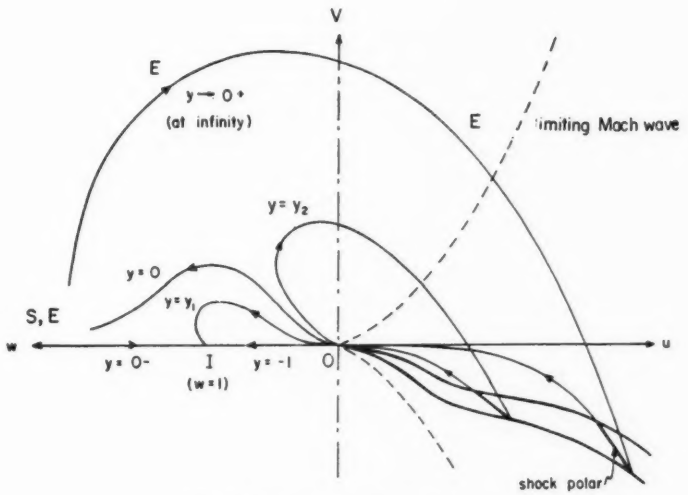

(b) HODOGRAPH PLANE

Figure 2.

The central streamline of the intake, $y = -1$, proceeds from O to I at zero slope. The internal flow is contained between $y = 0$, $y = 0-$, and $y = -1$; the external flow between $y = 0$, $y = 0+$, and the shock. The limiting Mach wave is the last of the expansion family emanating from the edge to meet the sonic line; hence disturbances downstream of this line do not affect the subsonic field. It maps on to $v = \zeta$.

In this section we consider only the flow up to the limiting Mach wave, that is, the problem in $\mathscr{R}(v-\zeta) \geqslant 0$. This is essentially a boundary value problem of the Tricomi type. The solution is constructed in two parts as follows ($\chi = \chi_1 + \chi_2$).

(i) The potential χ_1 is to represent the far field of the physical plane, that is, the flow near O. We require:

$$\left.\begin{aligned} &y_1 = \chi_{1v} \to \infty \text{ as } u, v \to 0, \\ &y_1 \to 0 \text{ as } u, v \to \infty, \\ &y_1 = 0 \text{ on } v = 0, \ w > 0, \\ &y_1 \text{ finite on } v = \zeta, \ v > 0, \end{aligned}\right\} \tag{3.2}$$

and a one-to-one mapping from the hodograph to the physical plane. This 'free stream singularity' for any symmetrical body has been found by Frankl (1947) and Guderley (1948). It is one of the similarity solutions $\chi = \zeta^{-m} fn(\alpha)$, where $\alpha = v^2/\zeta^2$ (Appendix I). In the present case $m = \frac{2}{3}$, and the $fn(\alpha)$, which is a hypergeometric function, reduces to elementary form. In fact

$$\chi_1 = -\mu \frac{\sqrt{3}}{\pi} \zeta^{1/3} \int_0^\infty e^{-\lambda v} K_{1/3}(\lambda\zeta)\, d\lambda, \tag{3.3a}$$

$$= -\mu 2 z^{-2/3} \frac{\cosh\{\frac{1}{3}\cosh^{-1}\sqrt{(1-\alpha)}\}}{\sqrt{(1-\alpha)}}, \qquad (v \geqslant 0, \quad \alpha \leqslant 0), \tag{3.3b}$$

$$= -\mu 2 \zeta^{-2/3} \frac{\sinh\{\frac{1}{3}\sinh^{-1}\sqrt{(\alpha-1)}\}}{\sqrt{(\alpha-1)}}, \qquad (v \geqslant 0, \quad \alpha \geqslant 1), \tag{3.3c}$$

where μ is a constant to be determined in any particular problem. Although it is irrelevant at this stage, we also note that

$$\chi_1 = -\mu 2 \zeta^{-2/3} \frac{\sin\{\frac{1}{3}\sin^{-1}\sqrt{(1-\alpha)}\}}{\sqrt{(1-\alpha)}}, \qquad (0 \leqslant \alpha \leqslant 1), \tag{3.3d}$$

where $\sin^{-1}\sqrt{(1-\alpha)}$ varies from 0 to π as v varies from ζ to $-\zeta$.

To formulate precisely the problem for χ_2, we observe that χ_1 gives velocities near the edge E which are altogether too large, and must be removed by χ_2. Indeed if χ_1 were to be the dominant term of the complete solution near E, this would result in an infinite drag, as will be shown in § 6.

(ii) The potential χ_2 is introduced to satisfy the boundary conditions on the body:

$$\left.\begin{aligned} &y_2 = -1 \text{ on } v = 0, \qquad 0 \leqslant w < 1, \\ &\quad = 0 \quad \text{on} \quad v = 0, \qquad w > 1, \\ &y_2 + y_1 \sim o(y_1) \quad \text{as } w, v \to \infty, \\ &y_2 \text{ is finite on } v = \zeta. \end{aligned}\right\} \tag{3.4}$$

Although μ is as yet unknown, the second of these conditions does fix the order of magnitude of y_2 at infinity in the hodograph plane. It is shown in Appendix II that (3.4) determine a unique boundary value problem in the sense of Tricomi.

We seek a solution of form

$$\chi_2 = -\frac{\sqrt{3}}{\pi}\zeta^{1/3}\int_0^\infty e^{-\lambda v}K_{1/3}(\lambda\zeta)f(\lambda)\frac{d\lambda}{\lambda}, \tag{3.5}$$

where the $I_{1/3}$-solution has been omitted because it leads, in general, to a singularity on the limiting Mach wave. (This step is justified rigorously by the fact that (3.5) will satisfy all the boundary conditions, and is therefore the unique solution.) $f(\lambda)$ is then determined from the integral equation

$$y_2(z,0) = z^{1/3}\int_0^\infty [J_{1/3}(\lambda z)+J_{-1/3}(\lambda z)]f(\lambda)\,d\lambda = -1, \quad \tfrac{2}{3} > z \geqslant 0,$$
$$= 0, \quad z > \tfrac{2}{3},$$

by means of the Mellin transform

$$\bar{\phi}(p) = \int_0^\infty z^{p-1}\phi(z)\,dz$$

(see Appendix I for further details). The integral equation transforms to

$$[\bar{J}_{1/3}(p+\tfrac{1}{3})+\bar{J}_{-1/3}(p+\tfrac{1}{3})]\bar{f}(-p+\tfrac{2}{3}) = -(\tfrac{2}{3})^p/p,$$

where (Erdélyi 1954)

$$\bar{J}_{1/3}(p)+\bar{J}_{-1/3}(p) = -\frac{\sin\frac{1}{2}\pi p\cos\frac{1}{6}\pi}{\cos\pi p-\cos\frac{1}{3}\pi}\frac{2^{p+1}}{\Gamma(-\frac{1}{2}p+\frac{5}{6})\Gamma(-\frac{1}{2}p+\frac{7}{6})}, (\tfrac{1}{3} < \mathscr{R}p < \tfrac{3}{2}). \tag{3.6}$$

Hence, with $-p+\frac{2}{3} = q$, we find after a little reduction that

$$\bar{f}(q) = (\tfrac{2}{3})^{2/3-q}\frac{2^{q-3}}{\pi}\frac{\cos\pi q+\cos\frac{1}{3}\pi}{\cos\frac{1}{2}\pi q\cos\frac{1}{6}\pi}\Gamma(\tfrac{1}{2}q-\tfrac{1}{3})\Gamma(\tfrac{1}{2}q+\tfrac{1}{3}), \quad (|\mathscr{R}q| < 1), \tag{3.7a}$$

and

$$f(\lambda) = \frac{1}{2\pi i}\int_{c-i\infty}^{c+i\infty}\lambda^{-q}\bar{f}(q)\,dq, \quad (|c| < 1). \tag{3.7b}$$

The only singularities of $\bar{f}(q)$ are simple poles at

$$q = \pm(2n+1), \qquad n = 0, 1, 2, \ldots,$$

the poles of the Γ-functions being removed by zeros of $\cos\pi q+\cos\frac{1}{3}\pi$. The evaluation of the contour integral in (3.7 b) is therefore straightforward: we close the contour with a large semi-circle in $\mathscr{R}q < 0$, whose contribution vanishes in the limit for all finite λ, because of the strong convergence induced by the Γ-functions in (3.7 a). Then

$$f(\lambda) = -\left(\frac{2}{3}\right)^{2/3}\frac{1}{\sqrt{3}}\sum_{n=0}^{\infty}(-)^n\left(\frac{\lambda}{3}\right)^{2n+1}\frac{1}{\Gamma(n+\frac{7}{6})\Gamma(n+\frac{11}{6})}, \tag{3.8a}$$

$$= -\left(\frac{2}{3}\right)^{2/3}\frac{2\sqrt{3}}{5\pi}\lambda+\left(\frac{2}{3}\right)^{2/3}\frac{8\sqrt{3}}{5.7.11.\pi}\lambda^3+\ldots. \tag{3.8b}$$

Now consider χ_2. If the substitution $\tilde{g} = -(\sqrt{3}/\pi)\bar{f}$ is made in equation (I.8), and the resulting integral is evaluated by contour integration, χ_2 is given by various series of hypergeometric functions. However, we are primarily interested in $x(w,0)$, which gives the pressure distribution along the centre-line and the inner wall of our intake. Now on $v = 0$

the hypergeometric functions take on simple values, or alternatively (3.5), (3.6) and (3.7a) may be used directly. In fact (3.5) may be written

$$\tilde{\chi}_2(-q-\tfrac{1}{3},0) = -[\tilde{J}_{1/3}(-q)+\tilde{J}_{-1/3}(-q)]\tilde{f}(q), \quad (-1<\mathscr{R}q<-\tfrac{1}{3}),$$

so that, substituting from (3.6) and (3.7a) and inverting, we have

$$\chi_2(z,0) = -\frac{1}{6}\frac{1}{2\pi i}\int_{c-i\infty}^{c+i\infty}\left(\frac{3}{2}z\right)^{q+1/3}\tan\tfrac{1}{2}\pi q\,\frac{\cos\pi q+\cos\frac{1}{3}\pi}{\cos\pi q-\cos\frac{1}{3}\pi}\times$$
$$\times\frac{\Gamma(\frac{1}{2}q-\frac{1}{3})\Gamma(\frac{1}{2}q+\frac{1}{3})}{\Gamma(\frac{1}{2}q+\frac{5}{6})\Gamma(\frac{1}{2}q+\frac{7}{6})}\,dq,$$

$$x_2(w,0) = \frac{1}{2}\frac{1}{2\pi i}\int_{c-i\infty}^{c+i\infty} w^{3q/2-1/2}\tan\tfrac{1}{2}\pi q\,\frac{\cos\pi q+\cos\frac{1}{3}\pi}{\cos\pi q-\cos\frac{1}{3}\pi}\times$$
$$\times\frac{\Gamma(\frac{1}{2}q-\frac{1}{3})\Gamma(\frac{1}{2}q+\frac{1}{3})}{\Gamma(\frac{1}{2}q+\frac{1}{6})\Gamma(\frac{1}{2}q+\frac{5}{6})}\,dq, \quad (-1<c<\tfrac{1}{3}). \tag{3.9}$$

The last integrand has simple poles at

$$q = \pm(2n+1), \quad 2n+\tfrac{1}{3}, \quad 2n+\tfrac{5}{3}, \qquad \text{where } n = 0, 1, 2, \ldots,$$

and for $w \gtrless 1$ we may use large semi-circles in $\mathscr{R}q \lesssim 0$, respectively. Then for $w > 1$,

$$\left.\begin{aligned} x_2(w,0) &= \frac{1}{\pi}\sum_{n=0}^{\infty} a_n\, w^{-3n-2}. \\ \text{where} \\ a_n &= \frac{\Gamma(n+\frac{4}{3})\Gamma(n+\frac{2}{3})}{\Gamma(n+\frac{7}{6})\Gamma(n+\frac{11}{6})} \sim \frac{1}{n} - \frac{3}{4n^2} + \ldots \quad \text{for } n\to\infty, \\ a_0 &= \tfrac{4}{5}\sqrt{3}\,; \end{aligned}\right\} \tag{3.10a}$$

and for $w < 1$,

$$\left.\begin{aligned} x_2(w,0) &= \frac{1}{3\pi}\sum_{n=0}^{\infty}(b_n+c_n w+d_n w^2)w^{3n}, \\ \text{where} \\ b_n &= \frac{\Gamma(n-\frac{1}{6})\Gamma(n+\frac{1}{2})}{\Gamma(n+\frac{1}{3})\Gamma(n+1)} \sim \frac{1}{n} + \frac{1}{12n^2} + \ldots \quad \text{for } n\to\infty, \\ c_n &= \frac{\Gamma(n+\frac{1}{6})\Gamma(n+\frac{5}{6})}{\Gamma(n+\frac{2}{3})\Gamma(n+\frac{4}{3})} \sim \frac{1}{n} - \frac{1}{4n^2} + \ldots, \\ d_n &= \frac{\Gamma(n+\frac{1}{2})\Gamma(n+\frac{7}{6})}{\Gamma(n+1)\Gamma(n+\frac{5}{3})} \sim \frac{1}{n} - \frac{7}{12n^2} + \ldots. \end{aligned}\right\} \tag{3.10b}$$

The asymptotic forms of the coefficients show that these series (which could also be written as *generalized* hypergeometric functions) converge rapidly except near $w = 1$, and that they diverge at $w = 1$. However, the singular part of the function is easily recognized and removed from the series. Equation (3.10a) may be written

$$\pi w^2 x_2(w,0) = -\log(1-w^{-3}) - \tfrac{3}{4}[(1-w^{-3})\log(1-w^{-3})+w^{-3}] +$$
$$+\sum_{n=0}^{\infty}\left(a_n - \frac{1}{n} + \frac{3}{4n(n-1)}\right)w^{-3n}, \tag{3.11}$$

where it is to be understood that the terms $-(1/n)$ and $3/\{4n(n-1)\}$ are to be included only for $n \geqslant 1$ and for $n \geqslant 2$, respectively. Equation (3.11) displays explicitly the logarithmic singularity of x (which corresponds to an exponential decay of the excess velocity in the duct), and the new series converges at $w = 1$ like $\sum n^{-3}$. Equation (3.10 b) can be put into a similar form.

It remains to find the constant μ, which determines the scale of the far-field solution χ_1: to this end we consider the flow at E $(w, v \to \infty)$. A suitable series for χ_2, as $v \to \infty$, is obtained by expanding $f(\lambda)$ in ascending powers of its argument:

$$\chi_2 = \frac{\sqrt{3}}{\pi}\zeta^{1/3}\int_0^\infty e^{-\lambda v}K_{1/3}(\lambda\zeta)\left[\left(\frac{2}{3}\right)^{2/3}\frac{2\sqrt{3}}{5\pi} - \right.$$
$$\left. -\left(\frac{2}{3}\right)^{2/3}\frac{8\sqrt{3}}{5.7.11.\pi}\lambda^2 + \ldots\right] d\lambda. \quad (3.12)$$

Applying the condition

$$\chi_2 + \chi_1 \sim o(\chi_1) \quad \text{for } v \to \infty,$$

which follows from the requirement of finite drag, and using (3.3 a) for χ_1, we obtain

$$\mu = \left(\frac{2}{3}\right)^{2/3}\frac{2\sqrt{3}}{5\pi}. \quad (3.13)$$

The asymptotic value of the complete solution near the edge E is now given by the second term of (3.12), and may be written

$$\chi_E = \left(\frac{2}{3}\right)^{2/3}\frac{8\sqrt{3}}{5.7.11.\pi}\frac{\partial^2}{\partial v^2}\left(\frac{\chi_1}{\mu}\right). \quad (3.14)$$

This is an elementary function which can be found from equations (3.3 b) to (3.3 d).

A more revealing (but less rigorous) method of evaluating μ is the following. The condition at the stagnation point S may be written

$$x = 0 \quad \text{at} \quad w = \delta^{-2/3}\Gamma^{1/3}, \qquad v = 0.$$

Since w is large, the leading term of an asymptotic series for $x_2(w, 0)$ suffices, and this is given by the first term of (3.10 a). Thus we require

$$x_1 + x_2 \sim -\mu 2\left(\frac{3}{2}\right)^{2/3}w^{-2} + \frac{4\sqrt{3}}{5\pi}w^{-2} = 0 \quad \text{at} \quad w = \delta^{-2/3}\Gamma^{1/3}.$$

In other words, as $w \to \infty$ on $v = 0$, x should $\to 0$ as rapidly as possible, in order that the stagnation point of the exact hodograph be simulated as closely as possible. This requirement leads to the same value of μ as before.

4. The far field and the edge field in the supersonic region

The far-field potential χ_1 and the edge-field potential χ_E are both similarity solutions up to the limiting Mach wave. Barish & Guderley (1953) have demonstrated that when the initial solution is a similarity one, the flow continues analytically to the shock wave, which is itself a similarity curve, and that the solution behind the shock, while a different function, has the same similarity as that before the shock. However, Barish &

Guderley, who studied plane and axi-symmetric flows simultaneously, used a non-linear differential equation associated with the flow in the physical plane, and had to integrate this equation numerically to obtain their results.

In this paper we prefer to work in the hodograph plane, where our asymptotic solutions are elementary functions, both before and after the shock. The only numerical work required will be to find the roots of certain algebraic equations, which provide the constants in the solutions.

In place of α we introduce the variable

$$\xi = \sin^{-1}(1-\alpha)^{1/2} = \sin^{-1}\frac{(\zeta^2 - v^2)^{1/2}}{\zeta},$$

which increases from 0 to π as v decreases from ζ to $-\zeta$. The upstream solutions are both of form

$$\left.\begin{aligned} &\chi = u^{-n} f n(\xi), && (n = \tfrac{3}{2}m), \\ &x = u^{-n-1} k_a f_a(\xi), && y = u^{-n-3/2} k_a g_a(\xi), \end{aligned}\right\} \tag{4.1}$$

and the solutions downstream of the shock will be written

$$x = u^{-n-1} k_b f_b(\eta), \qquad y = u^{-n-3/2} k_b g_b(\eta), \tag{4.2}$$

where

$$\eta = \xi - \tfrac{1}{2}\pi.$$

f_b and g_b are determined by the similarity index n, and by the boundary condition $y = 0$ on $\eta = 0$: they are, in fact, hypergeometric functions which again reduce to elementary form.

For the far field, by (3.3 d):

$$\left.\begin{aligned} n &= 1, \qquad k_a = \frac{2\sqrt{3}}{5\pi}, \\ f_a(\xi) &= \frac{2\sin\tfrac{1}{3}\xi}{\sin\xi} - \cos\xi\, g_a(\xi), \\ g_a(\xi) &= \frac{-\sin\tfrac{4}{3}\xi + 2\sin\tfrac{2}{3}\xi}{\sin^3\xi}, \\ f_b(\eta) &= \frac{2\cos\tfrac{1}{3}\eta}{\cos\eta} + \sin\eta\, g_b(\eta), \\ g_b(\eta) &= \frac{\sin\tfrac{4}{3}\eta + 2\sin\tfrac{2}{3}\eta}{\cos^3\eta}, \end{aligned}\right\} \tag{4.3}$$

and for the edge field, by (3.14):

$$\left.\begin{aligned} n &= 4, \qquad k_a = \frac{\sqrt{3}}{5\,.\,7\,.\,11\,.\,\pi}, \\ f_a(\xi) &= \frac{8(5\sin\tfrac{7}{3}\xi - 14\sin\tfrac{5}{3}\xi + 35\sin\tfrac{1}{3}\xi)}{\sin^5\xi} - \cos\xi\, g_a(\xi), \\ g_a(\xi) &= \frac{10(-2\sin\tfrac{10}{3}\xi + 7\sin\tfrac{8}{3}\xi - 30\sin\tfrac{4}{3}\xi + 42\sin\tfrac{2}{3}\xi)}{\sin^7\xi}, \\ f_b(\eta) &= \frac{8(-5\cos\tfrac{7}{3}\eta - 14\cos\tfrac{5}{3}\eta + 35\cos\tfrac{1}{3}\eta)}{\cos^5\eta} + \sin\eta\, g_b(\eta), \\ g_b(\eta) &= \frac{10(-2\sin\tfrac{10}{3}\eta - 7\sin\tfrac{8}{3}\eta + 30\sin\tfrac{4}{3}\eta + 42\sin\tfrac{2}{3}\eta)}{\cos^7\eta}. \end{aligned}\right\} \tag{4.4}$$

Let suffices $(\,)_1$ and $(\,)_2$ denote, for the moment, conditions immediately before and after the shock, let $u_2/u_1 = \sigma$, and let $k_b/k_a = \kappa$. The following conditions apply.

(i) x and y must be continuous across the shock:

$$\frac{f_b(\eta_2)}{f_a(\xi_1)} = \frac{\sigma^{n+1}}{\kappa}, \qquad \frac{g_b(\eta_2)}{g_a(\xi_1)} = \frac{\sigma^{n+3/2}}{\kappa}. \tag{4.5 a, b}$$

(ii) The jump in (u, v) must be along the transonic shock polar:

$$v_2 - v_1 = (u_1 - u_2)\left(\frac{u_1+u_2}{2}\right)^{1/2},$$

i.e.

$$\frac{2}{3}(-\sigma^{3/2}\sin\eta_2 - \cos\xi_1) - (1-\sigma)\left(\frac{1+\sigma}{2}\right)^{1/2} = 0. \tag{4.6}$$

(iii) The shock slope must be normal to the vectorial velocity jump:

$$\frac{dx_1}{dy_1} = \frac{dx_2}{dy_2} = \frac{v_2-v_1}{u_1-u_2} = \left(\frac{u_1+u_2}{2}\right)^{1/2},$$

i.e.

$$\frac{n+1}{n+\frac{3}{2}}\frac{f_a(\xi_1)}{g_a(\xi_1)} = \left(\frac{\sigma+1}{2}\right)^{1/2}, \qquad \frac{n+1}{n+\frac{3}{2}}\frac{f_b(\eta_2)}{g_b(\eta_2)} = \left(\frac{1+\sigma}{2\sigma}\right)^{1/2}. \tag{4.7 a, b}$$

These are four, rather than five, independent equations, since (4.5 a) and (4.5 b) combine to

$$\frac{f_b(\eta_2)g_a(\xi_1)}{f_a(\xi_1)g_b(\eta_2)} = \sigma^{-1/2},$$

and so do (4.7 a) and (4.7 b). The unknowns are ξ_1, η_2, σ, and κ; and the solution of these equations is not difficult. From (4.7) one can tabulate or plot ξ_1 and η_2 as functions of σ. The left-hand side of (4.6) is then a known function of σ, and one seeks its zero. There is only one such zero within the physically possible range of the variables. The results of this calculation are shown in the following table: here c is the constant in the equation of the shock wave $y = cx^{(2n+3)/(2n+2)}$.

	n	σ	ξ_1	η_2	κ	c
Far field	1	0·345	154·0°	27·2°	1·124	0·616
Edge field	4	0·735	126·7°	21·2°	1·004	1·430

5. The pressure distribution along the outer wall

The edge field and the far field are now completely determined, but the flow in the intermediate region is known only up to the shock, whose position is also not fully known. Strictly, the solution should be completed by means of the numerical method of characteristics, but in the present case the following empirical procedure was though to be sufficient.

There are two lines $u > 0$, $v = 0$ in the problem: the first lies between the limiting Mach wave and the shock, and on the first sheet of the hodograph plane; the second is the outer wall of the intake and lies on the second sheet of the hodograph. The first of these lines would probably be used as a starting point of the characteristics computation (cf. Guderley 1954). Let the values of x on these lines be denoted by $x_a(u,0)$ and $x_b(u,0)$, respectively. Both these functions are monotonic decreasing and might be expected to be qualitatively similar, since both represent a transition from the edge field to the far field. Now the foregoing results show that

$$\left.\begin{aligned} &\frac{x_b(u,0)}{x_a(u,0)} = 2{\cdot}248[1+O(u^2)] \quad \text{for } u\to 0,\\ \text{and}\quad &\frac{x_b(u,0)}{x_a(u,0)} = 2{\cdot}008[1+O(u^{-3})] \quad \text{for } u\to\infty. \end{aligned}\right\} \tag{5.1}$$

Accordingly it has been assumed here that

$$\frac{x_b(u,0)}{x_a(u,0)} \sim 2 \quad \text{for all } u. \tag{5.2}$$

$x_a(u,0)$ is easily calculated by the method already used for $x(w,0)$. We have

$$\begin{aligned} x_{a1}(u,0) &= \frac{2\sqrt{3}}{5\pi}u^{-2},\\ x_{a2}(u,0) &= -\frac{\sqrt{3}}{\pi}\frac{\partial}{\partial u}\left\{\zeta^{1\cdot3}\int_0^\infty K_{1\cdot3}(\lambda\zeta)f(\lambda)\frac{d\lambda}{\lambda}\right\},\\ &= \frac{1}{4}\frac{1}{2\pi i}\int_{c-i\infty}^{c+i\infty} u^{3q\cdot2-1\cdot2}\sec\tfrac{1}{2}\pi q\,\frac{\cos\pi q+\cos\frac{1}{3}\pi}{\cos\pi q-\cos\frac{1}{3}\pi}\times\\ &\qquad\times\frac{\Gamma(\frac{1}{2}q-\frac{1}{3})\Gamma(\frac{1}{2}q+\frac{1}{3})}{\Gamma(\frac{1}{2}q+\frac{1}{6})\Gamma(\frac{1}{2}q+\frac{5}{6})}\,dq, \qquad (-1<c<\tfrac{1}{3}),\\ &= -\frac{1}{2\pi}\sum_{n=0}^{\infty}a_n(-u)^{-3n-2}, \qquad (u\geqslant 1),\\ &= \frac{1}{3\pi}\sum_{n=0}^{\infty}(b_n+\tfrac{1}{2}c_n u+d_n u^2)(-u)^{3n}, \qquad (u\leqslant 1), \end{aligned} \tag{5.3}$$

where the coefficients are given in (3.10). These are alternating series, which converge at $u = 1$, but the convergence is improved by introducing terms in $\log(1+u^{-3})$ and $\log(1+u^3)$, as before.

6. The drag

In view of the singularity at the edge E, which makes our approximate solution locally invalid, the intake drag (as defined in § 1) must be calculated from the momentum flux across some suitable curve, such as BGO_2 in figure 3. (In this figure, O_1, O_2, I_1, I_2 represent points which are actually at infinity.) The general drag integral of transonic theory is derived in Appendix III; in the present case it becomes

$$\frac{1}{\delta^2}C_D = \frac{1}{\delta^2}\frac{\frac{1}{2}D}{\frac{1}{2}\rho_0 U_0^2 L} = \int_{BGO_2}\{2uv\,dx+(v^2+\tfrac{2}{3}u^3-\tfrac{1}{6}[u]^3)\,dy\}, \tag{6.1}$$

where $[u]$ denotes the velocity jump across the shock wave (downstream value minus upstream value), and is a function of y only. The term in $[u]^3$ accounts for the change in entropy and stagnation pressure across the shock, and is to be included only at points on BGO_2 behind the shock. The integral (6.1) is invariant under the changes of the path (provided that the termini remain at some point on the outer intake wall and at O_2), and the path may therefore be deformed to $BE_1E_2I_1I_2O_1O_2$. Then the integral around the small contour E_1E_2 gives the edge force, and that along I_1I_2 gives the pre-entry drag: the other parts of the path make no contribution.

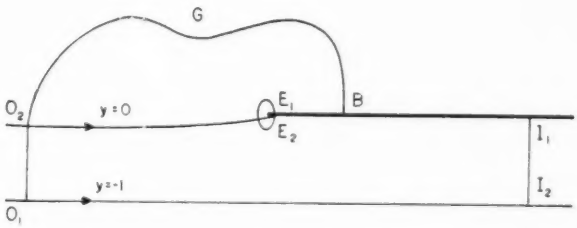

Figure 3.

Now near E the flow is represented asymptotically by a similarity solution, $\chi = u^{-n}f_n(\alpha)$, and the corresponding drag integral is

$$D_{E_1E_2} \sim O(u^{-n+3\cdot 2}) \sim O(y^{(2n-3)/(2n+3)}) \tag{6.2}$$

(details of this expression are given in Appendix III).

It follows that (i) the far-field solution χ_1 must be removed in the neighbourhood of the edge $(x, y \to 0;\ u, v \to \infty)$ because it would lead to an infinite force, and (ii) the true solution yields zero edge force. For χ_1 is the similarity solution with $n = 1$, so that the corresponding edge-force integral would $\to \infty$ as $u \to \infty$. (Since the geometry behind the limiting Mach wave may be varied without affecting the flow upstream, there is no general possibility of a cancellation between terms tending to infinity in the edge-force integral.) On the other hand the true edge flow is represented by the similarity solution with $n = 4$, so that the true edge-force integral $\to 0$ as $u \to \infty$.

The pre-entry drag is easily calculated from (6.1). On I_1I_2 this reduces to

$$\frac{1}{\delta^2} C_{D_{\text{pre}}} = \int_0^{-1} \tfrac{2}{3}u^3\, dy = \tfrac{2}{3}. \tag{6.3}$$

It remains to find the cowl drag of the slender-wedge intakes discussed in § 1. Let the slope of the wedge face be $\epsilon\delta$, and let its length be $lL(\delta\Gamma)^{1/3}$, where l is $O(1)$. For $\epsilon \to 0$ the pressure changes induced by the wedge

are $O(\epsilon\delta)$, and their contribution to the drag is therefore small compared with that of the flat-plate pressures. Hence, by (6.1)

$$\frac{1}{\delta^2} C_{D_{\text{cowl}}} \sim -2\epsilon \int_0^l u \, dx,$$

where u refers to values on the outside wall of the flat-plate intake. Numerical values are given in the next section.

7. Results

Pressure distributions along the centre-line, $y = -1$, along the inner wall $y = 0-$, and along the outer wall, $y = 0+$, are shown in figure 4.

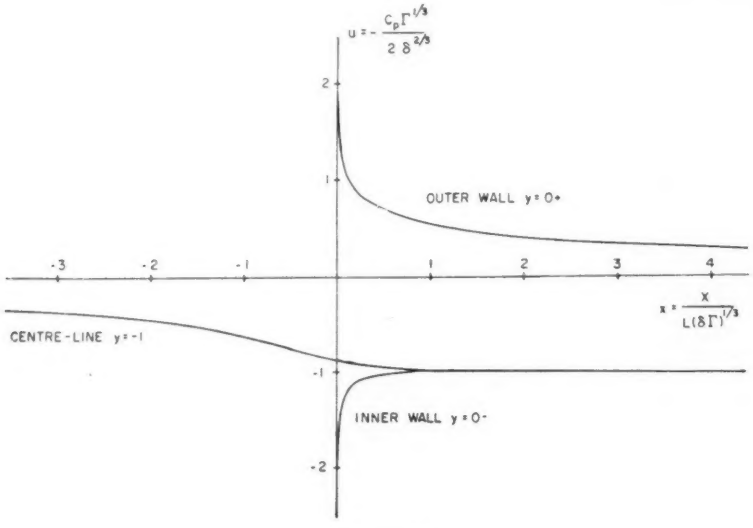

Figure 4.

This picture is supplemented by the following asymptotic approximations (which, for the external wall, are based on (5.1) rather than on the approximation (5.2))

$$\begin{aligned}
u(x,-1) &\sim -0{\cdot}664(-x)^{-1/2} && \text{for } x \to -\infty,\\
u(x,0+) &\sim 0{\cdot}704x^{-1{\cdot}2} && \text{for } x \to \infty,\\
u(x,0+) &\sim 0{\cdot}713x^{-1{\cdot}5} && \text{for } x \to 0,\\
u(x,0-) &\sim -0{\cdot}712x^{-1{\cdot}5} && \text{for } x \to 0,\\
u(x,0-) &\sim -1-0{\cdot}147e^{-\pi x} && \text{for } x \to \infty,\\
u(x,-1) &\sim -1+0{\cdot}147e^{-\pi x} && \text{for } x \to \infty.
\end{aligned}$$

It is evident that the external decay of disturbances before and after the inlet station is slow (although it must be remembered that x is a 'stretched' coordinate), and that the edge singularity is very weak. It is also striking

that over 90% of the compression of the entering fluid takes place ahead of the inlet station, and that the decay of disturbances within the duct is extremely rapid, so that one-dimensional theory provides a very good approximation to the flow within the duct.

As a basis for comparison, we quote some results for the present intake in an incompressible stream. In this case the reduced variables are given by

$$\delta = \frac{U_0 - U_1}{U_0}, \quad X = Lx, \quad Y = Ly, \quad U' = \delta u(x,y), \quad V' = \delta v(x,y),$$

and the small-disturbance solution is

$$x + iy = \frac{1}{\pi}\left(\frac{1}{u-iv} + \log\frac{u-iv}{u-iv+1}\right),$$

so that

$$\begin{aligned}
u(x,-1) &\sim 0{\cdot}318x^{-1} && \text{for } x \to -\infty,\\
u(x,0+) &\sim 0{\cdot}318x^{-1} && \text{for } x \to \infty,\\
u(x,0\pm) &\sim \pm 0{\cdot}399x^{-1/2} && \text{for } x \to 0,\\
u(x,0-) &\sim -1 - 0{\cdot}368e^{-\pi x} && \text{for } x \to \infty,\\
u(x,-1) &\sim -1 + 0{\cdot}368e^{-\pi x} && \text{for } x \to \infty.
\end{aligned}$$

Within the framework of reduced coordinates, the external disturbances of the incompressible flow are therefore more concentrated near the inlet station than are those of the transonic flow: the extent to which this effect is reversed, when physical coordinates are used, depends upon the magnitude of δ.

The pre-entry drag of the intake in transonic flow is

$$C_{D_{\text{pre}}} = \frac{D_{\text{pre}}}{\frac{1}{2}\rho_0 U_0^2 \cdot 2L} = \frac{2}{3}\delta^2.$$

Slender-wedge cowls, whose wedge face has slope $\epsilon\delta$, ($\epsilon \ll 1$), and length $lL(\delta\Gamma)^{1/3}$, have the following drag:

l	$\frac{1}{2}$	1	$\frac{3}{2}$
$\frac{1}{\delta^2\epsilon} C_{D_{\text{cowl}}}$	$-0{\cdot}9$	$-1{\cdot}5$	$-2{\cdot}0$

The decrease in drag with increasing frontal area is therefore quite rapid, at least initially.

I am indebted to Professor P. Germain and to Professor J. D. Cole for a number of most helpful discussions, and to Mrs A. Tingley for help with the numerical computations. This work was completed while I was on leave of absence at the Guggenheim Aeronautical Laboratory, California Institute of Technology, and was partly sponsored by the U.S. Air Force Office of Scientific Research, under Contract AF-18(600)-383.

Appendix I. Elementary solutions of the Tricomi equation

By separation of variables one finds the following elementary solutions of equation (2.5):

$$\left.\begin{aligned} e^{\pm\lambda v}\zeta^{1/3}K_{1/3}(\lambda\zeta) &= \frac{\pi}{\sqrt{3}}\,e^{\pm\lambda v}z^{1/3}[J_{1/3}(\lambda z)+J_{-1/3}(\lambda z)], \\ \text{and}\qquad e^{\pm\lambda v}\zeta^{1/3}I_{1/3}(\lambda\zeta) &= -e^{\pm\lambda v}z^{1/3}J_{1/3}(\lambda z). \end{aligned}\right\} \tag{I.1}$$

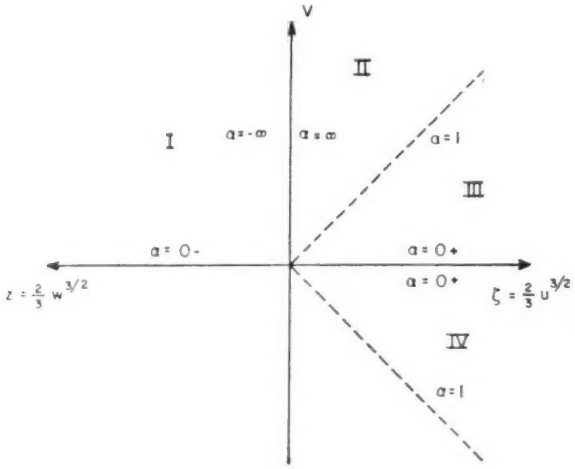

Figure 5.

Alternatively, if one seeks similarity solutions of form $\chi = \zeta^{-m} fn(\alpha)$, where $\alpha = v^2/\zeta^2 = 9v^2/4u^3$, these turn out to be, in a neighbourhood of the characteristic $v = \zeta$ (see figure 5),

$$\left.\begin{aligned} &\zeta^{-m}F\left(\frac{1}{2}m,\quad \frac{1}{2}m+\frac{1}{3};\quad m+\frac{5}{6};\quad 1-\alpha\right), \\ \text{and}\qquad &\zeta^{-m}(\alpha-1)^{-m+1/6}F\left(-\frac{1}{2}m+\frac{1}{6},\quad -\frac{1}{2}m+\frac{1}{2};\quad -m+\frac{7}{6};\quad 1-\alpha\right), \end{aligned}\right\} \tag{I.2}$$

with corresponding hypergeometric functions applying elsewhere in the field. The singularities of the hypergeometric equation, $\alpha = 0, \infty, 1$, correspond, respectively, to the line $v = 0$, to the sonic line, and to the important characteristics $\alpha = 1$. As Guderley (1948) has demonstrated, one of these two characteristics is generally the limiting Mach wave, which divides both the physical and the hodograph fields into (i) the subsonic region, together with an initial part of the supersonic region which influences the subsonic flow, and (ii) that part of the supersonic region which does not influence the upstream field.

Most analytic solutions of problems in transonic flow have been obtained by superposition of the solutions (I.1) and (I.2), but the relatively simple relation between these forms does not appear to have been emphasized in the literature. With a view to the present application, we discuss this relation here. Consider

$$\chi = \zeta^{1/3} \int_0^\infty e^{-\lambda v}[g(\lambda)K_{1/3}(\lambda\zeta) + h(\lambda)I_{1/3}(\lambda\zeta)]\,\frac{d\lambda}{\lambda}, \tag{I.3}$$

where g and h are assumed to be algebraic rather than exponential. Since for $\lambda \to \infty$

$$e^{-\lambda v}K_{1/3}(\lambda\zeta) \sim \left(\frac{\pi}{2\lambda\zeta}\right)^{1/2} e^{-\lambda(v+\zeta)},$$

$$e^{-\lambda v}I_{1/3}(\lambda\zeta) \sim \frac{1}{(2\pi\lambda\zeta)^{1/2}}\, e^{-\lambda(v-\zeta)},$$

the first part of (I.3) converges for $\mathscr{R}(v+\zeta) > 0$ (that is in the regions I, II, III, IV of the hodograph plane, figure 5), whereas the second converges for $\mathscr{R}(v-\zeta) > 0$ (that is, only in I and II). Thus we expect the $K_{1/3}$-solution to be associated with only the first solution in (I.2), which is analytic on $v = \zeta$. In fact by standard integrals, and by properties of the hypergeometric functions (Erdélyi 1954, 1953), one finds that

$$\zeta^{1/3} \int_0^\infty e^{-\lambda v}\lambda^{m-2/3}K_{1/3}(\lambda\zeta)\,d\lambda$$
$$= \frac{\pi^{1/2}\Gamma(m)\Gamma(m+\frac{2}{3})}{2^{m+1/3}\Gamma(m+\frac{5}{6})}\,\zeta^{-m}F\left(\frac{1}{2}m,\quad \frac{1}{2}m+\frac{1}{3};\quad m+\frac{5}{6};\quad 1-\alpha\right), \qquad (m>0). \tag{I.4}$$

A similar result for the $I_{1/3}$-solution involves both the hypergeometric functions in (I.2).

To obtain a further relation we introduce the Mellin transform. The definition integral of this transform is

$$\tilde{\phi}(p) = \int_0^\infty \zeta^{p-1}\phi(\zeta)\,d\zeta, \qquad (A < \mathscr{R}p < B), \tag{I.5}$$

which we also write $\tilde{\phi}(p) \doteqdot \phi(\zeta)$; the inversion integral is

$$\phi(\zeta) = \frac{1}{2\pi i}\int_{c-i\infty}^{c+i\infty} \zeta^{-p}\tilde{\phi}(p)\,dp, \qquad (A < c < B); \tag{I.6}$$

and the composition product is

$$\tilde{\phi}_1(p+a)\tilde{\phi}_2(-p+b) \doteqdot \zeta^a \int_0^\infty \lambda^{a+b-1}\phi_1(\lambda\zeta)\phi_2(\lambda)\,d\lambda \tag{I.7}$$

(provided that $\tilde{\phi}_1(p+a)$ and $\tilde{\phi}_2(-p+b)$ have a common strip of convergence). Now let

$$e^{-\lambda\alpha^{1/2}}K_{1/3}(\lambda) = G(\lambda,\alpha).$$

Then $\tilde{G}(p+\frac{1}{3},\alpha)$ is given by (I.4), with $m = p$, $v = \zeta\alpha^{1/2}$, $\zeta = 1$. Now if in (I.3) we set $h(\lambda) = 0$, and take the Mellin transform of both sides, we have, by (I.7),

$$\tilde{\chi}(p,\alpha) = \tilde{G}(p+\tfrac{1}{3},\alpha)\tilde{g}(-p-\tfrac{1}{3}),$$

provided that $\tilde{g}(q)$ converges somewhere in $\mathscr{R}q < -\frac{1}{3}$. Hence

$$\chi(\zeta,\alpha) = \zeta^{1/3}\int_0^\infty e^{-\lambda v}K_{1/3}(\lambda\zeta)g(\lambda)\,\frac{d\lambda}{\lambda}$$

$$= \frac{1}{2\pi i}\int_{c-i\infty}^{c+i\infty}\zeta^{-p}\,\frac{\pi^{1/2}\Gamma(p)\Gamma(p+\frac{2}{3})}{2^{p+1/3}\Gamma(p+\frac{5}{6})}\times$$

$$F\left(\frac{1}{2}p,\quad \frac{1}{2}p+\frac{1}{3}\,;\quad p+\frac{5}{6}\,;\quad 1-\alpha\right)\tilde{g}(-p-\tfrac{1}{3})\,dp, \qquad \text{(I.8)}$$

and we have transformed a superposition of the solutions (I.1) into a superposition of the solutions (I.2), the weighting function of the first form being replaced by its Mellin transform in the second. The complex integral can often be expressed as a series by contour integration.

Appendix II. Uniqueness of y_2

In this appendix the problem for y_2 is transformed into a problem of the standard Tricomi type by means of a certain inversion which leaves the equation invariant (see, for example, Germain & Bader (1952)). The $(z(\zeta), v)$-plane is mapped on to an $(\alpha(\gamma), \beta)$-plane by the transformation

$$\sqrt{\{(v+1)^2+z^2\}} \equiv \sqrt{\{(v+1)^2-\zeta^2\}} \equiv r = \frac{1}{\rho} \equiv \frac{1}{\sqrt{(\beta^2+\alpha^2)}} \equiv \frac{1}{\sqrt{(\beta^2-\gamma^2)}},$$

$$\frac{v+1}{\sqrt{\{(v+1)^2+z^2\}}} \equiv \frac{v+1}{\sqrt{\{(v+1)^2-\zeta^2\}}} \equiv t = \tau \equiv \frac{\beta}{\sqrt{(\beta^2+\alpha^2)}} \equiv \frac{\beta}{\sqrt{(\beta^2-\gamma^2)}},$$

$$y(r,t) = \rho^{1/3}\eta(\rho,\tau).$$

The line $v=0$, z real, maps on to the semi-circle $\rho=\tau$, or $\alpha^2+(\beta-\frac{1}{2})^2=\frac{1}{4}$, $0\leqslant\tau\leqslant 1$; the quarter-circle $r\to\infty$, $0\leqslant t\leqslant 1$, maps on to $\rho\to 0$, $0\leqslant\tau\leqslant 1$; the characteristic at infinity $v+\zeta=k$, $k\to\infty$, maps on to $\beta-\gamma=0$, $\gamma\leqslant\frac{1}{2}$; and the characteristic $v-\zeta=0$ maps on to $\beta+\gamma=1$, $\gamma\leqslant\frac{1}{2}$. The problem for y_2, namely

$$\text{(i)}\quad y_{rr}+\frac{1-t^2}{r^2}y_{tt}+\frac{4}{3r}\left(y_r-\frac{t}{r}y_t\right)=0,$$

$$\text{(ii)}\quad y=-1 \quad\text{on}\quad v=0,\ \tfrac{2}{3}>z\geqslant 0,$$

$$=0 \quad\text{on}\quad v=0,\ z>\tfrac{2}{3},$$

$$\text{(iii)}\quad y\sim O(r^{-5/3}) \quad\text{for } z \text{ real},\ r\to\infty,$$

$$\sim O(v^{-5/3}) \quad\text{for } \zeta \text{ real},\ v\to\infty,$$

then becomes

$$\text{(i)}\quad \eta_{\rho\rho}+\frac{1-\tau^2}{\rho^2}\eta_{\tau\tau}+\frac{4}{3\rho}\left(\eta_\rho-\frac{\tau}{\rho}\eta_\tau\right)=0,$$

$$\text{(ii)}\quad \eta=-\rho^{-1/3} \quad\text{on}\quad \rho=\tau, \qquad \frac{3}{\sqrt{13}}<\tau\leqslant 1,$$

$$=0 \quad\text{on}\quad \rho=\tau, \qquad 0\leqslant\tau<\frac{3}{\sqrt{13}},$$

$$\text{(iii)}\quad \eta=0 \quad\text{on}\quad \rho=0,\quad \gamma\leqslant\tfrac{1}{2}.$$

The uniqueness of such a problem, in which data are prescribed on an arc in the elliptic half-plane and on an adjacent characteristic in the hyperbolic half-plane, was established by Tricomi (1923).

Appendix III. The drag integral of transonic theory

In this appendix we first develop the general drag integral of transonic theory: this involves no more labour than the derivation of the particular form which is of interest here. Let ϕ be the perturbation velocity potential of a three-dimensional transonic flow, such that the total velocity at any point is $U_0(1+\nabla\phi)$. The governing differential equation is

$$(1-M_0^2-\Gamma\phi_X)\phi_{XX}+\phi_{YY}+\phi_{ZZ}=0. \tag{III.1}$$

Consider the drag on a portion A of some solid boundary, and let S be a surface in the fluid such that $S+A$ form a closed surface. Then by the equations of mass and momentum

$$D=\iint_A N_{(X)}(P-P_0)\,dA, \tag{III.2a}$$

$$=-\iint_S [N_{(X)}(P-P_0+\rho U_0^2\phi_X)+\rho U_0^2\phi_X(\mathbf{N}.\nabla\phi)]\,dS, \tag{III.2b}$$

where $\mathbf{N}$ is the normal outward from $S+A$, $N_{(X)}$ is its X-component, and P and ρ denote the pressure and density. If $P-P_0$ is bounded on A, (III.2a) and (III.2b) are wholly equivalent, but if there is a singularity on A, an approximate solution will not be physically valid in its neighbourhood. We assume, however, that the solution is valid in the field away from the singularity: then the drag is defined by (III.2b).

By expansion of the usual equations of inviscid, homenergic flow, we find that

$$\frac{P-P_0}{\frac{1}{2}\rho_0 U_0^2}=-2\phi_X-(\nabla\phi)^2+M_0^2\phi_X^2+M_0^2\phi_X(\nabla\phi)^2-\tfrac{1}{3}(2-\gamma)M_0^4\phi_X^3+$$
$$+\tfrac{1}{6}(\gamma+1)M_0^4\sum[\phi_X]^3+O\{(\nabla\phi)^4\}, \tag{III.3a}$$

$$\frac{\rho}{\rho_0}=1-M_0^2\phi_X-\tfrac{1}{2}M_0^2(\nabla\phi)^2+\tfrac{1}{2}(2-\gamma)M_0^4\phi_X^2+O\{(\nabla\phi)^3\}. \tag{III.3b}$$

Here $[\phi_X]$ denotes the velocity jump across a shock (downstream value minus upstream value) and the term in $[\phi_X]^3$ accounts for the change in stagnation pressure across any shock waves upstream of the point in question*. To our order of accuracy $[\phi_X]$ is a function of Y and Z only. If these expressions are now inserted in the drag integral (III.2b), there results

$$\frac{D}{\frac{1}{2}\rho_0 U_0^2}=\iint_S \{N_{(X)}((\nabla\phi)^2+M_0^2\phi_X^2-\tfrac{2}{3}(2-\gamma)M_0^4\phi_X^3-\tfrac{1}{6}(\gamma+1)M_0^4\sum[\phi_X]^3)-$$
$$-2\mathbf{N}.\nabla\phi(\phi_X-M_0^2\phi_X^2)\}\,dS. \tag{III.4}$$

* The need for this term was brought to my attention by Professor Germain and Professor Cole.

This is the drag integral of second-order compressible flow theory. For transonic flow we may make the further approximations

$$M_0^4 \phi_X^3 \sim M_0^2 \phi_X^3,$$
$$(\mathbf{N} \cdot \nabla\phi)\phi_X^2 \sim N_{(X)} \phi_X^3,$$

to obtain

$$\frac{D}{\frac{1}{2}\rho_0 U_0^2} = \iint_S \{N_{(X)}((\nabla\phi)^2 + M_0^2 \phi_X^2 + \tfrac{2}{3}\Gamma\phi_X^3 - \tfrac{1}{6}\Gamma \sum [\phi_X]^3) - 2\mathbf{N} \cdot \nabla\phi\, \phi_X\}\, dS. \tag{III.5}$$

It is readily verified, by means of Gauss's theorem, the differential equation (III.1), and the conservation equations for a shock wave, that this drag integral is invariant under changes of the surface S (provided that $S+A$ remains a closed surface and that there are no singularities between different surfaces S).

For plane flows with $M_0 = 1$, (III.5) reduces to

$$\frac{1}{\delta^2} C_D = \frac{1}{\delta^2} \frac{D}{\frac{1}{2}\rho_0 U_0^2 L} = \int_C \{2uv\, dx + (v^2 + \tfrac{2}{3}u^3 - \tfrac{1}{6}\sum [u]^3)\, dy\}, \tag{III.6}$$

where the integral is taken counter-clockwise in the physical plane, and where the reduced variables of (2.2) have been introduced.

Next, following Germain (1957), we consider the form of the drag integral when the flow may be represented on C by a similarity solution of the form considered in (I.2); that is, when

$$\chi = u^{-n} h(\alpha), \qquad (n = \tfrac{3}{2}m),$$

so that h is some solution of the hypergeometric equation

$$\alpha(1-\alpha)h'' + [\tfrac{1}{2} - (\tfrac{4}{3} + \tfrac{2}{3}n)\alpha]h' - \tfrac{1}{9}n(1+n)h = 0. \tag{III.7}$$

Equation (III.6) now becomes

$$\frac{1}{\delta^2} C_D = \int_{C'} \{u^{-n+1/2}[((\tfrac{8}{3}n+2)\alpha^{3/2} - (2n+3)\alpha^{1/2})h' + \tfrac{4}{3}(n^2+n)\alpha^{1/2}h]\, du + \\ + u^{-n+3/2}[(-\tfrac{8}{3}\alpha^{3/2} + 2\alpha^{1/2})h'' - ((\tfrac{4}{3}n + \tfrac{10}{3})\alpha^{1/2} - \alpha^{-1/2})h']\, d\alpha\} - \\ - \frac{1}{6}\int_C \sum [u]^3\, dy, \tag{III.8}$$

where C' is the image of C in the hodograph plane. Now the invariance property of the drag integral ensures that the integrand in (III.8) is an exact differential, and this may also be verified by means of (III.7). Hence it follows from the du-term that

$$\frac{1}{\delta^2} C_D = \left[\frac{u^{-n+3/2}}{-n+\frac{3}{2}}\{((\tfrac{8}{3}n+2)\alpha^{3/2} - (2n+3)\alpha^{1/2})h' + \tfrac{4}{3}(n^2+n)\alpha^{1/2}h\}\right]_{C'} - \\ - \frac{1}{6}\int_C \sum [u]^3\, dy. \tag{III.9}$$

In general C and C' cross shock waves, and the integrated term in (III.9) is then only piecewise continuous: its discontinuities must be taken into account when (III.9) is evaluated.

Germain (1957) has pointed out that if C is a large contour in the physical plane with termini on $y = 0$, $v = 0$, the appropriate solution is that with $n = 1$, so that the integrated term in (III.9) vanishes in the limit. The drag is then seen to be entirely due to the entropy gain across shock waves.

Note added in proof

It is clear from (III.8) and (III.9) that an edge force is possible, in transonic flow with $M_0 = 1$, only if $n = \frac{3}{2}$. Such a flow has been studied by Nonweiler (1958), who finds that the solution

$$\chi = \text{const. } w^{-3\cdot2}(1-\alpha)^{-5\cdot6} \qquad (w \geqslant 0)$$

corresponds to the flow past the body $Y \propto X^{2\cdot5}$, the velocity on this body being sonic for $X > 0$. Nonweiler calculates the edge force by integrating surface pressure on the related bodies $Y \propto X^{\nu}$ and letting $\nu \to \frac{5}{2}$. The same result is readily obtained from (III.8), in which the du-term and the shock term vanish. This shows that the only assumption implicit in Nonweiler's result is that the velocity in the field away from the singularity is given correctly to the lowest order.

References

Barish, D. T. & Guderley, G. 1953 Asymptotic forms of shock waves in flows over symmetrical bodies at Mach one, *J. Aero. Sci.* **20,** 491.

Erdélyi, A. (Ed.) 1953 *Higher Transcendental Functions*, vol. 1. New York : McGraw-Hill.

Erdélyi, A. (Ed.) 1954 *Tables of Integral Transforms*, vol. 1. New York : McGraw-Hill.

Frankl, F. I. 1947 An investigation of the theory of a wing of infinite span moving at the speed of sound, *Doklady Akad. Nauk. SSSR* (N.S.) **57,** 661.

Germain, P. & Bader, R. 1952 Sur quelques problèmes relatifs a l'équation de type mixte de Tricomi, *O.N.E.R.A. Publication* no. 54.

Germain, P. 1957 Lectures on transonic flow at the California Institute of Technology.

Guderley, G. 1948 Singularities at the sonic velocity, *Wright-Patterson Air Force Base Tech. Rep.* no. F–TR–1171–ND.

Guderley, G. 1954 The flow over a flat plate with a small angle of attack at Mach number one, *J. Aero. Sci.* **21,** 261.

Nonweiler, T. R. F. 1958 The sonic flow about some symmetric half-bodies, *J. Fluid Mech.* **4,** 140.

Spreiter, J. R. 1954 On alternative forms of the basic equations of transonic flow theory, *J. Aero. Sci.* **21,** 70.

Tricomi, F. 1923 Sulle equazioni lineari alle derivate parziali di 2° ordine di tipo misto, *Mem. Real. Acad. Lincei; classe Fis. Mat. e. Nat.*, **14** (5), 133.

A note on the compression of air through repeated shock waves

By J. L. STOLLERY and D. J. MAULL
Department of Aeronautics, Imperial College, University of London

(*Received* 10 *May* 1958)

SUMMARY

The results of calculations of the compression of air by repeated shock waves are compared with the perfect-gas values given by Evans & Evans (1956). The comparison emphasizes the increasing divergence of real from perfect-gas results as shock strengths are raised. The equations relating conditions across a shock wave are obtained in a convenient form for solution using a Mollier diagram.

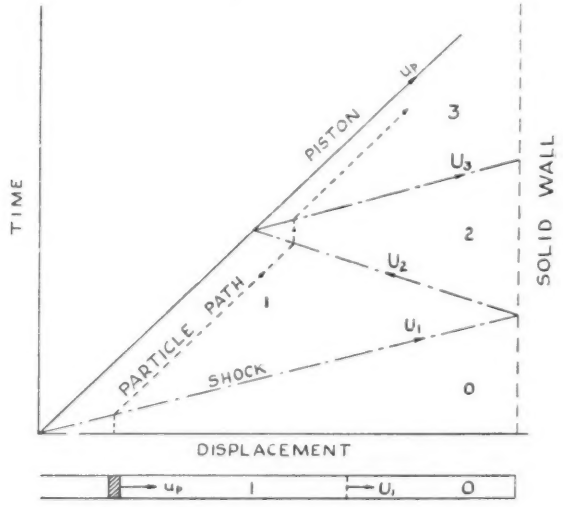

Figure 1. The displacement *vs* time diagram.

Figure 1 shows the problem considered. A piston instantaneously accelerated to a velocity u_p, which is subsequently held constant, generates a shock wave. The wave is reflected from the closed end and the piston face. The air pressure, density and temperature rise non-isentropically through the initial and reflected shocks, soon reaching values at which the excitation of vibrational modes, dissociation, electronic excitation and finally ionization become important. These real-gas effects are taken into

account here by using the Mollier diagram of Feldman (1957) prepared from the real-air tables of Hilsenrath & Beckett (1956). All viscous, heat transfer and relaxation effects are neglected and the flow is assumed to be one-dimensional.

The notation is as follows.

n An integer, referring to a flow region in the time–displacement diagram (figure 1). Thus H_n, ρ_n, p_n and T_n are the enthalpy, density, pressure and temperature in the nth region. The nth shock wave moves into the $(n-1)$th region and has the nth region behind it.

U_n Velocity of the nth shock wave.

u_n Flow velocity in the nth region ($u_n = u_p$ for n odd, $u_n = 0$ for n even).

q Velocity relative to the shock wave.

M_s Shock strength = (initial shock velocity)/(speed of sound in region 0) $= U_1/a_0$.

π A pressure of one atmosphere.

The equations for a stationary shock wave are:

energy $$H_0 + \tfrac{1}{2}q_0^2 = H_1 + \tfrac{1}{2}q_1^2, \tag{1}$$

momentum $$p_0 + \rho_0 q_0^2 = p_1 + \rho_1 q_1^2, \tag{2}$$

continuity $$\rho_0 q_0 = \rho_1 q_1. \tag{3}$$

These may be used for a moving shock wave by superposition of velocities, giving for the initial shock wave

$$q_0 = U_1, \qquad q_1 = U_1 - u_1.$$

Since $u_1 = u_p$, the above three equations yield

$$H_1 - H_0 = \tfrac{1}{2}u_p^2\left(\frac{\rho_1+\rho_0}{\rho_1-\rho_0}\right), \qquad p_1 - p_0 = u_p^2\left(\frac{\rho_1\rho_0}{\rho_1-\rho_0}\right), \qquad U_1 = \frac{u_p}{1-(\rho_0/\rho_1)}. \tag{4}$$

In the same way the following equations for the first reflected shock are obtained:

$$H_2 - H_1 = \tfrac{1}{2}u_p^2\left(\frac{\rho_2+\rho_1}{\rho_2-\rho_1}\right), \qquad p_2 - p_1 = u_p^2\left(\frac{\rho_2\rho_1}{\rho_2-\rho_1}\right), \qquad U_2 = \frac{u_p}{(\rho_2/\rho_1)-1}. \tag{5}$$

Similar formulae may be obtained for further shock reflections. The general forms of the equations are:

$$H_{n+1} - H_n = \tfrac{1}{2}u_p^2\left(\frac{\rho_{n+1}+\rho_n}{\rho_{n+1}-\rho_n}\right), \tag{6}$$

$$p_{n+1} - p_n = u_p^2\left(\frac{\rho_{n+1}\rho_n}{\rho_{n+1}-\rho_n}\right), \tag{7}$$

$$U_n = \frac{\mp u_p}{1-(\rho_{n-1}/\rho_n)} \qquad (+ \text{ for } n \text{ odd}, - \text{ for } n \text{ even}). \tag{8}$$

On the Mollier diagram, figure 2, enthalpy is plotted against entropy for lines of constant pressure, lines of constant density and lines of constant

temperature. Thus any two of these properties defines a point on the diagram. Given the initial conditions in region 0 and a value for M_s (or piston speed), two values for ρ_1 are chosen. The two corresponding values of H_1 calculated from (4) are plotted on the Mollier diagram, and the points joined by a straight line. The two values for the pressure p_1 from (4) are also plotted, and the line linking these points will cut that joining the enthalpy values if the chosen densities are reasonable. The point of intersection gives the approximate values for conditions in

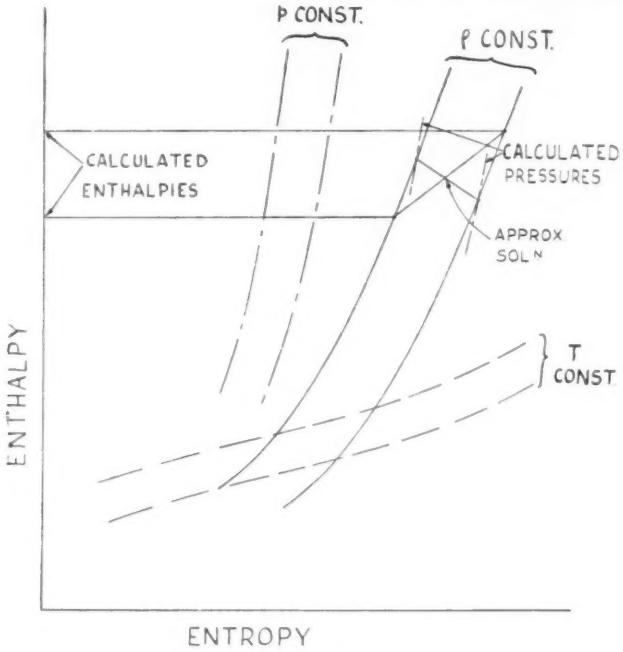

Figure 2. Mollier diagram showing method of solution.

region 1. The approximation may be improved by choosing two new density values just either side of the first intersection point and repeating the construction. With a little experience this becomes unnecessary. Now, knowing conditions in region 1, those in region 2 follow from (5) on using the same graphical construction. Similarly the method can be used for the other regions. The process is then repeated for further values of M_s. A comparison with Feldman's electronically-computed values for region 2 showed a maximum variation of 3%. The values for region 3 are thought to be accurate to 5%.

The results for an initial temperature T_0 of 290° K are shown in figures 3, 4 and 5. Conditions after one, two and three shocks are plotted against initial shock strength and compared with the perfect-gas solutions.

After two reflections only ($n = 3$), the perfect-gas solutions diverge from the air values for initial shock strengths greater than two. Table 1 presents a comparison at various piston speeds.

Thus perfect-gas performance calculations for shock tubes of the multiple reflection type are invalidated and real-gas tables must be used.

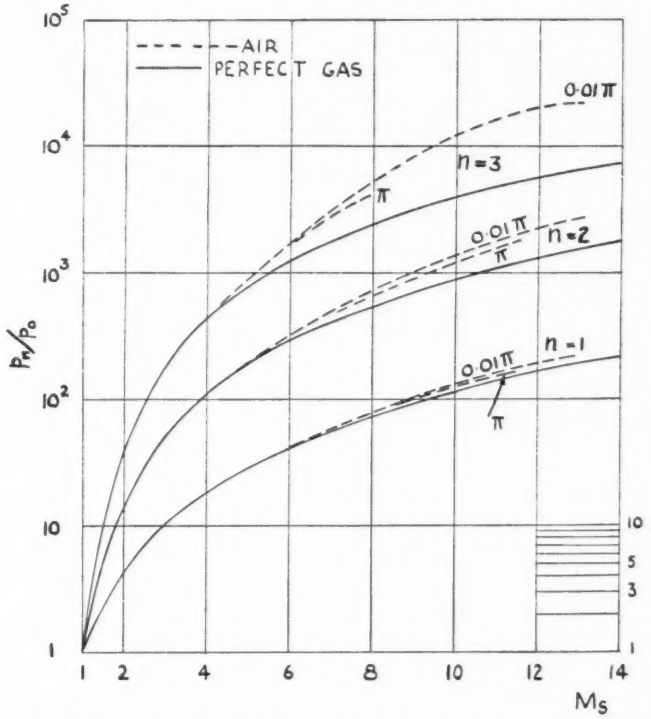

Figure 3. Pressure *vs* shock strength. π and $0{\cdot}01\pi$ refer to the values of p_0 ($\pi = 1$ atmos.). The curve for $p_0 = 0{\cdot}1\pi$ lies between the other two curves for air and has been omitted for the sake of clarity.

Piston speed (ft./sec)	Perfect gas			Air ($p_0 = 0{\cdot}01\pi$)		
	p_3/p_0	T_3/T_0	ρ_3/ρ_0	p_3/p_0	T_3/T_0	ρ_3/ρ_0
2 000	90	5·1	17·5	90	4·8	20·0
4 000	595	15·3	37·0	600	10·6	57·0
6 000	1 500	31·0	46·0	1 900	16·8	107·0
8 000	2 700	53·4	51·0	5 300	23·0	158·0
10 000	4 300	83·0	52·5	11 300	28·2	222·0
12 000	6 100	118·0	53·0	18 900	33·0	292·0

Table 1.

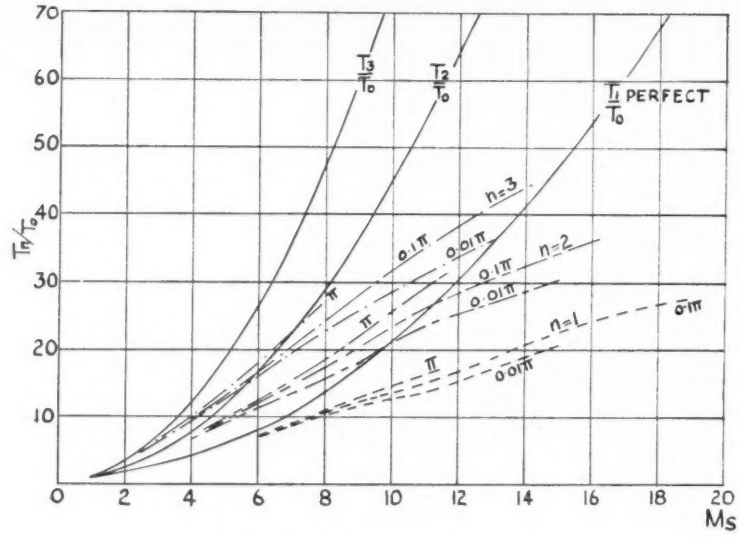

Figure 4. Density *vs* shock strength.

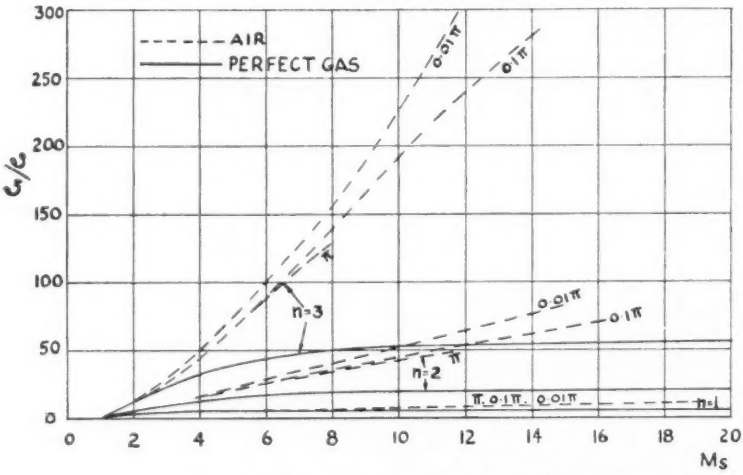

Figure 5. Temperature *vs* shock strength.

References

Evans, C. & Evans, F. 1956 Shock compression of a perfect gas, *J. Fluid Mech.* **1**, 399.

Feldman, S. 1957 Hypersonic gas dynamic charts for equilibrium air, *AVCO Research Laboratory Handbook.*

Hilsenrath, J. & Beckett, C. W. 1956 Tables of thermodynamic properties of argon-free air to 15 000° K, *Arnold Engineering Development Center, Rep.* no. TN–56–12.

REVIEWS

History of Hydraulics, by HUNTER ROUSE and SIMON INCE. Iowa City: Iowa Institute of Hydraulic Research, State University of Iowa, 1957. 269 pp. $5.00.

In these days of high blood pressure and rapid advancement in science and technology, it is refreshing to find a book which halts the headlong rush and contemplates the past. Here is a harmless tranquiliser to which all those interested in fluid mechanics should become addicted. The historical development of hydraulics since early antiquity is briefly but expertly recounted in a way which enables the reader to see the progress of the subject in its proper perspective. The aim has been to review the advances made in formulating the basic principles of fluid motion, together with those relevant aspects of experimental research, engineering design, related scientific progress and world history. Hydraulicists will be aware that much of the material for the book has already been published as a series of supplements to *La Houille Blanche* which has regularly featured historical and biographical notes.

The distinguished senior author, who is prominent in the advancement of engineering fluid mechanics, has also, most fortunately, been interested in the historical and philosophical progress of his subject. In 1950 he therefore encouraged a research student at Iowa, Simon Ince, to prepare a thesis on " A history of hydraulics at the end of the 18th century " which was submitted in 1952. When, some years later as a Fulbright Scholar, Professor Rouse spent a year at the University of Grenoble, it was an excellent opportunity to expand the original thesis. He was greatly aided by the unrivalled library facilities which had been built up in the neighbouring Laboratoire Dauphinoise d'Hydraulique under the genius of another eminent hydraulicist, Pierre Danel. With such a fusion of backgrounds it is little wonder that the book flourished.

Inevitably, because water is such an important element in life, ' Hydraulics ' must be one of the oldest subjects studied by man. Initially, its study was presumably empirical, but later it proved a fruitful field for theoreticians. One of the fascinating aspects of the book is its revelation of the close link in the past between the mathematician, the scientist and the hydraulic engineer, who in the 18th century were usually one and the same person. Nowadays in this era of specialization the field has broadened into what is fashionably termed fluid mechanics and the pursuit divided between aero- and hydro-dynamicists, engineers, meteorologists and a host of others who sometimes delude themselves that their own subject is ' different '. It is, in fact, often difficult to see the wood for the trees, and for this reason the book is welcome because of the clear view that it presents.

The story begins in the days, difficult for historians, when ancient civilizations were developing the middle east. Little is recorded, but it

is interesting, for instance, to note that the siphon dates at least from those times. The later periods of Greek and Roman culture are fortunately better documented in classical literature, from which numerous quotations are taken. The theoretical contributions to hydrostatics by Archimedes and the philosophy of Aristotle and others are famous but it may not always be appreciated that the Greeks were also competent hydraulic engineers, their skills as canal and tunnel builders probably being inherited from the middle east. On the mechanical side, Ctesibus is accredited with the first recorded positive displacement pump, and the steam-jet turbine described by Hero is well known. The Romans were outstanding as water handlers and have left behind many hydraulic structures as evidence of their engineering skill. Although illustrations from the middle ages depict the use of hydraulic machines in mills and forges, no outstanding figures in hydromechanics seem to have emerged. Examples are quoted of a few gropings towards mechanics made by Buridan of the University of Paris, Heytesbury of Oxford and others, but little is known of scientific progress during this period. In addition to the references quoted by Rouse and Ince the translated modern edition of *De Re Metallica* by Georgius Agricola might also have been mentioned as a valuable source of illustrations of hydraulic machinery used in mining during the middle ages. However, not until Leonardo da Vinci and the Renaissance do the individual contributions of hydraulicists become apparent. The drawings of hydraulic phenomena made by da Vinci and reproduced in the book show da Vinci's acute powers of observation, and extracts from his writings reveal a remarkable understanding of physical laws such as those of force and work. Others such as Copernicus, Stevin and Galileo also contributed to the progress of mechanics and the experimental method during this early period. From here on the story moves more rapidly through chapters on the naissance of the experimental method, post-renaissance hydraulics, 17th-century mathematics and mechanics, to the 18th century when theoretical hydrodynamics really began and remarkable advances were made. The 16th, 17th and 18th centuries may be the most fascinating periods for many readers, partly because they cover the birth and development of hydrodynamics as we know it and partly because we are less familiar with these times than with the more recent developments in the 19th and 20th centuries. The versatility of many of the scientists is remarkable. For instance, Newton is said to have discovered the contraction of jets in comparing the theoretical and measured flow through orifices and Euler was the first to consider cavitation in connection with the design of water turbines. The progress made in the 18th century is truly remarkable and it makes a fascinating story. The history is completed by chapters on the 19th century, the rise of fluid mechanics in the 20th century and an appraisal of the present situation at mid-century. Somehow the advances made in the 19th and 20th centuries lack the romance and glamour of the earlier golden age but the practical contributions, particularly to engineering, are nevertheless very great.

In the 18th century the distinguished tradition of the French Écoles was clearly established by the remarkable numbers of very eminent hydraulicists which they produced. Because of the easier availability of French records for this period, there may be a tendency to neglect the work of other countries during this time. Balance is always difficult to preserve, particularly in such a concise history, and although one may have doubts here and there, the authors have maintained a good general level of equilibrium.

Most of the important figures seem to have been mentioned, although a few distinguished names may have been omitted because they did not come within the particular scope of the book. Perhaps some mention should have been made of such names as Stodola, Schoklitsch and a few others.

This book provides a good many details which present-day scholars miss by not having easy access to original or translated versions of the great technical works. How much is lost by reference to second-hand and often incorrect versions resulting from successive generations of textbooks ! " One of the ironies of history is the fact that Froude's name has since become inseparably associated with a law of similarity and a non-dimensional number, the first of which he did not originate and the second of which he never even used." The authors have rendered a service by pointing out such anomalies and by quoting direct from old works whenever possible.

The standard of printing is high, and there are many illustrations, including reproductions of portraits of the outstanding figures. The book is written in a concise and easily readable style and is remarkably complete and well-documented for a brief survey. In fact, it whets the appetite for a larger version and it is to be hoped that the authors may consider writing a more detailed history on the same lines. To all those wandering in the maze of modern technology, this history of hydraulics is warmly commended.

S. P. Hutton

Fundamentals of Gas Dynamics, edited by H. W. Emmons (Volume III of High Speed Aerodynamics and Jet Propulsion). Princeton University Press, 1958. 749 pp. $20.00.

Here is a book written by some of the world's experts on gas dynamics. The result, as one would expect, is a book of great value which will be used continually by everyone interested in the subject. It must also be said, however, that this reviewer found it disappointing in a number of ways. This should not be unduly emphasized, and if a relatively large amount of space is devoted here to points of adverse criticism, it is with the understanding that the reader does not need or want to be told many times that articles by people like T. von Kármán and G. I. Taylor have much to offer!

The eight main sections are:

A. The equations of gas dynamics (Tsien).
B. One-dimensional treatment of steady gas dynamics (Crocco).
C. One-dimensional treatment of unsteady gas dynamics (Kantrowitz).
D. The basic theory of gas dynamic discontinuities (Hayes).
E. Shock wave interactions (Polachek and Seeger).
F. Condensation phenomena in high speed flows (Stever).
G. Gas dynamics of combustion and detonation (von Kármán, Emmons, Tankin, Taylor).
H. Flow of rarefied gases (Schaaf and Chambré).

One of the main criticisms is that these sections remain essentially separate, each one having a different purpose and scope, and a different assumption as to the type of reader. The material is not combined into a connected comprehensive account. There are practically no cross-references between sections, and there is considerable duplication. All this could have been just a minor irritation but it turns out to be more. For as a consequence, the value of some articles is reduced, matter of interest is left out and some basic questions emerge confused. Let us consider the articles in turn.

A first section of the standard type on the equations of motion is appropriate if the book is planned as a complete account that a newcomer would read. But the later sections (with the possible exception of C) are not of that type. Thus A loses much of its value. Most of it is in fact not used at all in the rest of the book; each section rederives the few equations needed from first principles. There would be a good case for omitting the section altogether (since there is no shortage of references) and replacing it by a careful review of the results of kinetic theory, the physical chemistry of dissociation, etc., topics which have become so important and yet are not familiar to many gas dynamicists. (It is true that Vol. I of the series is *Thermodynamics and Properties of Matter* but that is another 700 pages!).

Although a detailed discussion of the contents of each section would be too long, it must be noted that some of the derivations in A are misleading and some appear to be wrong. For example, in deriving the energy equation (pages 10 and 11), the work done by the stresses π_{ij} per unit time per unit volume is calculated to be $\pi_{ij}\,\partial u_i/\partial x_j$ instead of $\partial(\pi_{ij}u_i)/\partial x_j$; the resulting equation is correct because the increase of kinetic energy is also omitted from this energy equation. In the treatment of Helmholtz's equation for the vorticity $\boldsymbol{\Omega}$ (pages 30 and 31), the term $(\boldsymbol{\Omega}\,.\,\nabla)\mathbf{u}$ is interpreted as a 'bending' of vortex lines and the term $-\boldsymbol{\Omega}(\nabla\,.\,\mathbf{u})$ as the 'stretching'. This is wrong, of course; the former represents the stretching as well and the latter would be absent altogether in incompressible flow. The so-called 'intrinsic coordinates' n, s, the distances along and perpendicular to streamlines, are used on pages 53, 61 and 63. These variables cannot be introduced in the large and

$\partial/\partial n$, $\partial/\partial s$ are not derivatives in the usual sense; they stand for $h_1^{-1}\,\partial/\partial\alpha$, $h_2^{-1}\,\partial/\partial\beta$, where α and β are generalized coordinates defining the streamlines and orthogonals, and $h_1\,d\alpha$ and $h_2\,d\beta$ are the line elements; for instance $\partial/\partial s(\partial f/\partial n) \neq \partial/\partial n(\partial f/\partial s)$. A final example: the equations of motion are deduced by considering conservation of mass, etc., for a parallelepiped, and are then integrated over an arbitrary volume, the results being *interpreted* as conservation laws. Why not treat an arbitrary volume in the first place ?

Section B is a complete book in itself. It is nearly 300 pages long, out of about 750 for the whole book, and is completely independent of the rest. All aspects of one-dimensional steady flow are developed and applied in considerable detail. This must surely be the most thorough treatment that exists. Particularly impressive is the amount of useful information that can be got out of rather a small number of basic ideas, supplemented by careful physical arguments. There are many practical applications, some of which are far from one-dimensional at first sight. Like most of the other articles, great care is taken to be realistic about the thermodynamics; after reading this book, it will be almost embarassing to assume $p \propto e^{S/c_v}$. This section is perhaps more suitable for reference as needed than for continuous reading; reading it from beginning to end required some persistence.

In contrast to B, section C is relatively short and not compendious, with a general reference to *Supersonic Flow and Shock Waves* by Courant & Friedrichs for full mathematical details. Here some of the space wasted elsewhere in duplication could have been used. For instance, Riemann's classical solution for the interaction of two simple waves and the hodograph transformation are mentioned only in a footnote. On the other hand, there are some physical arguments about simple waves, with or without weak shock waves, and Professor Kantrowitz's original work on the stability of shock waves in steady channel flows, which do not appear in Courant & Friedrichs. It should be noted that this particular section was written in 1952 and as a consequence is a little out of date now.

Part of D is concerned with the Navier–Stokes structure of shock waves. This is very well done and indeed some of the original ideas, such as the precise use of Burgers's equation, have less impact than they deserve because they were introduced independently, but published earlier, by Lighthill in *Surveys in Mechanics* (the G. I. Taylor 70th Anniversary Volume). It is disappointing, however, to find that the kinetic theory approaches to the question are not also included in some detail. The author claims correctly that their foundations are a little shaky and their results seem to be less successful than the Navier–Stokes treatment, but these are not sufficient reasons unless space is scarce. But space is used elsewhere on much less respectable theories, and section B is certainly not limited in this respect. After all, the beginner can find the classical treatment of shock structure in many books, and the more experienced reader would welcome an authoritative account of some of the more recent attempts just because they do pose considerable difficulties.

The remainder of D concerns ' discontinuities ' in which reactions and change of state occur, examples being condensation shocks, flame fronts and detonations. This has to be considered in conjunction with sections F and G where these topics are studied in detail. Now, F and G make no serious reference to the longish discussion in D; instead there is appreciable overlap. For example, the classification of combustion phenomena into weak and strong deflagrations and detonations is given in D3, G1 and G10, in each case as if for the first time. Both D3 and G10 include detailed discussions of the properties of the Hugoniot curve which are essentially the same. The equations for a plane stationary flame front are given in both G1 and G2 (which are by different authors) in different form and notation without explaining why this was necessary. In a difficult and only partially understood subject, the lack of a unified treatment is very confusing. Moreover, what is the relation of these articles on combustion to Vol. II of the series which is an equally large volume devoted *entirely* to combustion ?

The interesting question of the existence of strong deflagrations and weak detonations is clouded by some of the statements. After referring to Friedrichs extensively in the arguments suggesting that strong deflagrations cannot exist, the final paragraph of D6 begins: " With regard to the weak detonation, which has not been observed (again to the writer's knowledge) in explosion experiments, there is no theoretical evidence for non-existence." Yet such evidence is given in Courant & Friedrichs and on p. 231 of their book there is the italicized statement: " Consequently, weak detonations are impossible." I am open to arguments that their reasoning is unsound but not that it is not there.

Of course, in spite of the above criticism, F and G are bulging with information, and one can really get some idea of the present state of these complicated fields. There is again the feeling of reality which is an outstanding feature of the book. For example, in G10 we are led through the details of calculating the Hugoniot curve for the mixture $H_2 + \frac{1}{2}O_2 + 2{\cdot}5N_2$, first without and then with dissociation, before going on to discuss the propagation of detonation waves. At every stage there are checks with whatever experiments are available.

Section E requires little comment. It is a complete account of the present knowledge of the interaction of plane shock waves with other waves, solid walls and interfaces. The methods of deriving theoretical formulae, the subsequent computations, the comparison with experiment (and lack of agreement for Mach reflection of weak shocks) are all set out exactly as they should be.

The final section H stands out as a piece of careful exposition. All the ideas and results are presented clearly and concisely; it makes interesting and informative reading. It even remedies earlier deficiencies in part. For example, the section on slip flow contains an excellent review of the derivation of the Navier–Stokes, Burnett and Thirteen-moment equations from the Boltzmann equation, with a sober consideration of the validity

and degree of success of the various approximations involved. This is of general value for the book, quite apart from its relevance to slip flow. Some brief comments on shock structure also appear here. Odd though it may seem, section H was added on to this volume as an afterthought; it was originally prepared for Vol. IV.

After a classification of the various flow regimes, with the significant relative magnitudes of Mach number and Reynolds number, section H is divided into three main sections; free molecule flow, slip flow, and experimental results in slip flow and transition regimes. The first of these shows how theories of the heat transfer and the forces, for bodies moving at the appropriate high speeds, may be developed assuming a Maxwellian distribution about the main stream velocity for the molecules incident on the body surface and using empirical coefficients to specify the interaction of the incident molecules with the surface. Typical cases are worked out and detailed references are given for further work. In the chapter on slip flow, the review noted above is given and the conclusion reached that the Navier–Stokes equations, together with the slip velocity and temperature jump boundary conditions, are at present more successful than any of the intended improvements. The final chapter sets out the comparison of theoretical results worked out in this way with experiment.

G. B. WHITHAM

INDEX

Binnie, A. M. and Phillips, O. M. The mean velocity of slightly buoyant and heavy particles in turbulent flow in a pipe, 87.

Blackman, Vernon H. *See* **Niblett and Blackman.**

Boyle, P. *See* **King, Boyle and Ogle.**

Brenner, Howard and Happel, John Slow viscous flow past a sphere in a cylindrical tube, 195.

Broadwell, James E. A simple model of the non-equilibrium dissociation of a gas in Couette and boundary-layer flows, 113.

Broer, L. J. F. Characteristics of the equations of motion of a reacting gas, 276.

Cann, Gordon L. and Ducati, Adriano C. Energy content and ionization level in an argon gas jet heated by a high intensity arc, 529.

Carrier, G. F. Shock waves in a dusty gas, 376.

Carrier, G. F. The mixing of ground water and sea water in permeable subsoils, 479.

Carrier, G. F. and Greenspan, H. P. Water waves of finite amplitude on a sloping beach, 97.

Cheng, S. I. and Kovitz, A. A. Mixing and chemical reaction in the laminar wake of a flat plate, 64.

Clarke, John F. Energy transfer through a dissociated diatomic gas in Couette flow, 441.

Crease, J. The propagation of long waves into a semi-infinite channel in a rotating system, 306.

Cumberbatch, E. Two-dimensional planing at high Froude number, 466.

Drazin, P. G. The stability of a shear layer in an unbounded heterogeneous inviscid fluid, 214.

Ducati, Adriano C. *See* **Cann and Ducati.**

Fraenkel, L. E. A two-dimensional air intake in a sonic stream, 629.

Freeman, N. C. Non-equilibrium flow of an ideal dissociating gas, 407.

Grant, H. L. The large eddies of turbulent motion, 149.

Greenspan, H. P. On the breaking of water waves of finite amplitude on a sloping beach, 330.

Greenspan, H. P. *See* **Carrier and Greenspan.**

Gundersen, Roy A note on shock flow in a channel, 501.

Happel, John *See* **Brenner and Happel.**

Kakutani, T. *See* **Tatsumi and Kakutani.**

Keller, Joseph B. Surface waves on water of non-uniform depth, 607.

Kemp, Nelson H. and Petschek, Harry E. Two-dimensional incompressible magneto-hydrodynamic flow across an elliptical solenoid, 553.

King, J. L., Boyle, P. and Ogle, J. B. Instability in slotted wall tunnels, 283.

Kovitz, A. A. *See* **Cheng and Kovitz.**

Lighthill, M. J. On displacement thickness, 383.

Lock, R. C. An extension of the linearized theory of supersonic flow past quasi-cylindrical bodies, with applications to wing-body interference, 33.

Malkus, W. V. R. and Veronis, G. Finite amplitude cellular convection, 225.

Maull, D. J. *See* **Stollery and Maull.**

Miles, John W. On the disturbed motion of a plane vortex sheet, 538.

Niblett, Bryan and Blackman, Vernon H. An approximate measurement of the ionization time behind shock waves in air, 191.

Nonweiler, T. R. F. The sonic flow about some symmetric half-bodies, 140.

Ogle, J. B. *See* **King, Boyle and Ogle.**

Payne, R. B. Calculations of unsteady viscous flow past a circular cylinder, 81.

Pearson, J. R. A. On convection cells induced by surface tension, 489.

Petschek, Harry E. *See* **Kemp and Petschek.**

Phillips, O. M. The equilibrium range in the spectrum of wind-generated waves, 426.

Phillips, O. M. *See* **Binnie and Phillips.**

Power, G. and Smith, P. A modified tangent-gas approximation for two-dimensional steady flow, 600.

Pridmore-Brown, D. C. Sound propagation in a fluid flowing through an attenuating duct, 393.

Riley, N. Effects of compressibility on a laminar wall jet, 615.

Roberts, Leonard. On the melting of a semi-infinite body of ice placed in a hot stream of air, 505.

Smith, P. *See* **Power and Smith.**

Spalding, D. B. Heat transfer from surfaces of non-uniform temperature, 22.

Sparrow, E. M. The thermal boundary layer on a non-isothermal surface with non-uniform free stream velocity, 321.

Stollery, J. L. and Maull, D. J. A note on the compression of air through repeated shock waves, 650.

Stuart, J. T. On the non-linear mechanics of hydrodynamic stability, 1.

Tatsumi, T. and Kakutani, T. The stability of a two-dimensional laminar jet, 261.

Townsend, A. A. The effects of radiative transfer on turbulent flow of a stratified fluid, 361.

Veronis, G. *See* **Malkus and Veronis.**

White, Donald R. Influence of diaphragm opening time on shock tube flows, 585.

Whitham, G. B. On the propagation of shock waves through regions of non-uniform area or flow, 337.

REVIEWS

An Introduction to Fluid Mechanics and Heat Transfer, by J. M. Kay, 110.

Fluid Models in Geophysics, edited by Robert R. Long, 335.

Water Waves: The Mathematical Theory with Applications, by J. J. Stoker, 435.

Proceedings of the 5th Midwestern Conference on Fluid Mechanics, edited by A. M. Kuethe, 439.

History of Hydraulics, by Hunter Rouse and Simon Ince, 655.

Fundamentals of Gas Dynamics, edited by H. W. Emmons (Volume III of High Speed Aerodynamics and Jet Propulsion), 657.

JOURNAL OF FLUID MECHANICS

Volume 4, Part 6 November 1958

CONTENTS

Two-dimensional incompressible magneto-hydrodynamic flow across an elliptical solenoid
by NELSON H. KEMP and HARRY E. PETSCHEK 553

Influence of diaphragm opening time on shock-tube flows
by DONALD R. WHITE 585

A modified tangent-gas approximation for two-dimensional steady flow
by G. POWER and P. SMITH 600

Surface waves on water of non-uniform depth
by JOSEPH B. KELLER 607

Effects of compressibility on a laminar wall jet
by N. RILEY 615

A two-dimensional air intake in a sonic stream
by L. E. FRAENKEL 629

A note on the compression of air through repeated shock waves
by J. L. STOLLERY and D. J. MAULL 650

Reviews 655

Index to Volume 4 662

Printed in Great Britain by Taylor & Francis Ltd.

7898